Supporting Information

Thiosquaramides: pH switchable anion transporters

Nathalie Busschaert,[a‡] Robert B.P. Elmes,[b‡] Dawid D. Czech,[a] Xin Wu,[a] Isabelle L. Kirby,[a] Evan M. Peck,[c] Kevin D. Hendzel,[c] Scott Shaw,[c] Bun Chan,[b] Bradley D. Smith,[c] Katrina A. Jolliffe,[b*] and Philip A. Gale,[a,d*]

[a] Chemistry, University of Southampton, Southampton, SO17 1BJ, UK; Tel: +44 (0)23 8059 3332; E-mail: philip.gale@soton.ac.uk

[b] School of Chemistry (F11), The University of Sydney, 2006 NSW, Australia; Fax: +61 2 9351 3329; Tel: +61 2 9351 2297; E-mail: kate.jolliffe@sydney.edu.au

[c] Department of Chemistry and Biochemistry, University of Notre Dame, Notre Dame, Indiana, 46556, United States

[d]Department of Chemistry, Faculty of Science, King Abdulaziz University, Jeddah 21589, Saudi Arabia

[‡]These authors contributed equally to this work

Contents

S1. Synthesis S3

S2. NMR and HPLC-MS data S6

S3. Conformational analysis in solution (DNMR) S14

S4. Single crystal X-ray diffraction S17

S4.1. Crystal structure of 4 with DMSO (CCDC 1005459) S18

S4.2. Crystal structure of 5 with DMSO (CCDC 1005460) S20

S4.3. Crystal structure of 8 with DMSO (CCDC 1005461) S21

S4.4. Crystal structure of 6 with TMACl (CCDC 1005458) S23

S5. ^{1}H NMR Chloride Binding Titrations S25

S6. Determination of pK_a values S29

S7. Anion transport studies S34

S7.1. General protocol S34

S7.2. Chloride/nitrate transport at pH 7.2 and pH 4.0 ..... S34

S7.3. Hill plots S36

S7.4. Cholesterol tests S39

S7.5. Calcein leakage assays S41

S7.6. Antiport tests S43

S7.7. HPTS assays S45

S7.8. Apparent pK_a determination S54

S8. Thiosquaramide stability S61

S9. References S64

S1. Synthesis

^{1}H NMR spectra were recorded using a Bruker Avance III 500 at a frequency of 500.13 MHz, and are reported as parts per million (ppm) with DMSO-d_6 (δ_H 2.50 ppm) or CD_3CN (δ_H 1.94 ppm) as internal references. The data are reported as chemical shift (δ), multiplicity (br = broad, s = singlet, d = doublet, m = multiplet), coupling constant (*J*, Hz) and relative integral. ^{13}C NMR spectra were recorded using a Bruker Avance III 500 at a frequency of 125.76 MHz and are reported as parts per million (ppm) with DMSO-d_6 (δ_C 39.52 ppm) or CD_3CN (δ_C 118.26 ppm) as internal references. High resolution ESI spectra were recorded on a BrukerBioApex Fourier Transform Ion Cyclotron Resonance mass spectrometer (FTICR) with an Analytica ESI source, operating at 4.7 T or a BrukerDaltonics Apex Ultra FTICR with an Apollo Dual source, operating at 7 T. Infrared (IR) absorption spectra were recorded on a Bruker ALPHA Spectrometer with Attenuated Total Reflection (ATR) capability, using OPUS 6.5 software. LC-MS was performed on a Shimadzu LC-MS 2020 instrument consisting of a LC-M20A pump and a SPD-20A UV/Vis detector coupled to a Shimadzu 2020 mass spectrometer (ESI) operating in positive mode. Separations were performed on a Waters Sunfire 5 μm, 2.1 x 150 mm column (C18) operating at a flow rate of 0.2 mL min^{-1}. Separations were performed using a mobile phase of 0.1% formic acid in water (Solvent A) and 0.1% formic acid in acetonitrile (Solvent B) and a linear gradient of 0-100% B over 30 min. Analytical TLC was performed using precoated silica gel plates (Merck Kieselgel 60 F254). Squaramide starting materials **1** - **3** were synthesised as previously described,[1] thionating agent P_4S_{10}.pyridine was synthesised according to the method of Bergman *et. al.*[2] and all other reagents were commercially available and used as supplied. All reactions were carried out under an inert atmosphere and undertaken using anhydrous solvents dried using an Innovative Technologies PureSolve solvent purification system.

3,4-bis(3,5-di-tert-butylphenylamino)cyclobut-3-ene-1,2-dione (4).

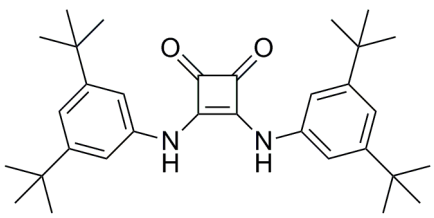

Compound **4** was synthesised according to the previously reported method of Taylor *et al.*[3] using 3,5-ditertbutyl-aniline (0.3 g, 1.46 mmol, 2.2 equiv), 3,4-diethoxy-cyclobut-3-ene-1,2-dione (0.11 g, 0.66 mmol, 1.0 equiv) and zinc trifluoromethanesulfonate (0.05 g, 0.13 mmol, 0.2 equiv). Purification by flash column chromatography eluting with 5% acetone in DCM yielded **4** as a

beige solid. (0.293 g, 90%). **m.p.** 333 ◦C; **^{1}H NMR** (500.13 MHz, DMSO-d_6): 1.30 (s, 36 H, tBu),7.12 (t, *J* = 1.4 Hz, 2 H, Ar H), 7.36 (d, *J* = 1.4 Hz, 4 H, Ar H), 9.77 (br s, 2 H, NH); **^{13}C NMR** (125.76 MHz, DMSO-d_6): 15.8, 31.8, 35.4, 65.5, 113.4, 117.6, 152.3, 166.2.; **HRMS** (ESI) m/z calcd. for $C_{32}H_{44}N_2O_2Na$ $[M + Na]^+$ 511.3295, found 511.3295; **ν_{max} (film)/cm^{-1}:** 2962, 1790, 1679, 1626, 1584, 1554, 1482, 1436, 1363, 1309, 1249.

3,4-bis(phenylamino)cyclobut-3-ene-1,2-dithione (5).

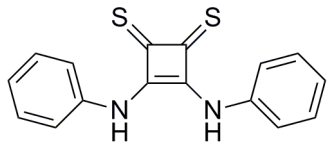

3,4-bis(phenylamino)cyclobut-3-ene-1,2-dione (0.2 g, 0.76 mmol, 1.0 equiv) and P_4S_{10}·pyridine (0.575 g, 1.5 mmol, 2.0 equiv) were suspended in anhydrous MeCN (15 mL) and heated at 90° C for 4 hrs. The resultant precipitate was isolated by suction filtration and washed with 2M HCl (3 x 5 mL) and MeCN (3 x 5 mL) to yield **5** as a yellow solid. (0.147 g, 66%). **m.p.** 243 ◦C; **^{1}H NMR** (500.13 MHz, DMSO-d_6): 7.00 – 7.26 (m, 10 H, Ar H),10.79 (br s, 2 H, NH); **^{13}C NMR** (125.76 MHz, DMSO-d_6): 122.2, 125.4, 128.6, 169.49; **HRMS** (ESI) m/z calcd. for $C_{16}H_{13}N_2s_2$ $[M + H]^+$ 297.0515, found 297.0517; **ν_{max} (film)/cm^{-1}:** 3156, 2957, 1683, 1604, 1546, 1463, 1447, 1327, 1295, 1275, 1233, 1204, 1130, 1074, 1028, 960, 932, 898.

3,4-bis(4-(trifluoromethyl)phenylamino)cyclobut-3-ene-1,2-dithione (6).

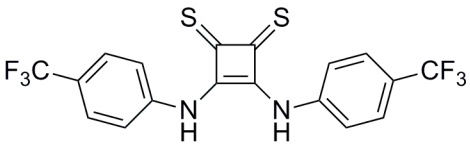

3,4-bis(4-(trifluoromethyl)phenylamino)cyclobut-3-ene -1,2-dione (0.2 g, 0.5 mmol, 1.0 equiv) and P_4S_{10}·pyridine (0.380 g, 1.0 mmol, 2.0 equiv) were suspended in anhydrous MeCN (15 mL) and heated at 90° C for 4 hrs. The solvent was removed under reduced pressure and the crude residue was stirred in 2M HCl before being subjected to flash column chromatography eluting with 5% MeCN in DCM to yield **6** as a yellow solid. (0.103 g, 48%). **m.p.** 193 ◦C decomp; **^{1}H NMR** (500.13 MHz, CD_3CN): 7.25 (d, *J* = 8.3 Hz, 4 H, Ar H),7.37 (d, *J* = 8.3 Hz, 4 H, Ar H),8.97 (br s, 2 H, NH); **^{13}C NMR** (125.76 MHz, CD_3CN): 123.4, 123.9, 126.09, 127.0, 127.6 (q, *J* = 34.1) , 141.7, 170.4; **HRMS** (ESI) m/z calcd. for $C_{18}H_{11}F_6N_2S_2$ $[M + H]^+$ 433.0262, found 433.0264; **ν_{max} (film)/cm^{-1}:** 3156, 3014, 1701, 1614, 1597, 1537, 1422, 1377, 1318, 1298, 1273, 1221, 1177, 1126, 1111, 1065, 997, 867, 834.

3,4-bis(3,5-bis(trifluoromethyl)phenylamino)cyclobut-3-ene-1,2-dithione (7).

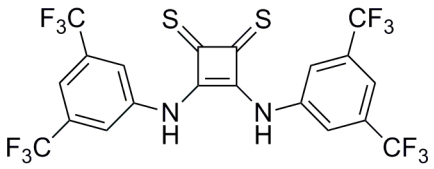

3,4-bis(3,5-bis(trifluoromethyl)phenylamino)cyclobut-3-ene-1,2-dione (0.2 g, 0.37 mmol, 1.0 equiv) and P_4S_{10}·pyridine (0.282 g, 0.74 mmol, 2.0 equiv) were suspended in anhydrous MeCN (15 mL) and heated at 90° C for 4 hrs. The solvent was removed under reduced pressure and the crude residue was stirred in 2M HCl before being subjected to flash column chromatography eluting with DCM to yield **7** as a yellow solid. (0.157 g, 37%). **m.p.** 220 ◦C decomp; **^{1}H NMR** (500.13 MHz, CD_3CN): 7.93 (s, 2 H, Ar H), 8.30 (s, 4 H, Ar H), 9.92 (br s, 2 H, NH); **^{13}C NMR** (125.76 MHz, CD_3CN): 120.5, 122.2, 124.4, 124.6, 187.8; **HRMS** (ESI) m/z calcd. for $C_{20}H_9F_{12}N_2S_2$ $[M + H]^+$ 569.0010, found 569.0009; **ν_{max} (film)/cm^{-1}:** 3101, 2971, 1738, 1536, 458, 1434, 1367, 1328, 1302, 1273, 1217, 1195, 1181, 1145, 1126, 1109, 934, 912, 898, 882, 846, 812.

3,4-bis(3,5-di-tert-butylphenylamino)cyclobut-3-ene-1,2-dithione (8).

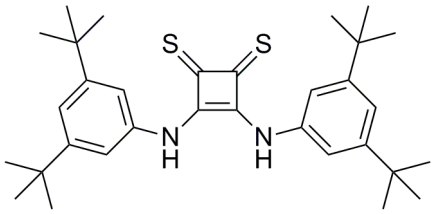

3,4-bis(3,5-di-tert-butylphenylamino)cyclobut-3-ene-1,2-dione (0.1 g, 0.2 mmol, 1.0 equiv) and P_4S_{10}·pyridine (0.233 g, 0.6 mmol, 3.0 equiv) were suspended in anhydrous MeCN (8 mL) and heated at 90° C for 7 hrs. The solvent was removed under reduced pressure and the crude residue was stirred in 2M HCl before being subjected to flash column chromatography eluting with 2% MeCN in DCM to yield **8** as a yellow solid (0.063 g, 60%). **m.p.** 235 ◦C; **^{1}H NMR** (500.13 MHz, DMSO-d_6): 1.24 (s, 36 H, tBu), 7.3 (m, 6 H, Ar H), 10.48 (br s, 2 H, NH); **^{13}C NMR** (125.76 MHz, DMSO-d_6): 1.1, 34.6, 116.4, 118.0, 119.1, 151.0, 169.4; **HRMS** (ESI) m/z calcd. for $C_{32}H_{44}N_2S_2Na$ $[M + Na]^+$ 543.2838, found 543.2838. **ν_{max} (film)/cm^{-1}:** 2963, 2364, 2340, 2326, 1680, 1572, 1466, 1297.

S2. NMR and HPLC-MS data

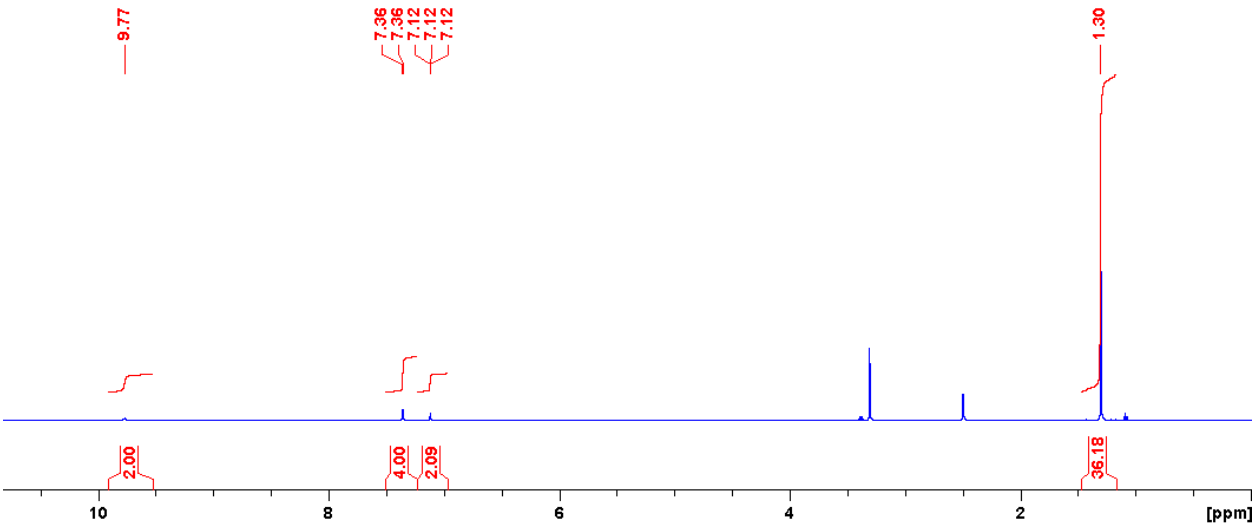

Figure S1: ^{1}H NMR (DMSO-d_6, 500 MHz) spectra of **4**.

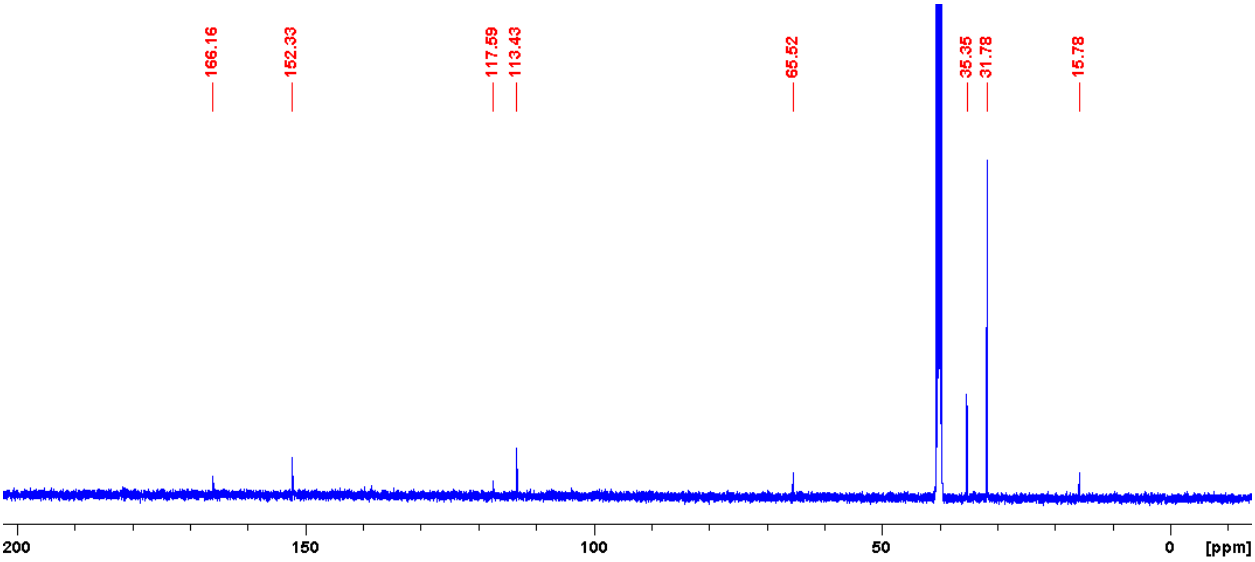

Figure S2: ^{13}C NMR (DMSO-d_6, 125 MHz) spectra of **4**.

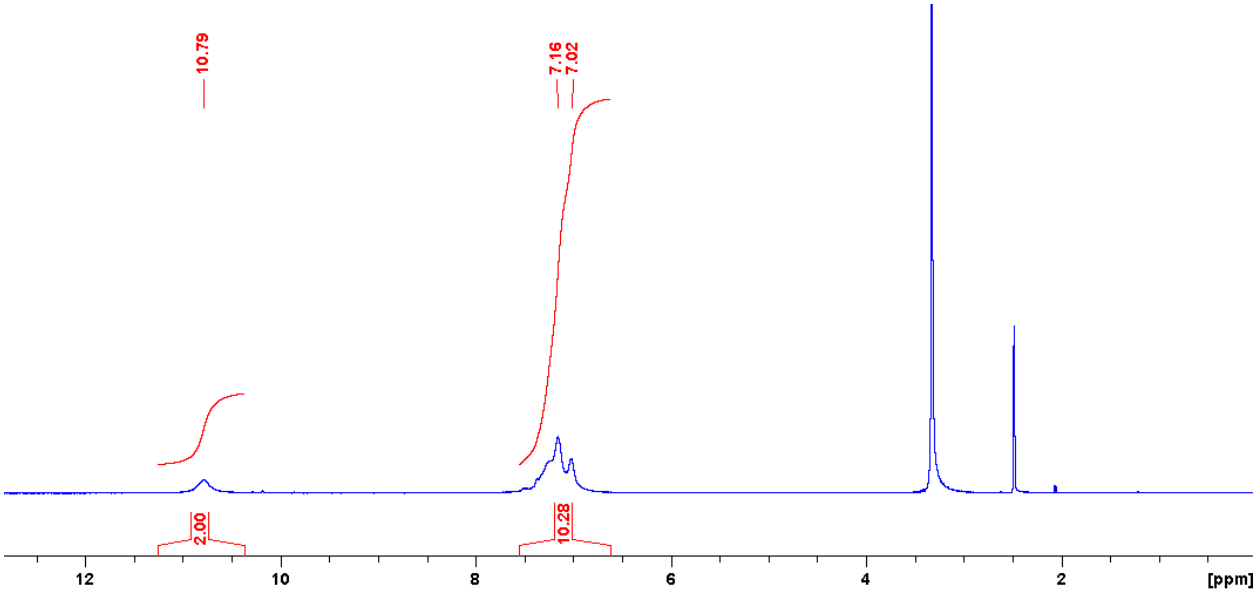

Figure S3: ^{1}H NMR (DMSO-d_6, 500 MHz) spectra of **5**.

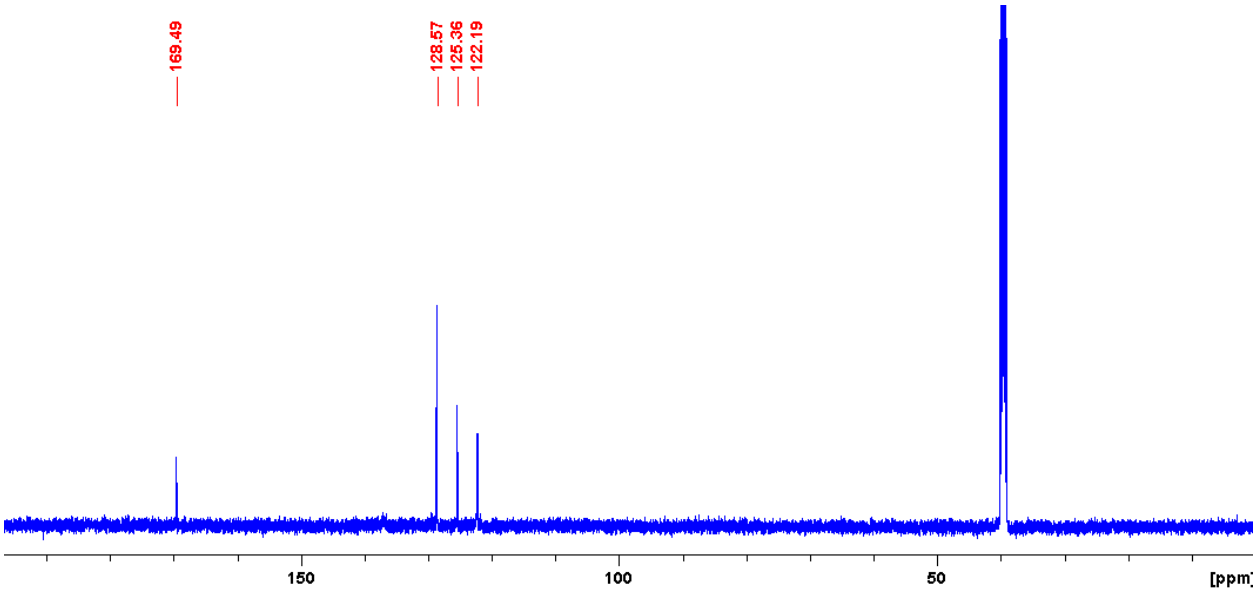

Figure S4: ^{13}C NMR (DMSO-d_6, 125 MHz) spectra of **5**.

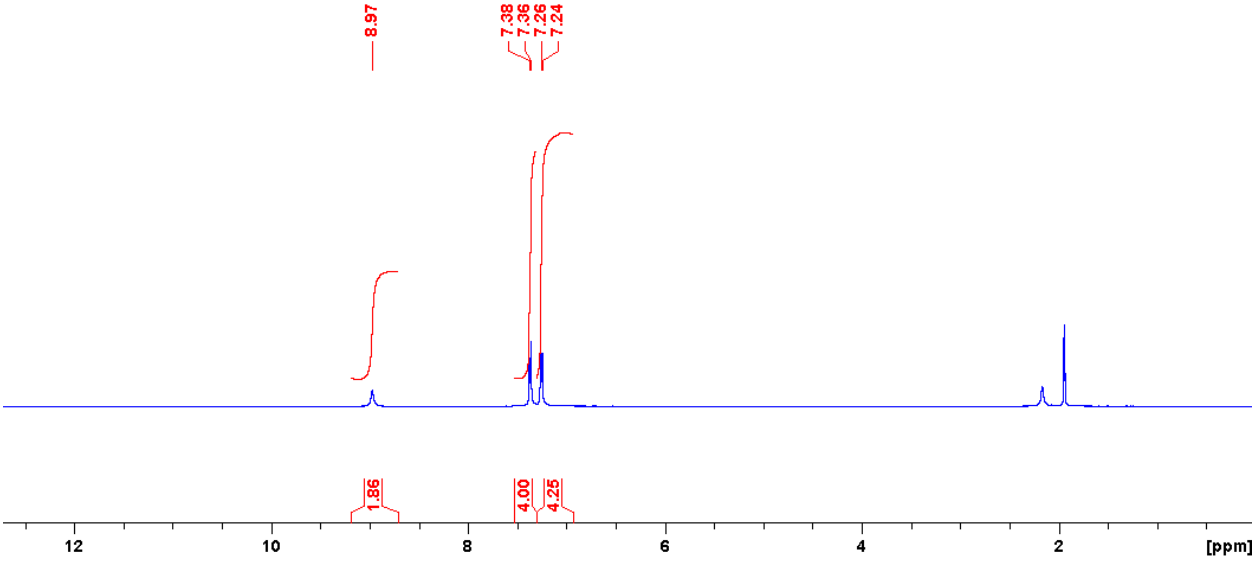

Figure S5: ^{1}H NMR (CD_3CN, 500 MHz) spectra of **6**.

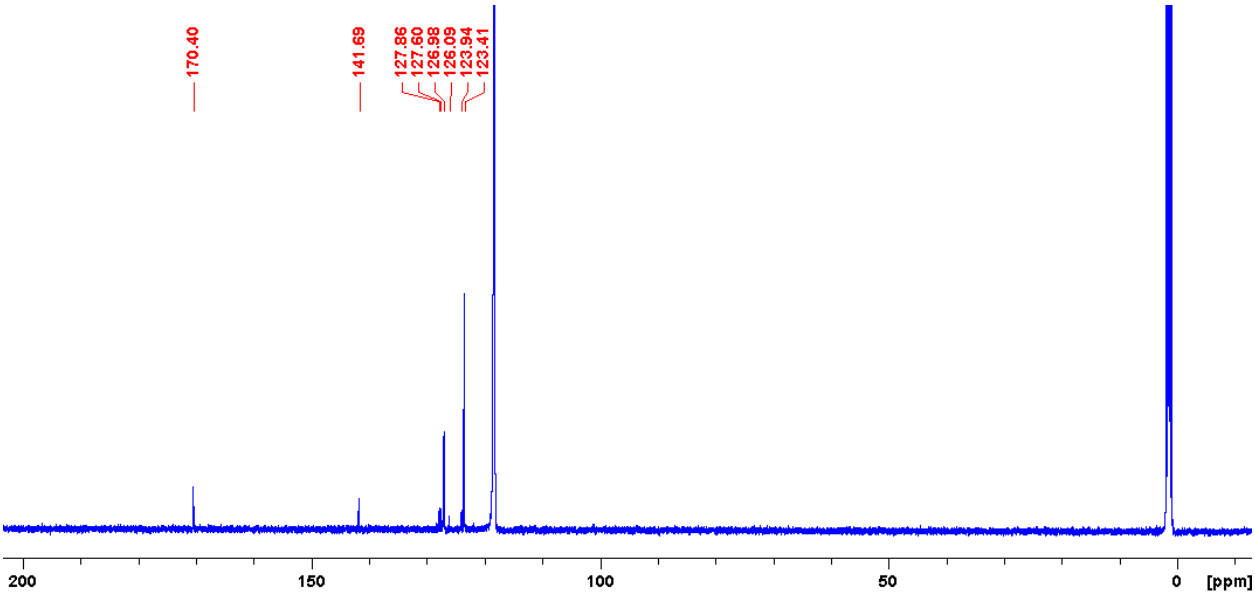

Figure S6: ^{13}C NMR (CD_3CN, 125 MHz) spectra of **6**.

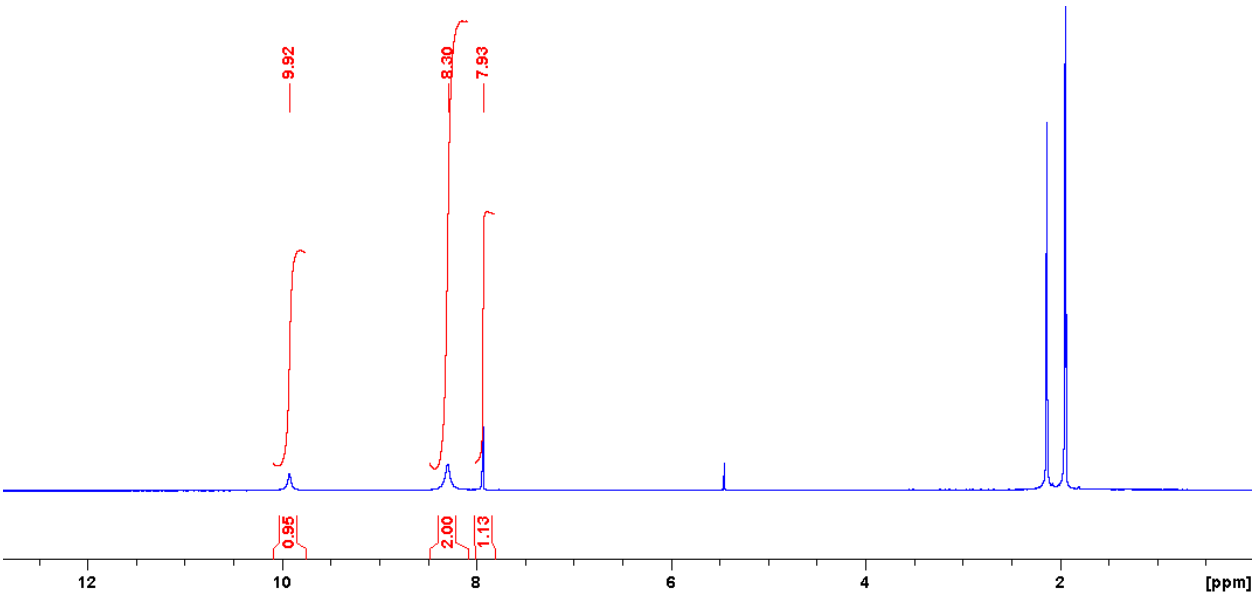

Figure S7: ^{1}H NMR (CD_3CN, 500 MHz) spectra of 7.

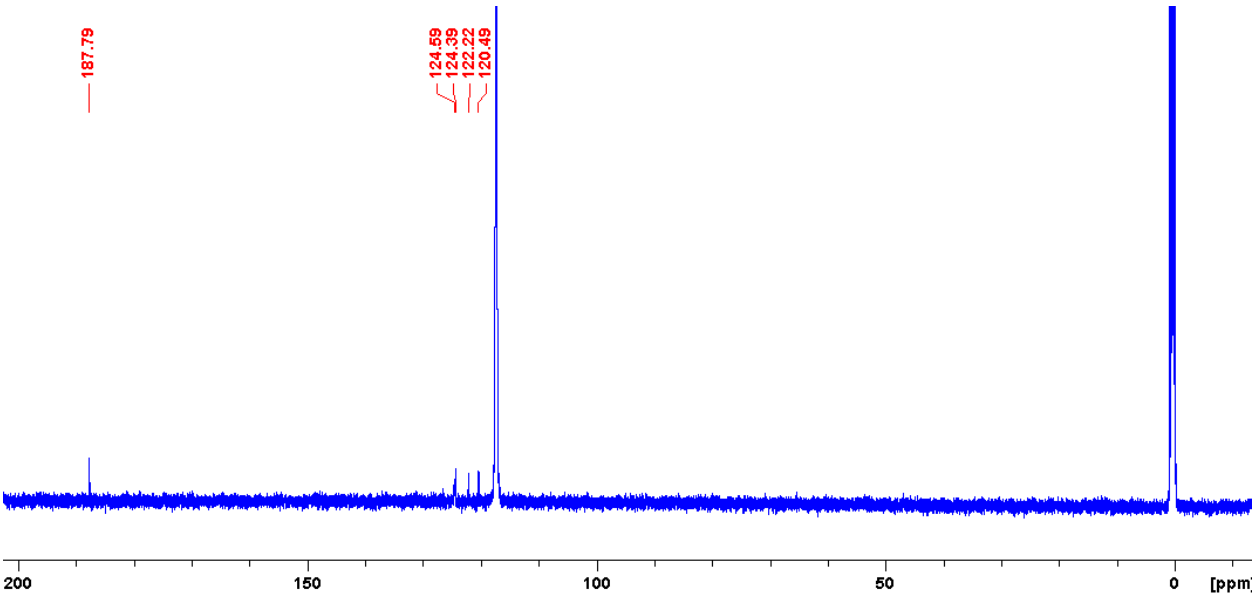

Figure S8: ^{13}C NMR (CD_3CN, 125 MHz) spectra of 7.

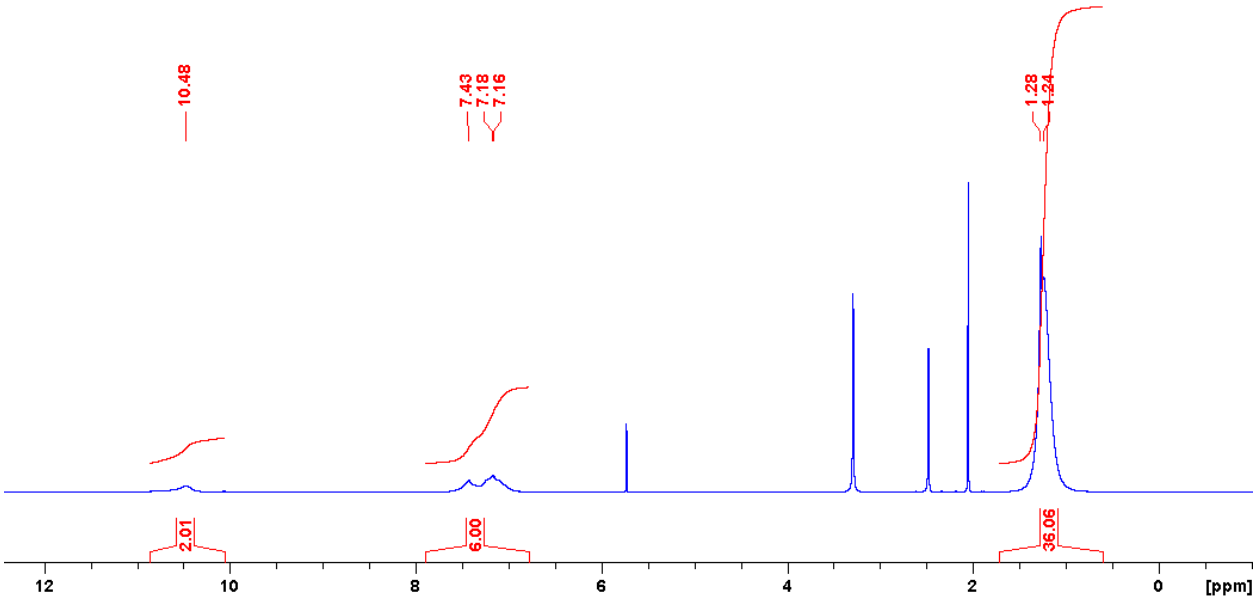

Figure S9: ^{1}H NMR (CD_3CN, 500 MHz) spectra of **8**.

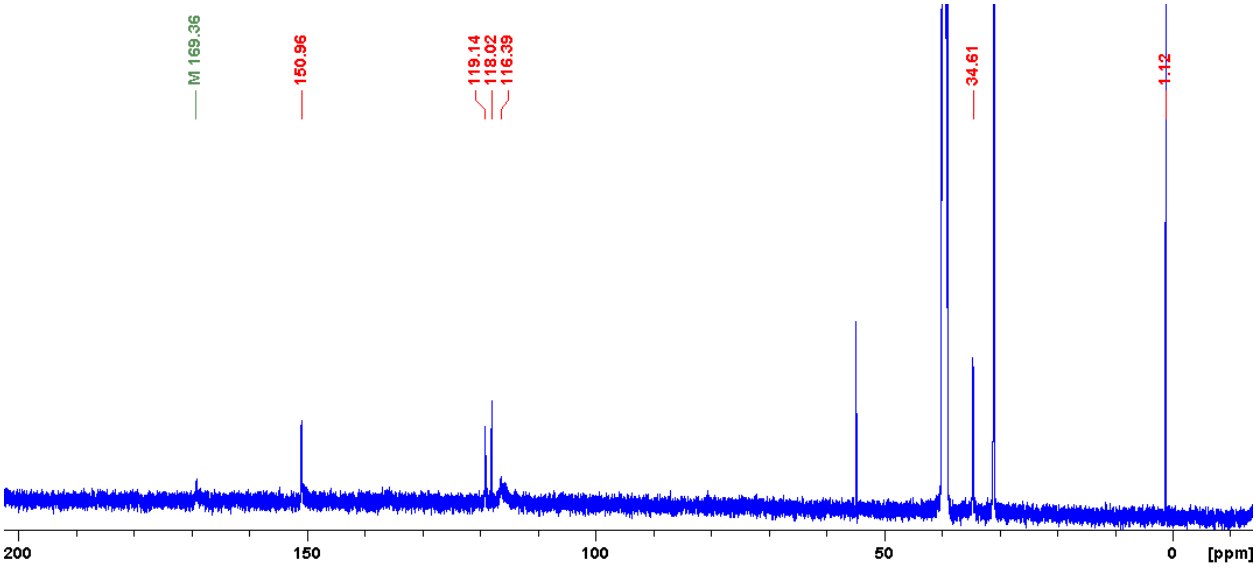

Figure S10: ^{13}C NMR (CD_3CN, 125 MHz) spectra of **8**.

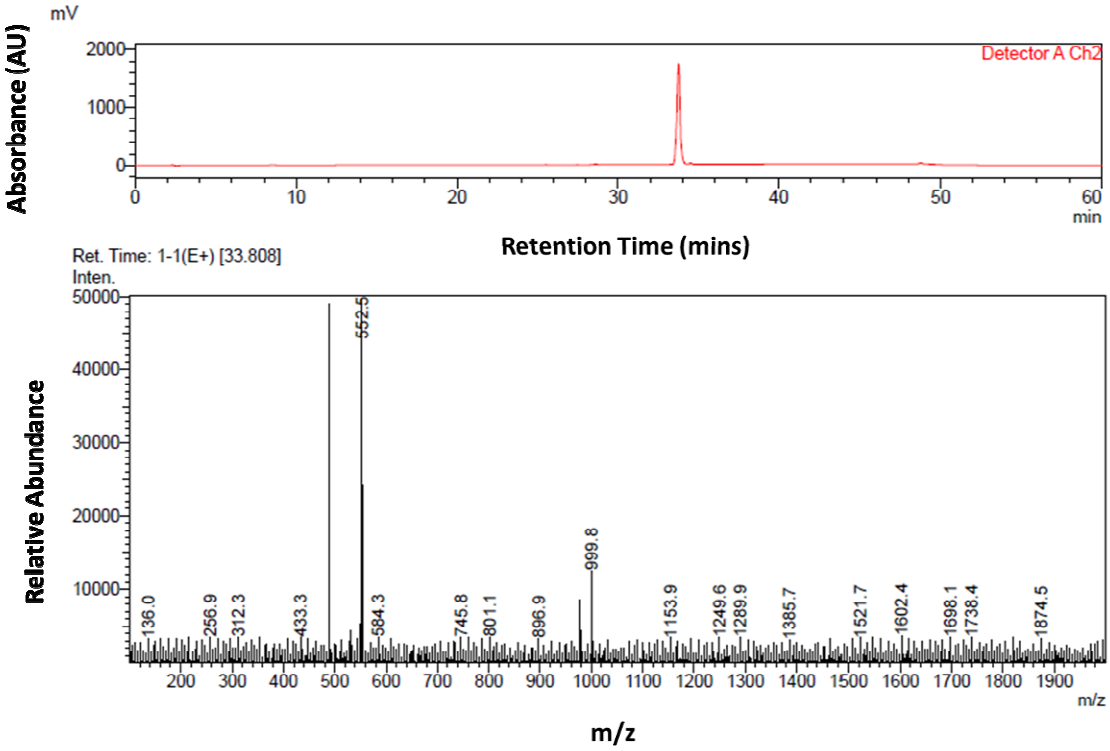

Figure S11: Analytical LCMS trace of receptor **4**; Rt 33.81 min (0-100% B over 30 min, 0.1% Formic Acid, λ = 254 nm); Calculated Mass $[M+H]^+$: 489.7; Mass Found (ESI^+); 489.5

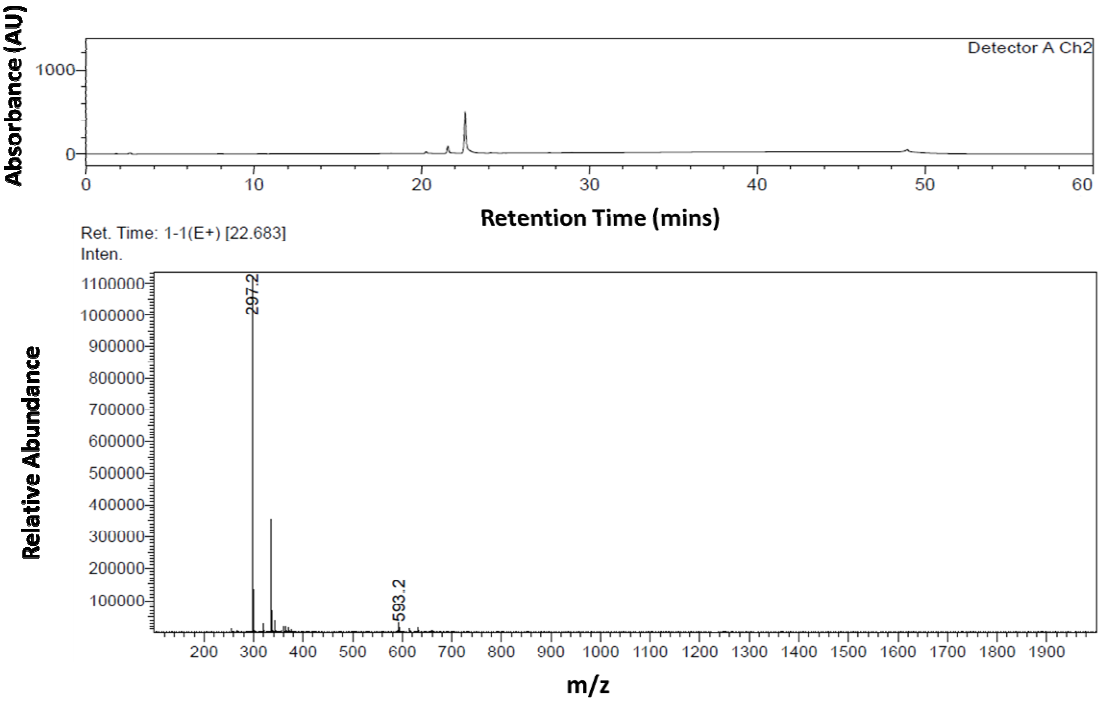

Figure S12: Analytical LCMS trace of receptor **5**; Rt 22.68 min (0-100% B over 30 min, 0.1% Formic Acid, λ = 254 nm); Calculated Mass $[M+H]^+$: 297.1; Mass Found (ESI^+); 297.2

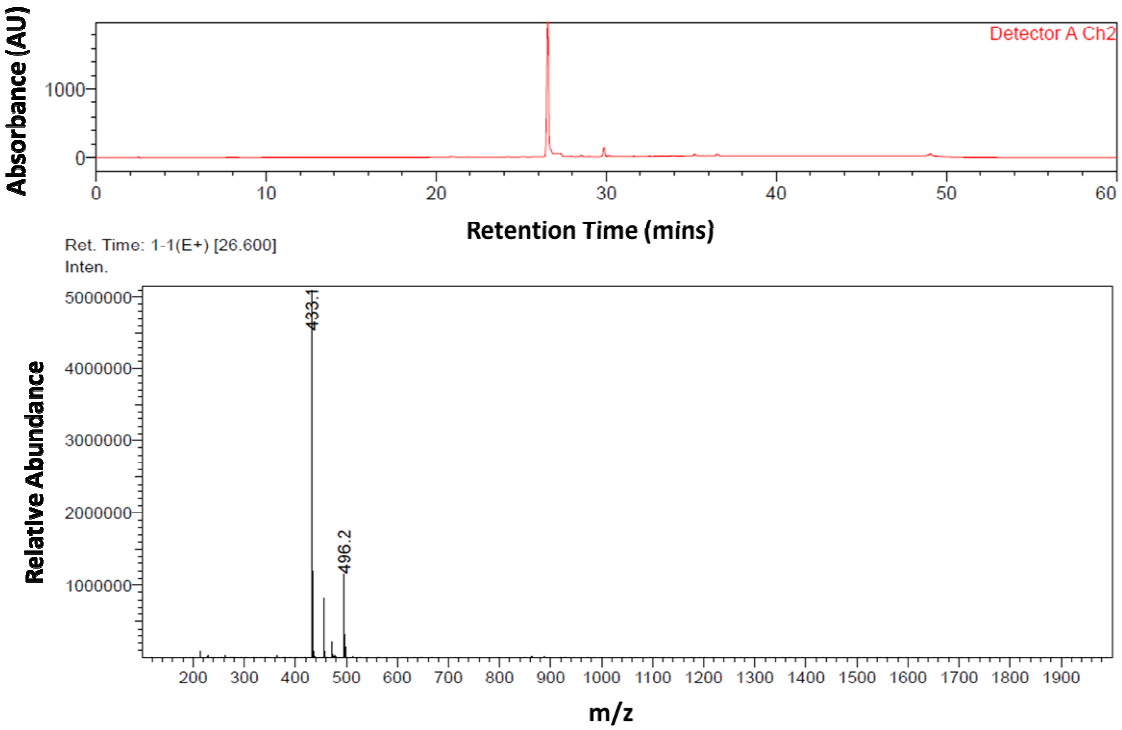

Figure S13: Analytical LCMS trace of receptor **6**; Rt 26.6 min (0-100% B over 30 min, 0.1% Formic Acid, λ = 254 nm); Calculated Mass $[M+H]^+$: 433.0; Mass Found (ESI^+); 433.1

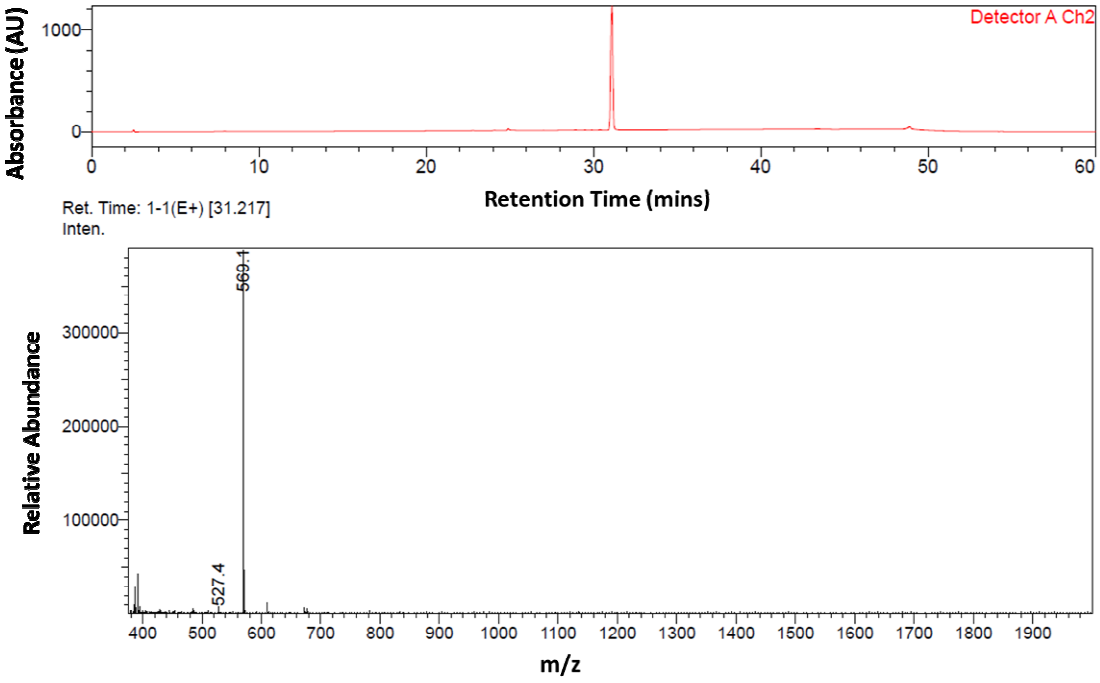

Figure S14: Analytical LCMS trace of receptor **7**; Rt 31.2 min (0-100% B over 30 min, 0.1% Formic Acid, λ = 254 nm); Calculated Mass $[M+H]^+$: 569.0; Mass Found (ESI^+); 569.

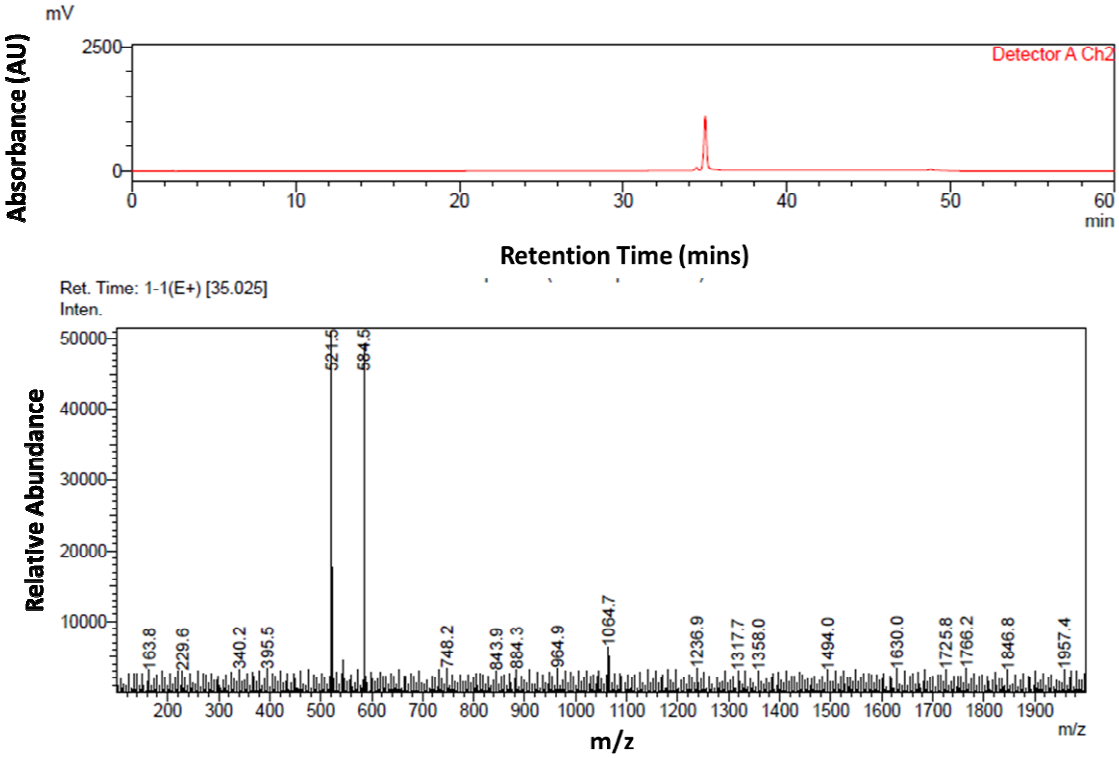

Figure S15: Analytical LCMS trace of receptor **8**; Rt 35.0 min (0-100% B over 30 min, 0.1% Formic Acid, λ = 254 nm); Calculated Mass $[M+H]^+$: 521.5; Mass Found (ESI^+); 521.5

S3. Conformational analysis in solution (DNMR)

Squaramides exist in two well-documented conformations: the *anti/anti* (open) and *anti/syn* (closed) conformations (Figure S16). Lone pair conjugation of the nitrogen into the π-system of the cyclobutadenedione ring contributes sp^2-like character to the nitrogen,[4] and therefore limits rotation of the C-N bonds making squaramides fairly rigid scaffolds.[5] While the *anti/syn* conformation is not sterically favoured, there are reports of engineered systems where the *anti/syn* conformation is favoured due to intramolecular hydrogen bonding that can occur to the adjacent amide hydrogen.[6] The *anti/syn* conformation is also dependent on the ligand and can be induced if a mixed acceptor-donor ligand is present.[7] The *syn/syn* conformer has not been reported due to the heavy steric strain that would entail.[5]

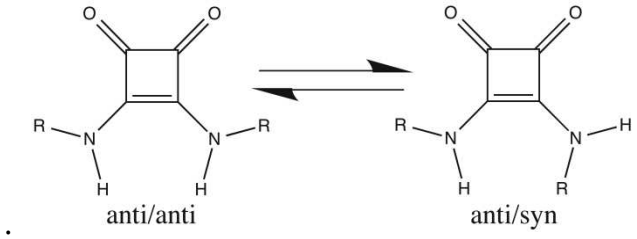

Figure S16: The two reported conformations of squaramides: the *anti/anti* and *anti/syn* conformations, respectively**.**

The ^{1}H NMR spectrum of compound **4** in non-polar CD_2Cl_2 is made complicated by self-aggregation processes. For example, upon cooling the sample to -55°C, a new set of peaks emerges (indicated in Figure S17 with *) that are due to intermolecular aggregates. A second feature in Figure S17 is the chemical shift sensitivity of aryl signal **C** to squaramide conformation. At high temperatures, the signal appears at 7.10 ppm, but the signal shifts dramatically to 7.48 ppm (Figure S17) upon cooling, which favors the *anti/anti* conformer. This signal can be used a diagnostic tool to determine the conformation of the squaramide in different solvents. For example, in a 50:50 $CDCl_3$/DMSO-d_6 solution, the chemical shift of **C** now appears at 7.3 ppm, indicating the molecule is locked into an *anti/anti* conformation. Cooling of the sample shows no broadening of the spectrum, confirming a lack of conformational exchange (Figure S18). Binding of **4** to DMSO could explain the observed behaviour (see also Section S4: X-ray), as this would cause compound **4** to adopt an *anti/anti* conformation, allowing hydrogen bonding to the DMSO oxygen

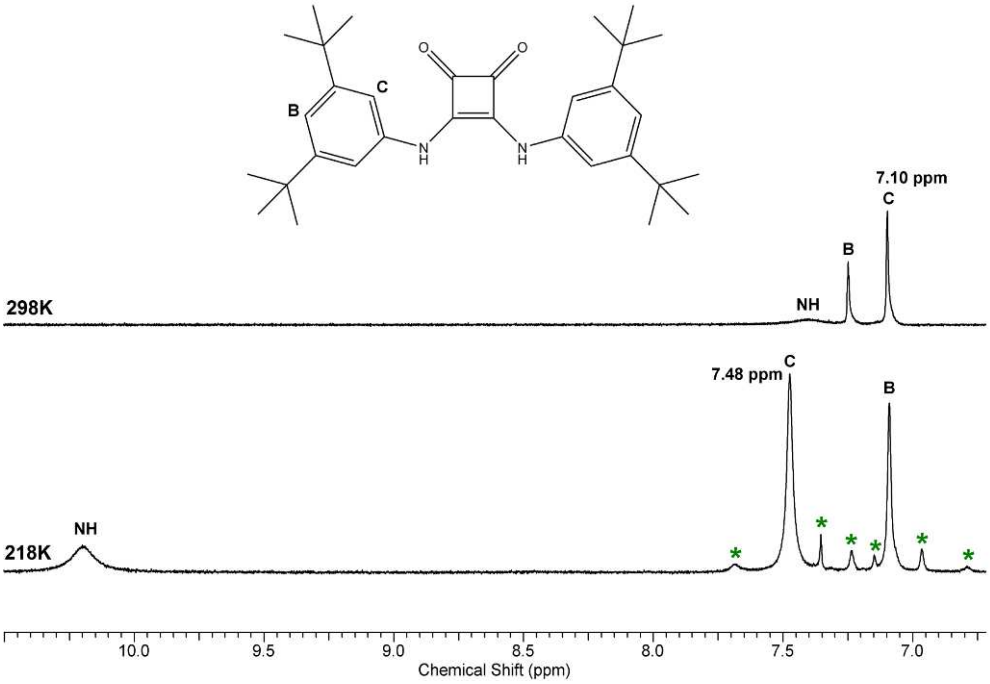

Figure S17: Variable temperature NMR of **4** in CD_2Cl_2.

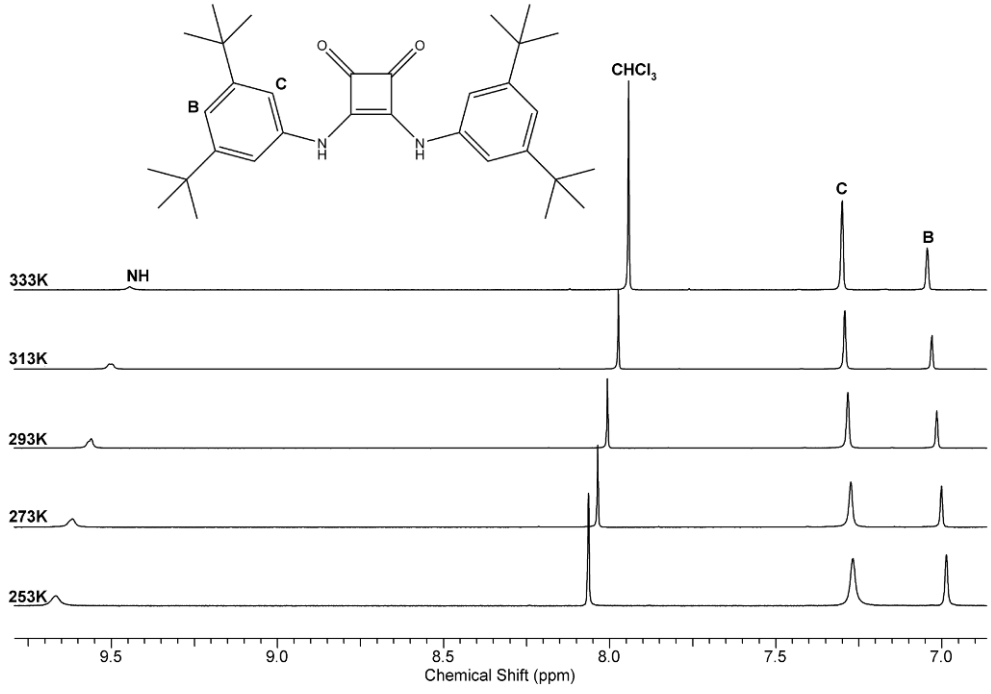

Figure S18: Variable temperature NMR of **4** in 50:50 $CDCl_3$/DMSO-d_6.

In contrast to **4**, the spectrum for **8** in a 50:50 $CDCl_3$/DMSO-d_6 exhibits dynamic behaviour (Figure S19), indicating that **8** is present in both the *anti/anti* and the *anti/syn* conformations.

It appears that substitution with sulfur has an effect on the *anti/anti* and *anti/syn* conformation equilibrium and also the barrier for C-N bond rotation. But at low temperature, the molecule adopts the *anti/anti* conformation as indicated by the symmetric nature of the pattern and the chemical shift of **C** (7.39 ppm).

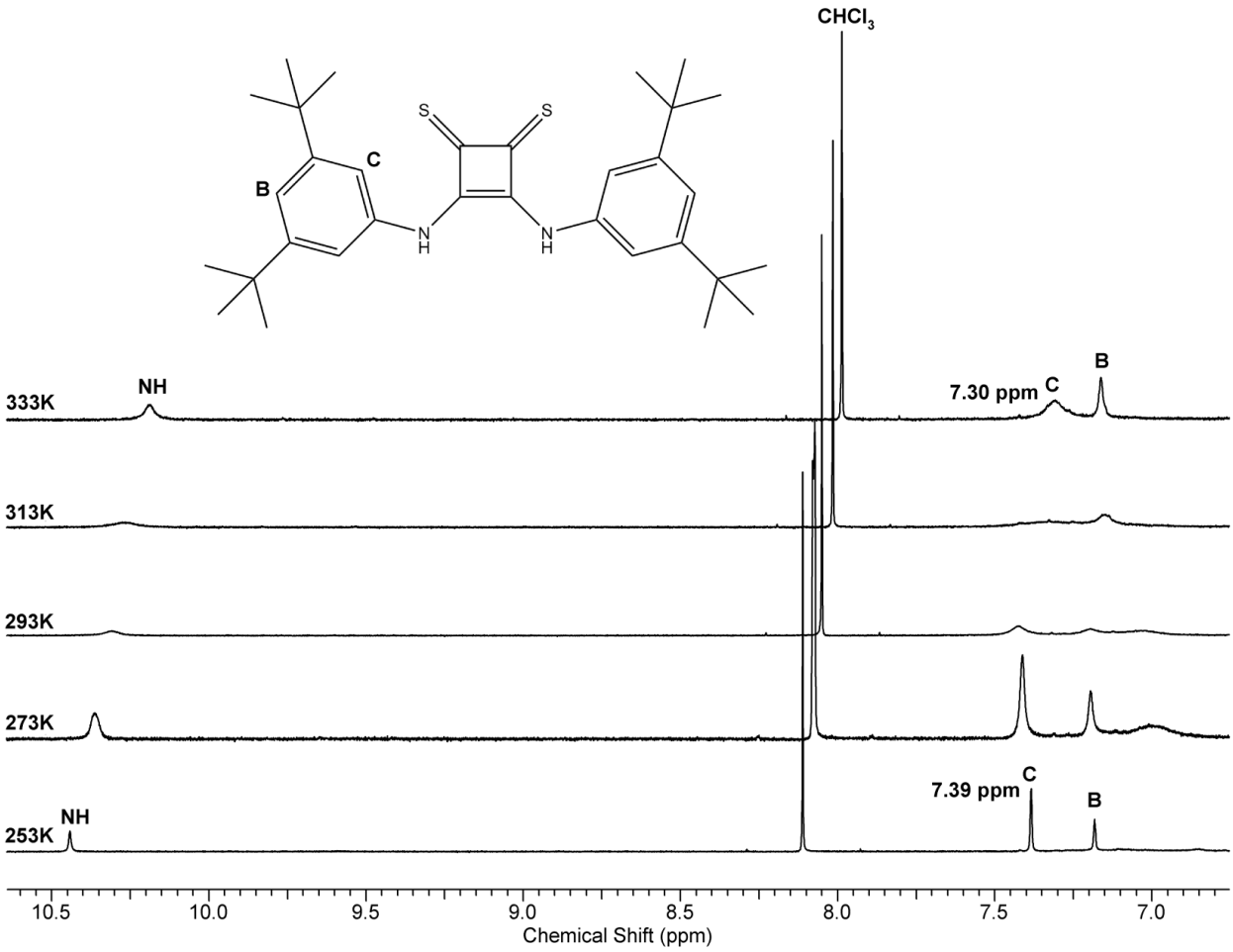

Figure S19: Variable temperature NMR of **8** in 50:50 $CDCl_3$/DMSO-d_6.

S4. Single crystal X-ray diffraction

Data were collected on various diffractometers (details below). Graphics are generated using ORTEP-III, MERCURY 3.0 or ViewerLite and Pov-Ray. In all cases the non-hydrogen atoms are refined anisotropically till convergence. Hydrogen atoms were stereochemically fixed at idealized positions and then refined isotropically. Hydrogen bonds are calculated using MERCURY 3.0. Structures were deposited with the Cambridge Crystallographic Database Centre (CCDC).

CCDC 1005458:

A single crystal was mounted on MiTeGen and the data was subsequently collected on a Rigaku AFC12 goniometer equipped with an enhanced sensitivity (HG) Saturn724+ detector mounted at the window of an FR-E+ SuperBright molybdenum rotating anode generator with HF Varimax optics (100 µm focus) operating at 100 K. Cell determination, Data collection, Data reduction, cell refinement and absorption correction were performed using CrystalClear-SM Expert 2.0 r7 (Rigaku, 2011). The structure was solved with SHELXS97 (G. M. Sheldrick, Acta Cryst. (1990) A**46** 467–473) and further refined with SHELXL97 (G. M. Sheldrick (1997), University of Göttingen, Germany).

CCDC 1005459:

An arbitrary sphere of data was collected on a Bruker Kappa X8-APEX-II diffractometer operating at 120 K using a combination of ω-and φ-scans of 0.5°. Data were corrected for absorption and polarization effects and analyzed for space group determination using SADABS (Sheldrick, 2013). The structure was solved with SHELXT-2014/2 and further refined with SHELXL-2013. All non-hydrogen atoms were refined with anisotropic thermal displacement parameters. Unless otherwise noted, hydrogen atoms were included in calculated positions. Thermal parameters for the hydrogens were tied to the isotropic thermal parameter of the atom to which they are bonded (1.5 × for methyl, 1.2 × for all others).

CCDC 1005460-1005461:

Crystal were attached with Exxon Paratone N, to a short length of fibre supported on a thin piece of copper wire inserted in a copper mounting pin. The crystal was quenched in a cold nitrogen gas stream from an Oxford Cryosystems Cryostream. A SuperNova Dual equipped

with an Atlas detector and employing mirror monochromated Cu (Kα) radiation from a micro-source was used for the data collection cell constants were obtained from a least squares refinement against 12339 reflections located between 8.85 and 152.00º 2θ. Data was collected at 150 K with ω scans to 152.94º 2θ. The data processing was undertaken with CrysAlis Pro (CrysAlisPro Version 1.171.36.28. Agilent Technologies, 2013) and subsequent computations were carried out with WinGX (WinGX, Farrugia, L. J. (1999) J. Appl. Cryst., 32, 837-838) and ShelXle (ShelXle: graphical user interface for SHELXL; C. B. Hübschle, G. M. Sheldrick and B. Dittrich. J. Appl. Cryst. (2011). 44, 1281-1284). A multi-scan absorption correction was applied[1] to the data. The structure was solved with SHELXS97 (G. M. Sheldrick, Acta Cryst. (1990) A**46** 467–473) and further refined with SHELXL97 (G. M. Sheldrick (1997), University of Göttingen, Germany).

S4.1. Crystal structure of 4 with DMSO (CCDC 1005459)

Single crystals suitable for X-ray diffraction were obtained by slow evaporation of an 95:5 $CHCl_3$:DMSO solution of compound **4**. Crystal data for (**4**·DMSO). $C_{34}H_{50}N_2O_3S$, M_r = 566.82 g/mol, crystal size = 0.165 x 0.129 x 0.082 mm³, colourless tablet, triclinic, space group *P-1*, a = 11.0175(6) Å, b = 12.8086(7) Å, c = 12.9025(7) Å, α = 91.871(2) º, β = 113.774(2) º, γ = 96.730(2) º, V = 1648.39(16) Å^3, Z = 2, ρ_c = 1.142 g cm^{-3}, μ = 0.132 mm^{-1}, radiation and wavelength = MoK\a (0.71073), T = 120(2) K, θ_{max} = 28.467, reflections collected: 33121, independent reflections: 8308 (R_{int} = 0.0530), 375 parameters, R indices (all data): R_1 = 0.0840, wR_2 = 0.1109, final R indices [$I > 2\sigma I$]: R_1 = 0.0460, wR_2 = 0.0965, *GOOF* = 1.015, largest diff. peak and hole = 0.332 and -0.380 e Å³.

Table S1. Hydrogen bond properties for (**4**·DMSO) calculated using *Mercury 3.0*.

Donor--H···Acceptor	**H···A (Å)**	**D···A (Å)**	**D-H···A (°)**
N1--H1···O3	2.018	2.860	159.73
N2--H2···O3	1.928	2.797	169.23
C10--H10···O3	3.325	3.932	123.66
C20--H20···O3	3.124	3.769	126.72

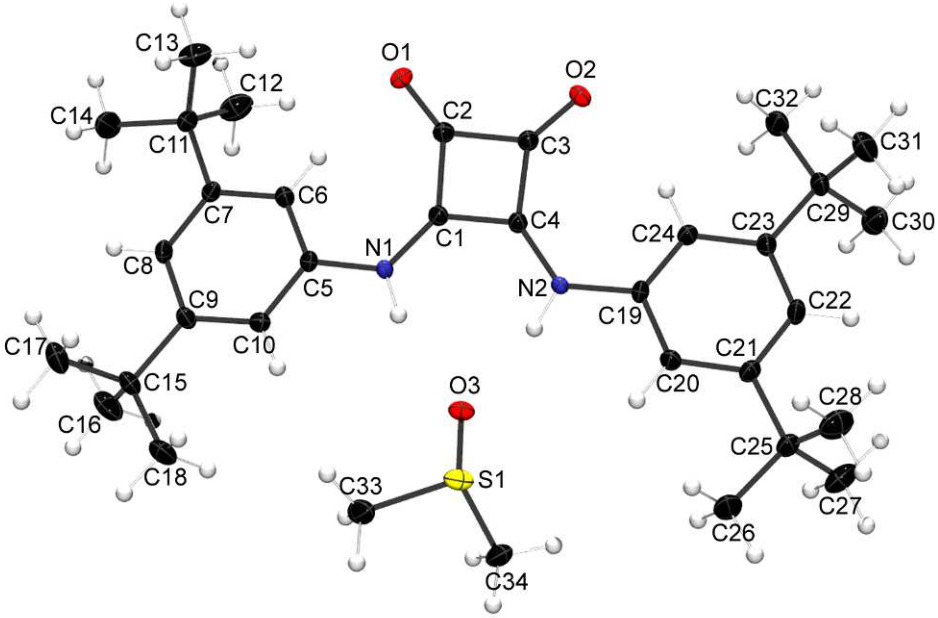

Figure S20: ORTEP diagram of (**4**·DMSO) with atom numbering, showing 50% probability factor for the thermal ellipsoids.

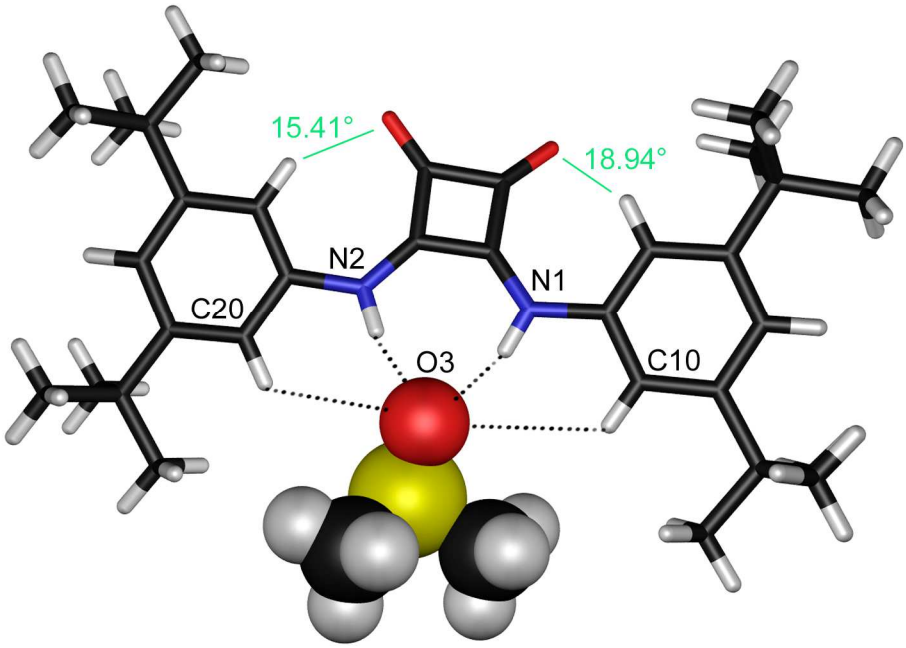

Figure S21: Schematic representation of the intermolecular hydrogen bonds in the crystal of (**4**·DMSO). For clarity, only atoms involved in hydrogen bonding are labelled. Hydrogen bonds are represented by dashed lines. Torsion angles between the planes defined by the cyclobutene ring and the aromatic substituents are shown in turquoise (calculated using *Mercury 3.0*).

S4.2. Crystal structure of 5 with DMSO (CCDC 1005460)

Single crystals suitable for X-ray diffraction were obtained by recrystallization from a concentrated DMSO solution of compound **5**. Crystal data for (**5**·DMSO). $C_{18}H_{18}N_2OS_3$, M_r = 374.52 g/mol, crystal size = 0.117 x 0.080 x 0.068 mm³, yellow prism, monoclinic, space group *P21/n*, a = 8.0488(1) Å, b = 11.6233(1) Å, c = 19.2104(1) Å, α = 90 º, β = 90.883(1) º, γ = 90 º, V = 1796.99(3) Å^3, Z = 4, ρ_c = 1.384 g cm^{-3}, μ = 3.826 mm^{-1}, radiation and wavelength = CuK\a (1.5418), T = 150.01(10) K, θ_{max} = 76.402, reflections collected: 40089, independent reflections: 3762 (R_{int} = 0.0260), 228 parameters, R indices (all data): R_1 = 0.0315, wR_2 = 0.1199, final R indices [$I > 2\sigma I$]: R_1 = 0.0296, wR_2 = 0.1166, *GOOF* = 1.098, largest diff. peak and hole = 0.513 and -0.385 e Å³.

Table S2. Hydrogen bond properties for (**5**·DMSO) calculated using *Mercury 3.0*.

Donor--H···Acceptor	H···A (Å)	D···A (Å)	D-H···A (°)
N5--H5N···O24	2.084	2.815	166.01
N6--H6N···O24	2.023	2.774	170.22
C12--H12···O24	3.233	3.850	124.44
C16--H16···O24	3.260	3.814	119.16

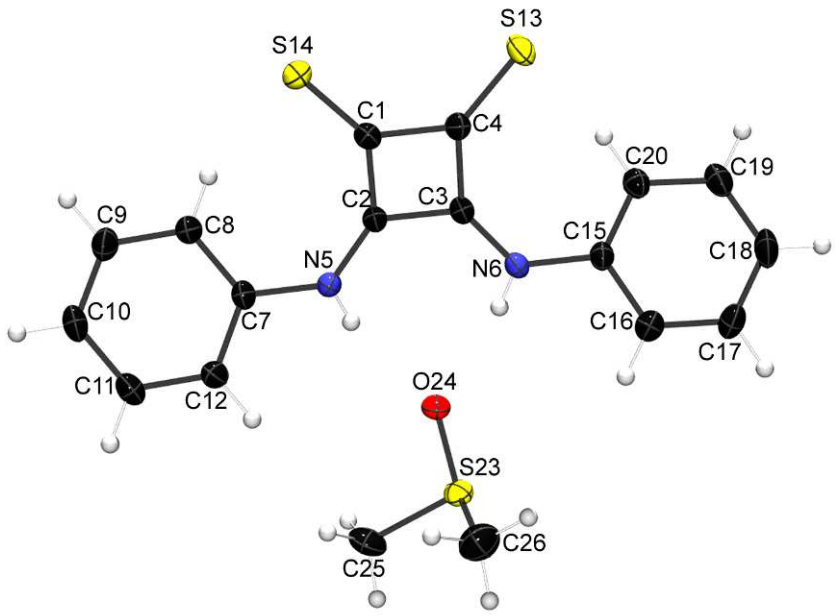

Figure S22: ORTEP diagram of (**5**·DMSO) with atom numbering, showing 50% probability factor for the thermal ellipsoids.

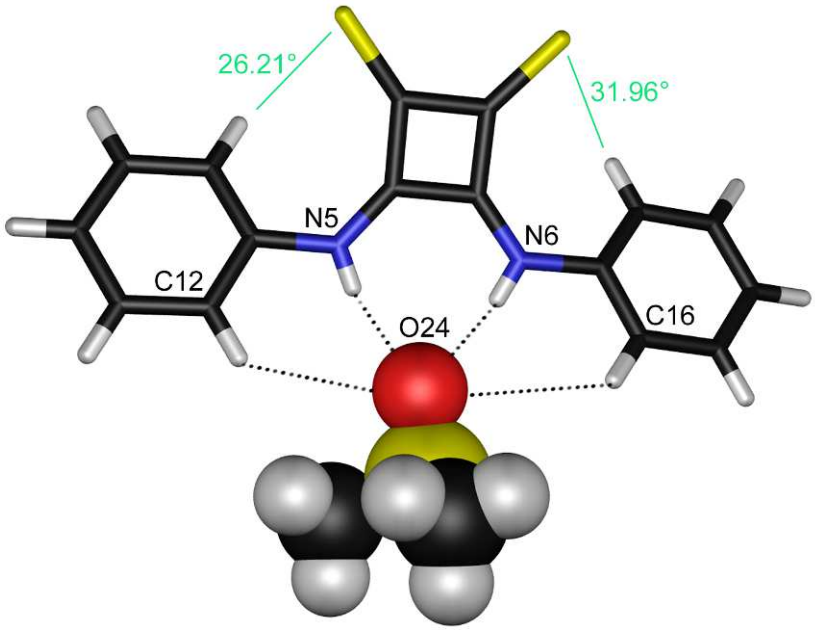

Figure S23: Schematic representation of the intermolecular hydrogen bonds in the crystal of (**5**·DMSO). For clarity, only atoms involved in hydrogen bonding are labelled. Hydrogen bonds are represented by dashed lines. Torsion angles between the planes defined by the cyclobutene ring and the aromatic substituents are shown in turquoise (calculated using *Mercury 3.0*).

S4.3. Crystal structure of 8 with DMSO (CCDC 1005461)

Single crystals suitable for X-ray diffraction were obtained by recrystallization from a concentrated DMSO solution of compound **8**. Crystal data for (**8**·DMSO). $C_{36}H_{56}N_2O_2S_4$, M_r = 677.11 g/mol, crystal size = 0.21 x 0.12 x 0.07 mm³, orange prism, monoclinic, space group *P21/c*, *a* = 18.2073(6) Å, *b* = 11.9379(2) Å, *c* = 19.5492(6) Å, α = 90 °, β = 115.355(4) °, γ = 90 °, *V* = 3839.8(2) Å^3, *Z* = 4, ρ_c = 1.171 g cm^{-3}, μ = 2.511 mm^{-1}, radiation and wavelength = CuK\a (1.54184), *T* = 150(2) K, θ_{max} = 76.470, reflections collected: 60156, independent reflections: 8007 (R_{int} = 0.0871), 391 parameters, *R* indices (all data): R_1 = 0.1040, wR_2 = 0.2305, final *R* indices [$I > 2\sigma I$]: R_1 = 0.0742, wR_2 = 0.2098, *GOOF* = 1.110, largest diff. peak and hole = 0.661 and -0.440 e Å³. Disorder is present in some of the *tert*-butyl groups, which were modelled by splitting it over two parts and keeping the disordered carbon atoms isotropically.

Table S3. Hydrogen bond properties for (**8**·DMSO) calculated using *Mercury 3.0*.

Donor--H···Acceptor	H···A (Å)	D···A (Å)	D-H···A (°)
N1--H101···O3	1.881	2.755	160.55
N2--H102···O3	1.872	2.776	164.12
C10--H10···O3	3.503	3.931	110.78
C16--H16···O3	3.272	3.800	118.22

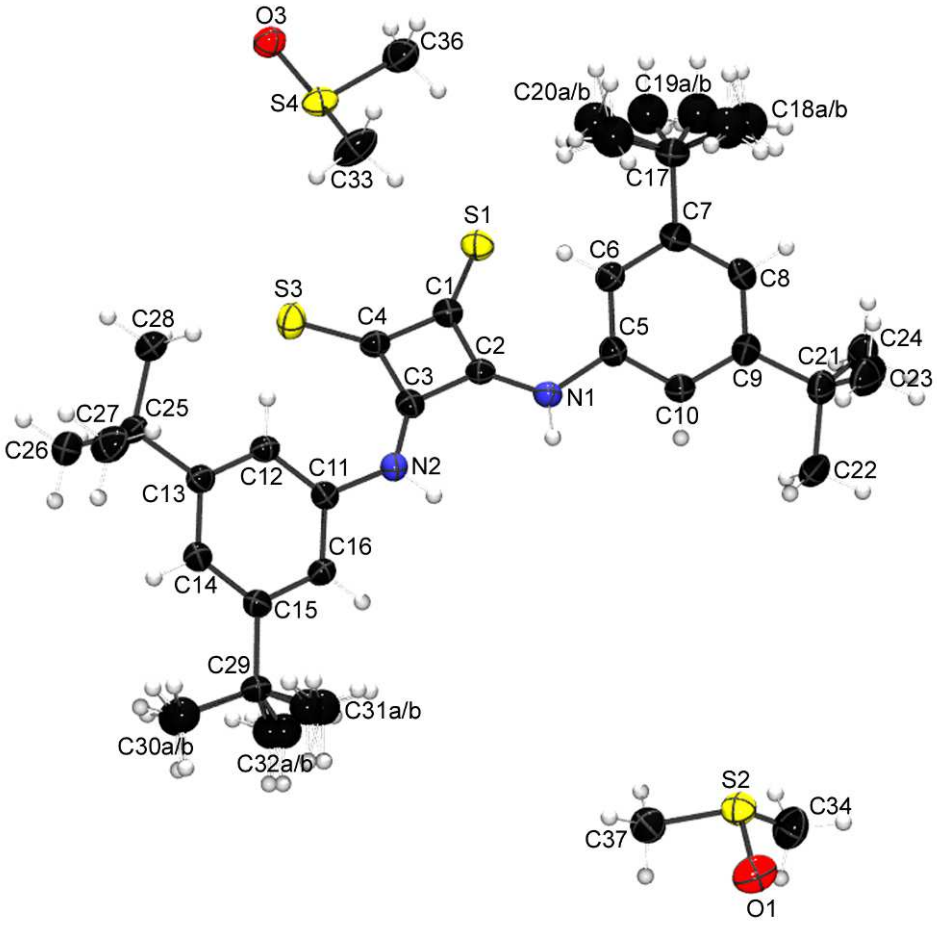

Figure S24: ORTEP diagram of (**8**·DMSO) with atom numbering, showing 50% probability factor for the thermal ellipsoids.

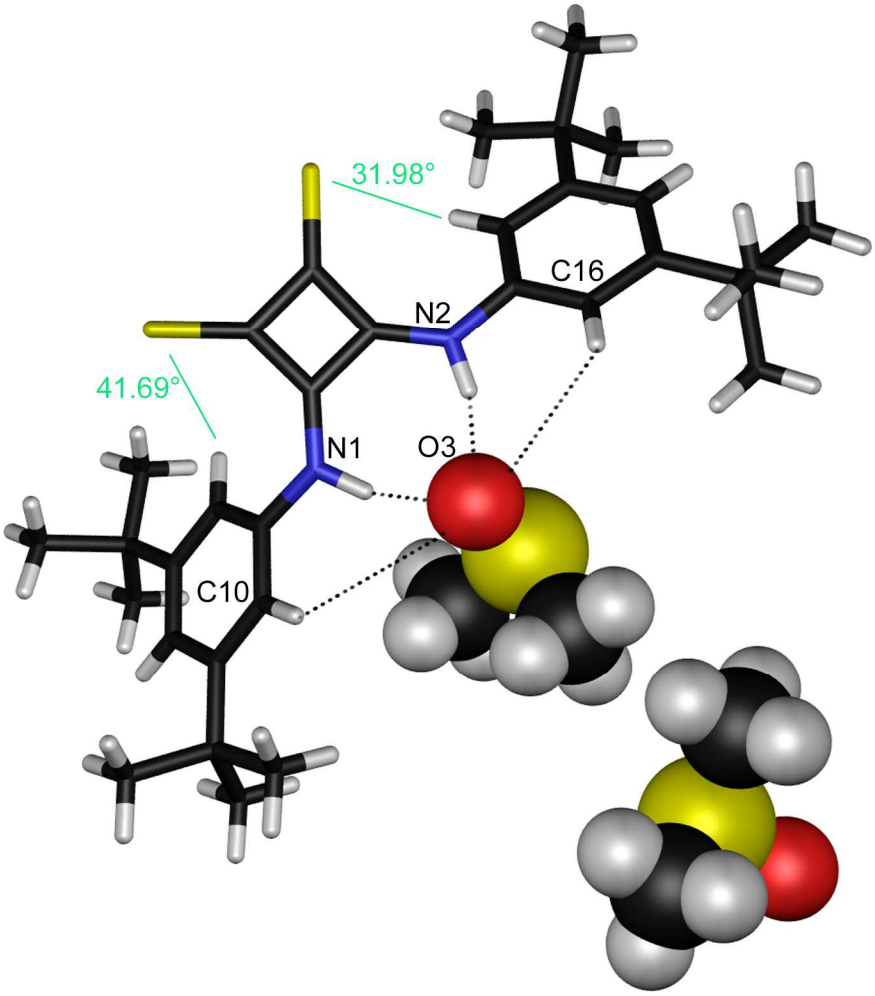

Figure S25: Schematic representation of the intermolecular hydrogen bonds in the crystal of (**8**·DMSO). For clarity, only atoms involved in hydrogen bonding are labelled. Hydrogen bonds are represented by dashed lines. Torsion angles between the planes defined by the cyclobutene ring and the aromatic substituents are shown in turquoise (calculated using *Mercury 3.0*).

S4.4. Crystal structure of 6 with TMACl (CCDC 1005458)

Single crystals suitable for X-ray diffraction were obtained by slow evaporation of a 1:9 water:acetonitrile solution of compound **6** in the presence of excess TMACl (~5 equivalents). Crystal data for $[(\mathbf{6})_2 \cdot Cl][TMA]^+$. $C_{40}H_{32}F_{12}N_5S_4Cl$, M_r = 974.40 g/mol, crystal size = 0.07 x 0.02 x 0.01 mm³, orange block, triclinic, space group *P-1*, a = 8.0301(5) Å, b = 16.9861(11) Å, c = 17.5950(11) Å, α = 64.243(4) °, β = 80.825(6) °, γ = 77.765(5) °, V = 2106.2(2) Å^3, Z = 2, ρ_c = 1.536 g cm^{-3}, μ = 0.380 mm^{-1}, radiation and wavelength = MoK\a (0.71075), T = 100(2) K, θ_{max} = 27.50, reflections collected: 25975, independent reflections: 9528 (R_{int} =

0.0749), 587 parameters, *R* indices (all data): R_1 = 0.1221, wR_2 = 0.1769, final *R* indices [$I > 2\sigma I$]: R_1 = 0.0683, wR_2 = 0.1492, *GOOF* = 1.051, largest diff. peak and hole = 0.708 and -0.597 e Å^3. Rotational disorder was present in the –CF_3 groups, which was modelled by splitting over 2 positions. Geometric restraints (SADI) were applied.

Table S4. Hydrogen bond properties for [(**6**)$_2$·Cl][TMA]$^+$ calculated using *Mercury 3.0*.

Donor--H···Acceptor	H···A (Å)	D···A (Å)	D-H···A (°)
N1--H1···Cl1	2.293	3.163	169.85
N2--H2···Cl1	2.338	3.209	170.80
N3--H3···Cl1	2.323	3.175	162.63
N4--H4···Cl1	2.317	3.183	168.67
C6--H6···Cl1	3.553	4.134	121.90
C15--H15···Cl1	3.525	4.147	125.20
C24--H24···Cl1	3.442	4.023	121.65
C35--H35···Cl1	3.547	4.105	119.99

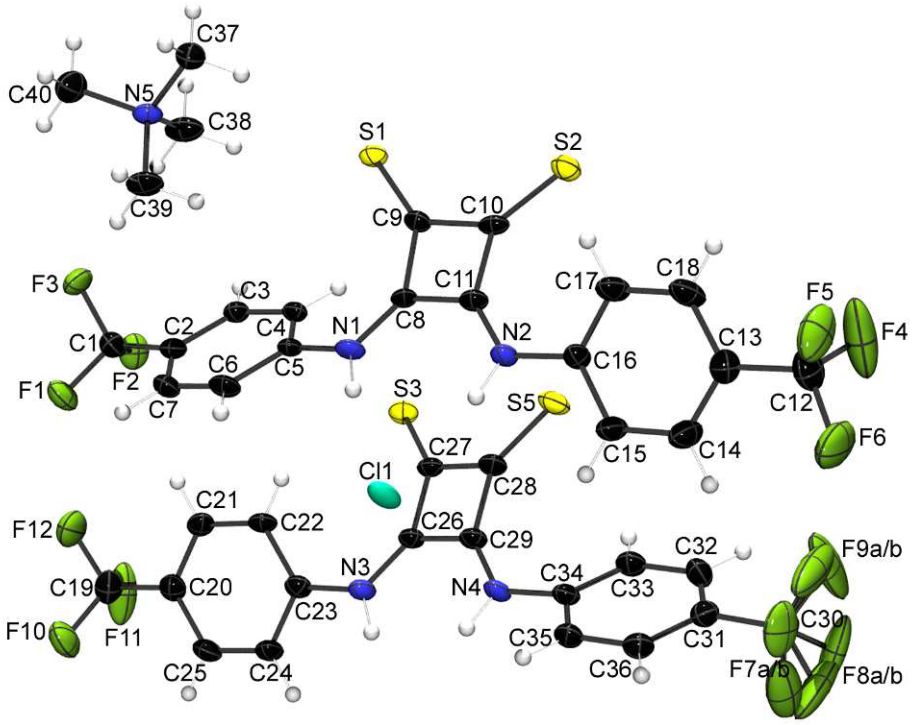

Figure S26: ORTEP diagram of [(**6**)$_2$·Cl][TMA]$^+$ with atom numbering, showing 50% probability factor for the thermal ellipsoids.

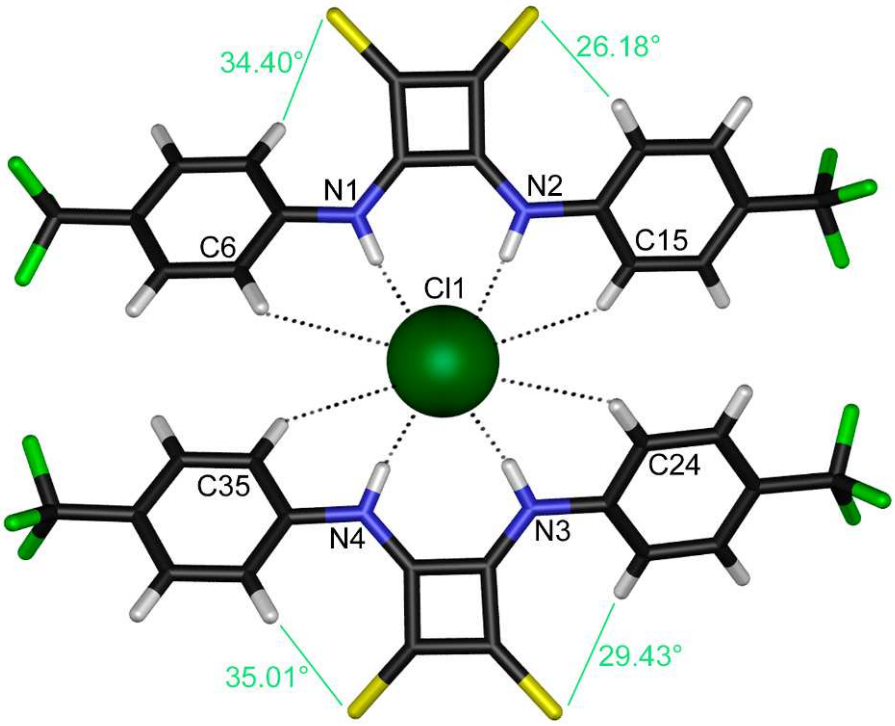

Figure S27: Schematic representation of the intermolecular hydrogen bonds in the crystal of $[(\mathbf{6})_2 \cdot Cl][TMA]^+$. For clarity, only atoms involved in hydrogen bonding are labelled. Hydrogen bonds are represented by dashed lines. Torsion angles between the planes defined by the cyclobutene ring and the aromatic substituents are shown in turquoise (calculated using *Mercury 3.0*).

S5. ^{1}H NMR Chloride Binding Titrations

^{1}H NMR titrations were performed by additions of aliquots of chloride as the tetrabutylammonium (TBA) salt (0.15 – 0.2 M), in a solution of the receptor (2.5×10^{-3} M) in either 0.5% H_2O in DMSO-d_6 or CD_3CN to a 2.5×10^{-3} M solution of the receptor in either 0.5% H_2O in DMSO-d_6 or CD_3CN. Typically, up to 12 equivalents of the anion were added to the solution. Both salt and receptor were dried under high vacuum prior to use. ^{1}H NMR spectra were recorded on a BrukerAvance III 500 spectrometer at a frequency of 500.13 MHz and calibrated to the residual protio solvent peak in DMSO-d_6 (δ = 2.50 ppm) or CD_3CN (δ =

1.94 ppm). Stack plots were made using MestReNova Version 6.0. Where possible and when the change in chemical shift was larger than 0.2 ppm, non-linear curve fitting of the experimentally obtained titration isotherms (equivalents of anion *vs.* chemical shift of the squaramide NH protons or thiosquaramide NH protons) using the commercially available software program HypNMR® (Hyperquad® package) enabled the calculation of association constants (K_a/M^{-1}) using a 1:1 model.

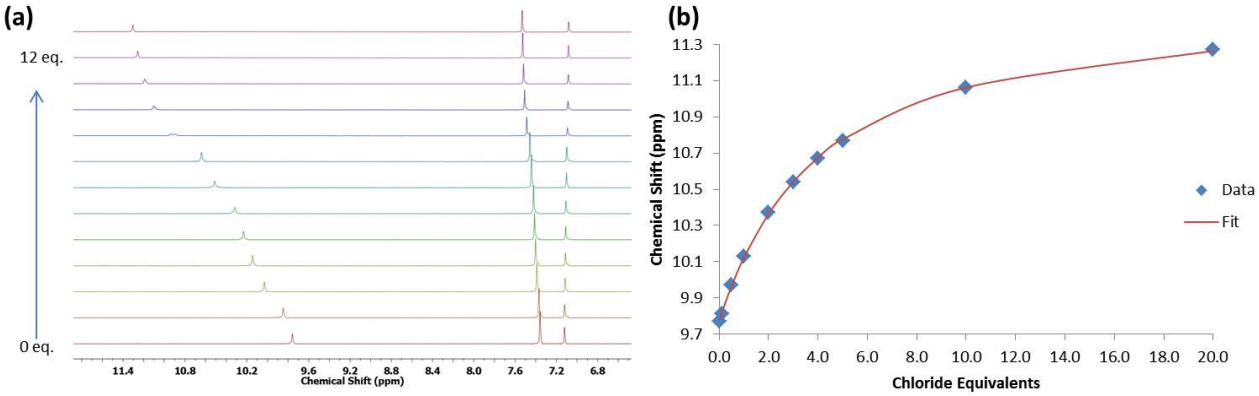

Figure S28: (a): ^{1}H NMR stackplot of **4** with TBACl in 0.5% H_2O in DMSO-d_6 at 300 K. (b): Fitplot for NH proton at δ =9.8 ppm.

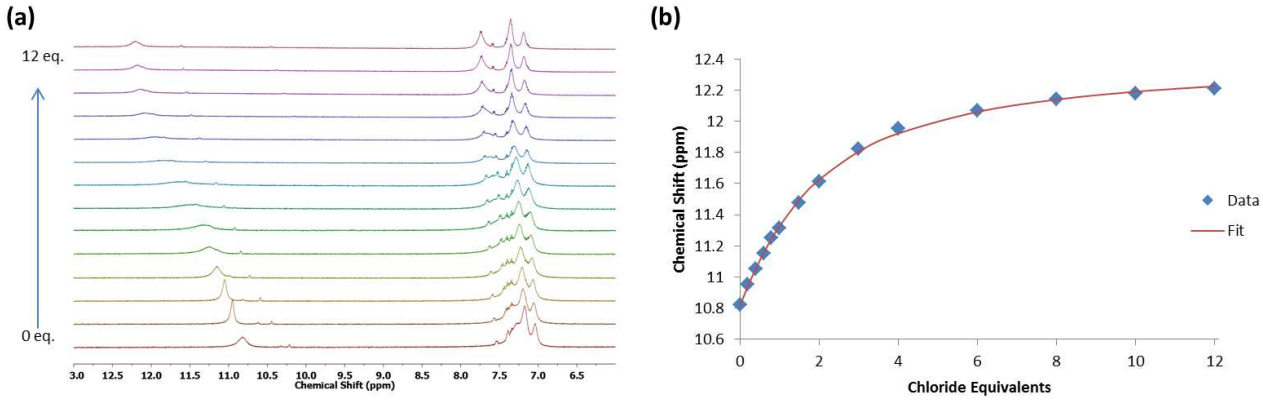

Figure S29: (a): ^{1}H NMR stackplot of **5** with TBACl in 0.5% H_2O in DMSO-d_6 at 300 K. (b): Fitplot for NH proton at δ = 10.8 ppm.

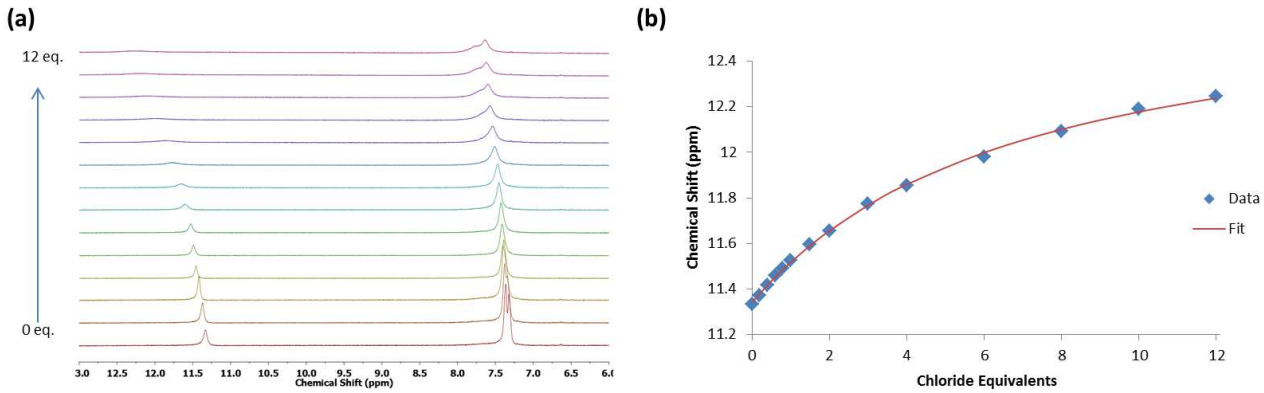

Figure S30: (a): ^{1}H NMR stackplot of **6** with TBACl in 0.5% H_2O in DMSO-d_6 at 300 K. (b): Fitplot for NH proton at δ = 11.3 ppm.

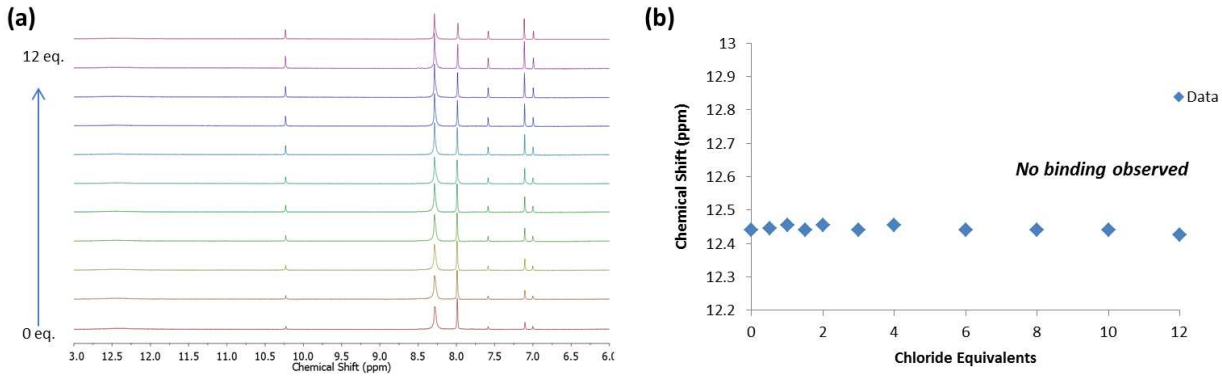

Figure S31: (a): ^{1}H NMR stackplot of **7** with TBACl in 0.5% H_2O in DMSO-d_6 at 300 K. (b): Fitplot for NH proton at δ = 12.5 ppm.

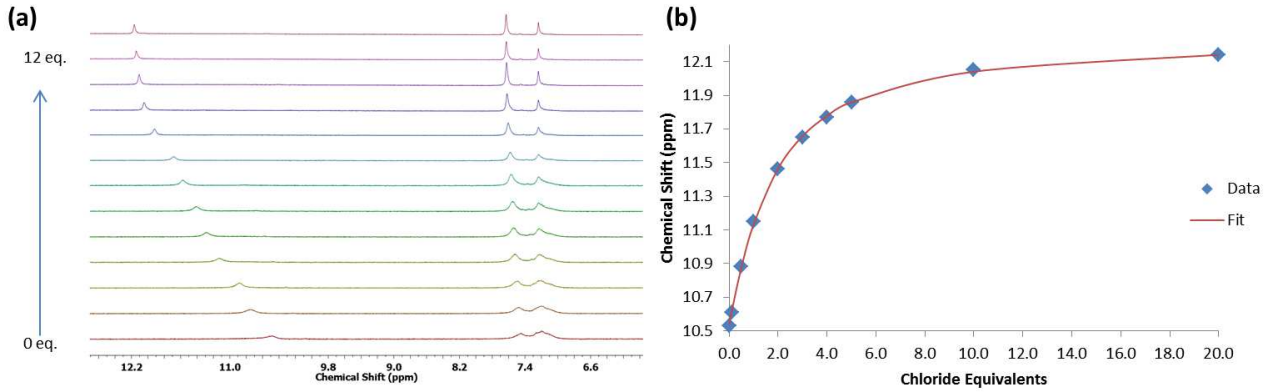

Figure S32: (a): ^{1}H NMR stackplot of **8** with TBACl in 0.5% H_2O in DMSO-d_6 at 300 K. (b): Fitplot for NH proton at δ = 10.5 ppm.

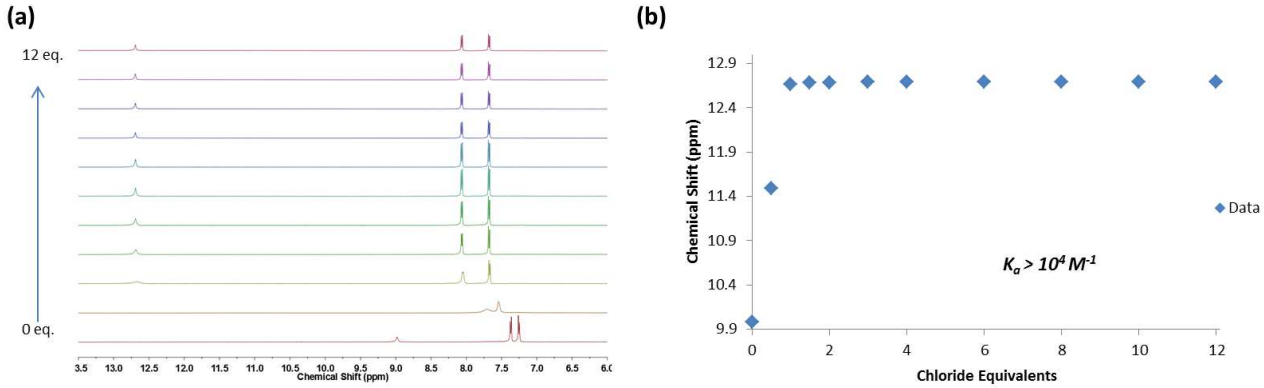

Figure S33: (a): ^{1}H NMR stackplot of **6** with TBACl in CD_3CN at 300 K. (b): Fitplot for NH proton at δ = 9.98 ppm.

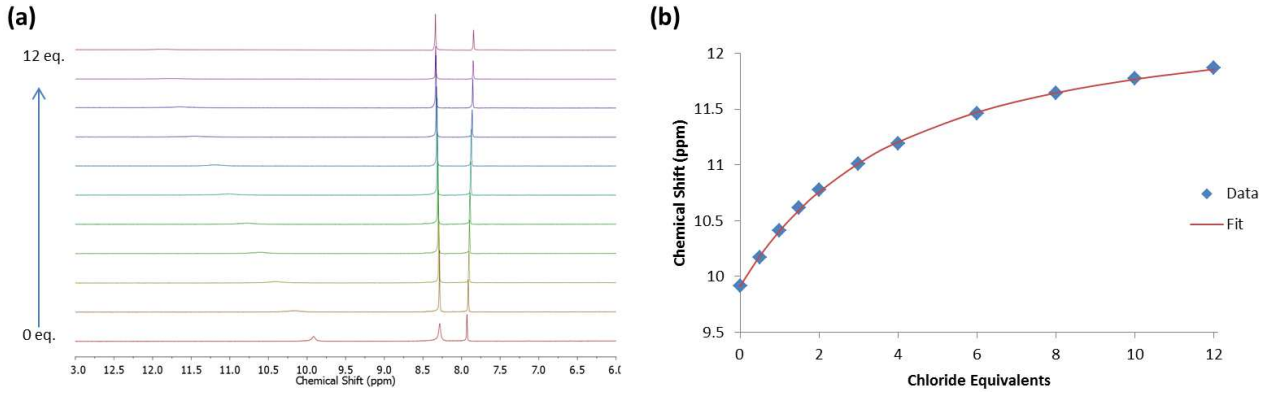

Figure S34: (a): ^{1}H NMR stackplot of **7** with TBACl in CD_3CN at 300 K. (b): Fitplot for NH proton at δ = 9.91 ppm.

S6. Determination of pK_a values

pK_a values were experimentally determined using the wavelength of maximum difference in absorbance between the UV/Vis spectra of the anionic and the neutral species. For each compound the absorbance was measured on a solution in MeCN/H_2O (9:1) containing 0.1M $TBAPF_6$ with pH values between 2.5 and 14. The solutions were adjusted to acidic pH using an excess of HNO_3 before being slowly basified by small aliquots of an aqueous 0.1 M NaOH solution. The absorbance values at the wavelength of maximal difference were plotted against the pH values. A four parameter sigmoid curve using Sigma Plot (Systat Software Inc., Chicago, IL, USA) was fitted through the data points with the point of inflexion corresponding to the pK_a value.

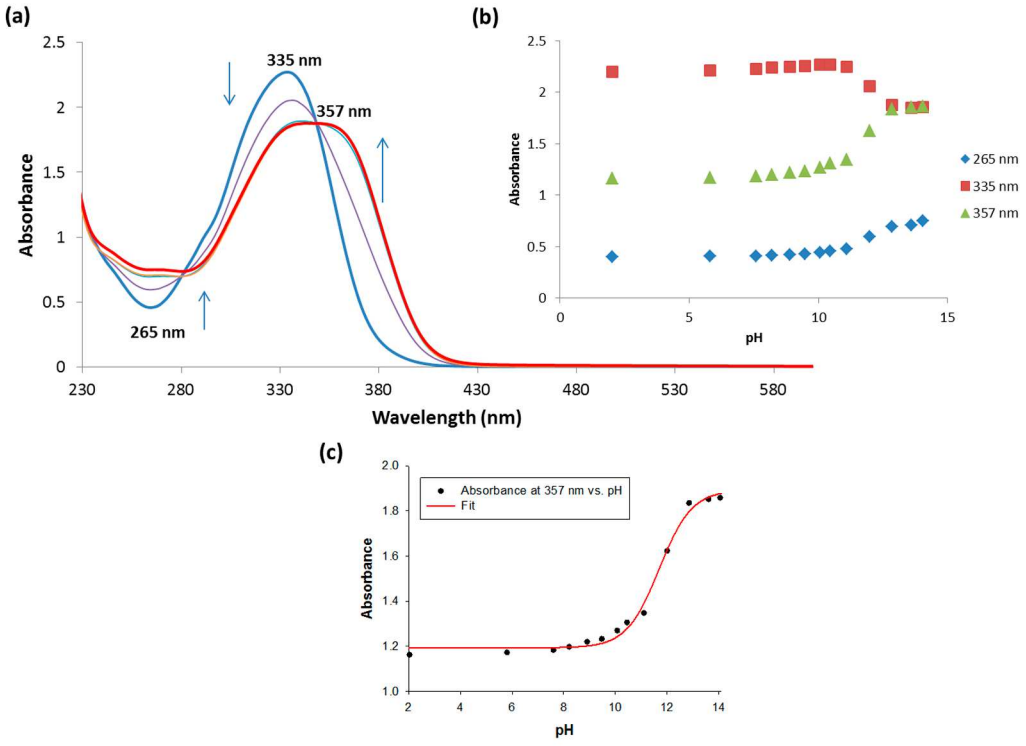

Figure S35: (a) Absorption spectra taken over the course of a pH-spectrophotometric titration of **1** (8×10^{-5} M) in an acetonitrile/water mixture (9/1 v/v; 0.1 M in $TBAPF_6$). (b) Comparison plots of absorbance at 265 nm (♦), 335 nm (■) and 357 nm (▲) vs. pH.(c) Four parameter sigmoid curve fit with the point of inflexion corresponding to the pK_a value.

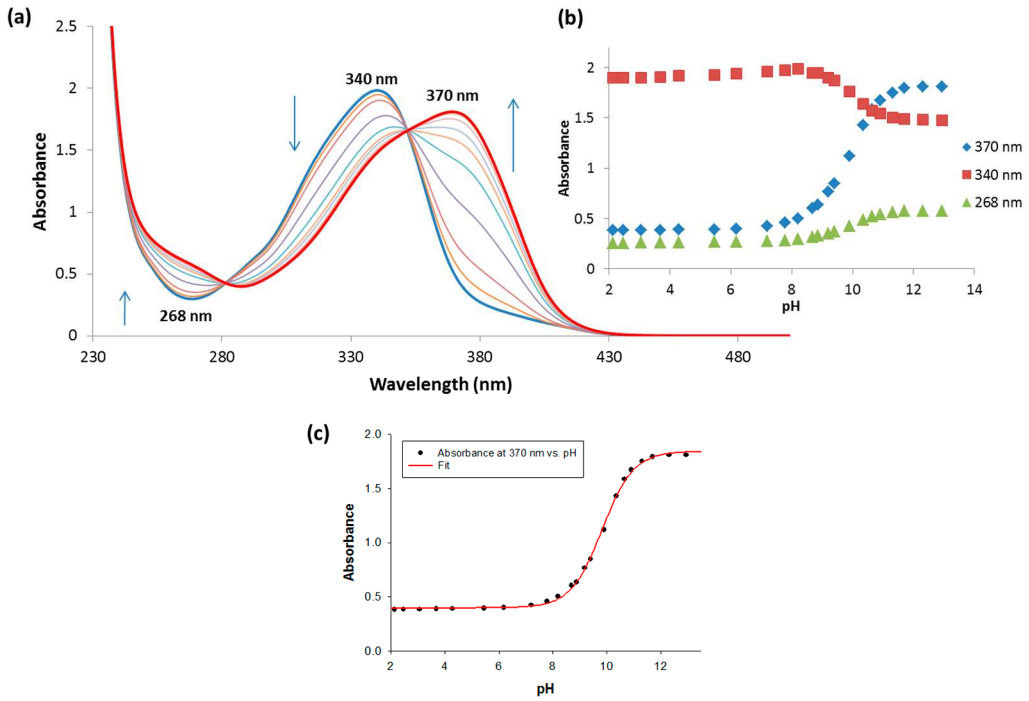

Figure S36: (a) Absorption spectra taken over the course of a pH-spectrophotometric titration of **2** (6×10^{-5} M) in an acetonitrile/water mixture (9/1 v/v; 0.1 M in $TBAPF_6$). (b) Comparison plots of absorbance at 268 nm (▲), 340nm (■) and 370 nm (♦) vs. pH.(c) Four parameter sigmoid curve fit with the point of inflexion corresponding to the pK_a value.

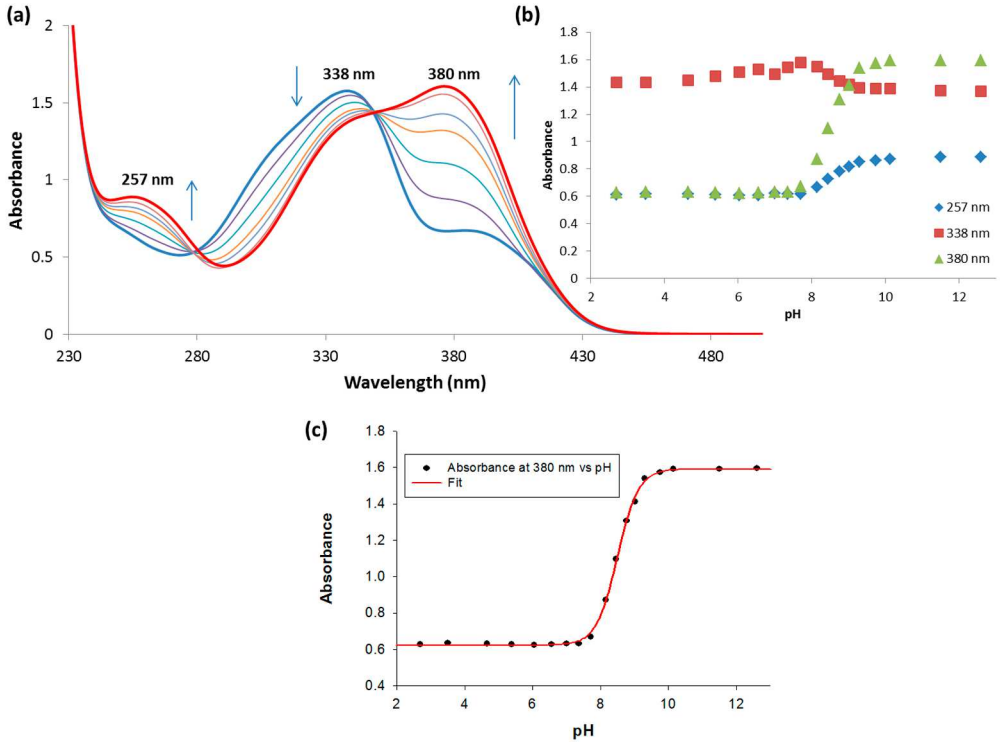

Figure S37: (a) Absorption spectra taken over the course of a pH-spectrophotometric titration of **3** (6×10^{-5} M) in an acetonitrile/water mixture (9/1 v/v; 0.1 M in $TBAPF_6$). (b) Comparison plots of absorbance at 257 nm (♦), 338nm (■) and 380 nm (▲) vs. pH.(c) Four parameter sigmoid curve fit with the point of inflexion corresponding to the pK_a value.

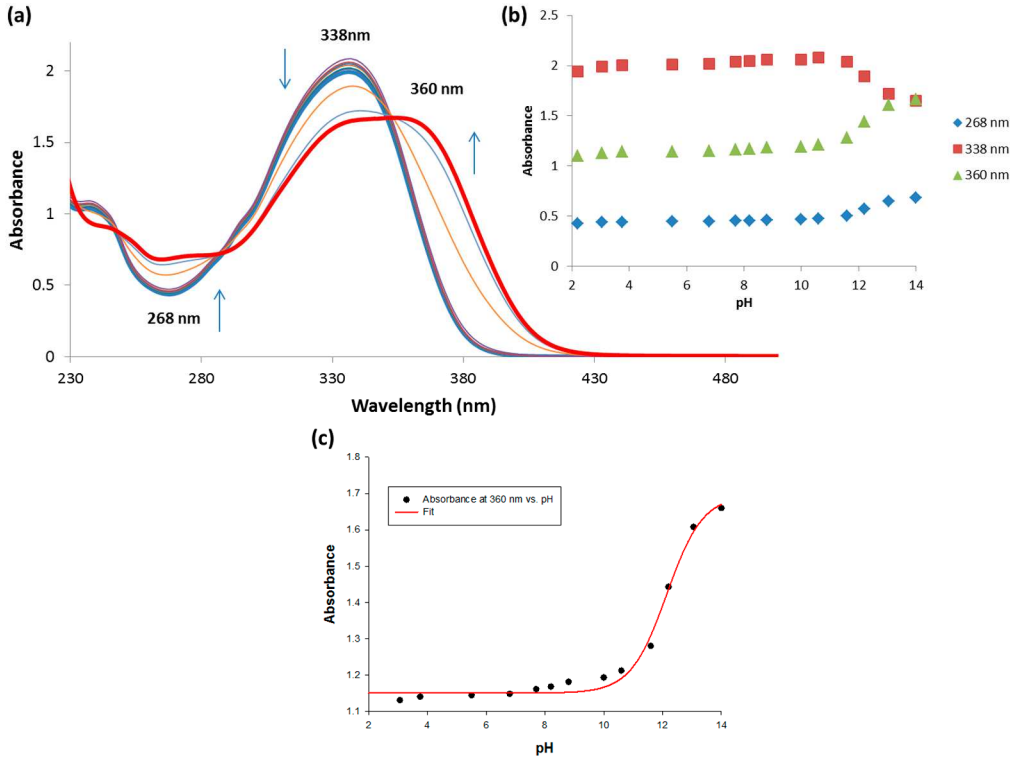

Figure S38: (a) Absorption spectra taken over the course of a pH-spectrophotometric titration of **4** (6×10^{-5} M) in an acetonitrile/water mixture (9/1 v/v; 0.1 M in $TBAPF_6$). (b) Comparison plots of absorbance at 268 nm (♦), 338nm (■) and 360 nm (▲) vs. pH.(c) Four parameter sigmoid curve fit with the point of inflexion corresponding to the pK_a value.

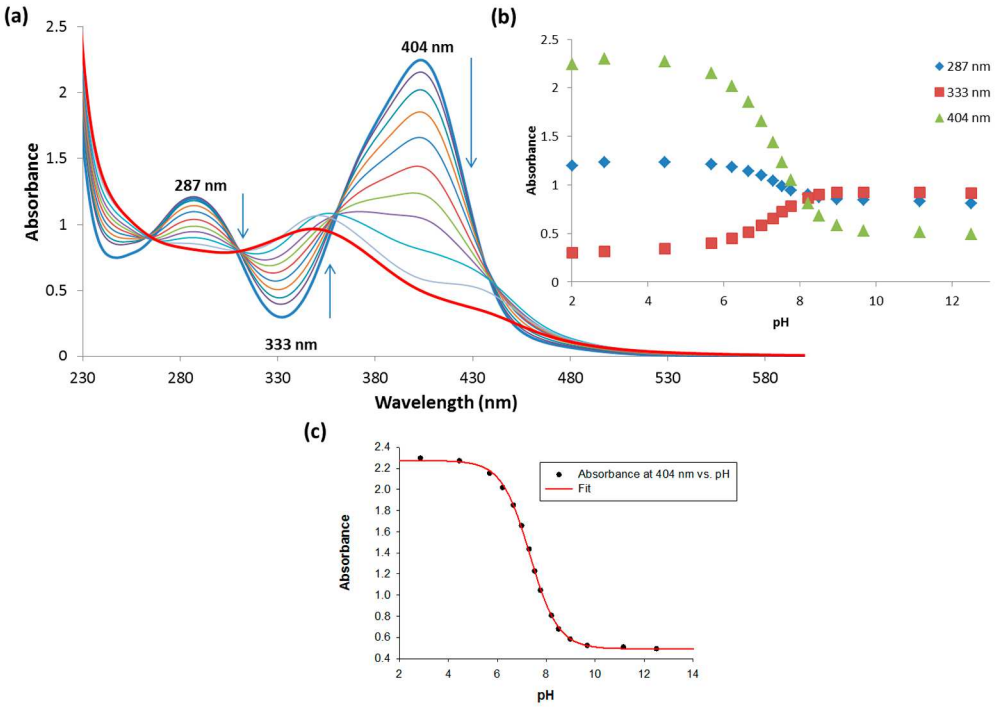

Figure S39: (a) Absorption spectra taken over the course of a pH-spectrophotometric titration of **5** (6×10^{-5} M) in an acetonitrile/water mixture (9/1 v/v; 0.1 M in $TBAPF_6$). (b) Comparison plots of absorbance at 287 nm (♦), 333nm (■) and 404 nm (▲) vs. pH.(c) Four parameter sigmoid curve fit with the point of inflexion corresponding to the pK_a value.

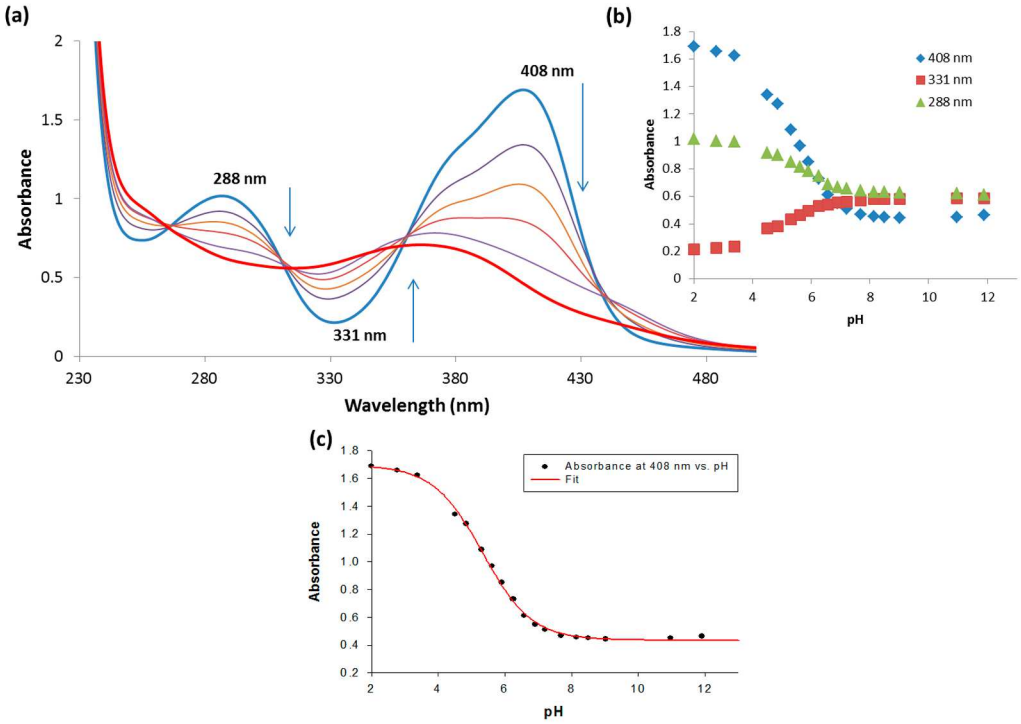

Figure S40: (a) Absorption spectra taken over the course of a pH-spectrophotometric titration of **6** (5×10^{-5} M) in an acetonitrile/water mixture (9/1 v/v; 0.1 M in $TBAPF_6$). (b) Comparison plots of absorbance at 288 nm (▲), 331nm (■) and 408 nm (♦) vs. pH.(c) Four parameter sigmoid curve fit with the point of inflexion corresponding to the pK_a value.

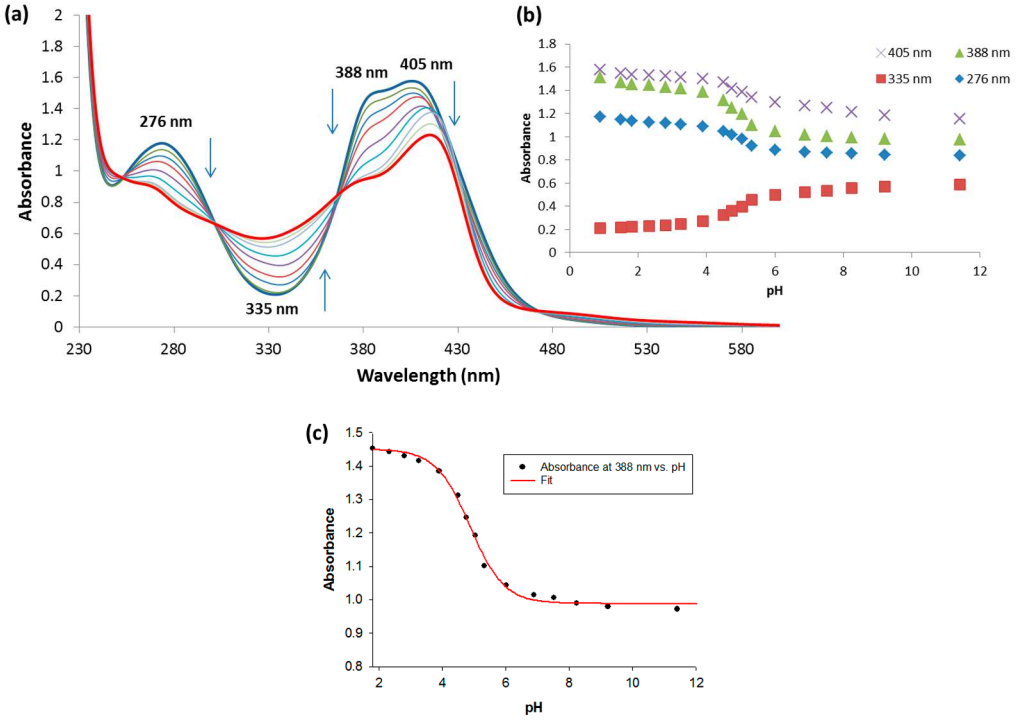

Figure S41: (a) Absorption spectra taken over the course of a pH-spectrophotometric titration of **7** (6×10^{-5} M) in an acetonitrile/water mixture (9/1 v/v; 0.1 M in $TBAPF_6$). (b) Comparison plots of absorbance at 276 nm (♦), 335 nm (■), 388 nm (▲) and 405 nm (×) vs. pH.(c) Four parameter sigmoid curve fit with the point of inflexion corresponding to the pK_a value.

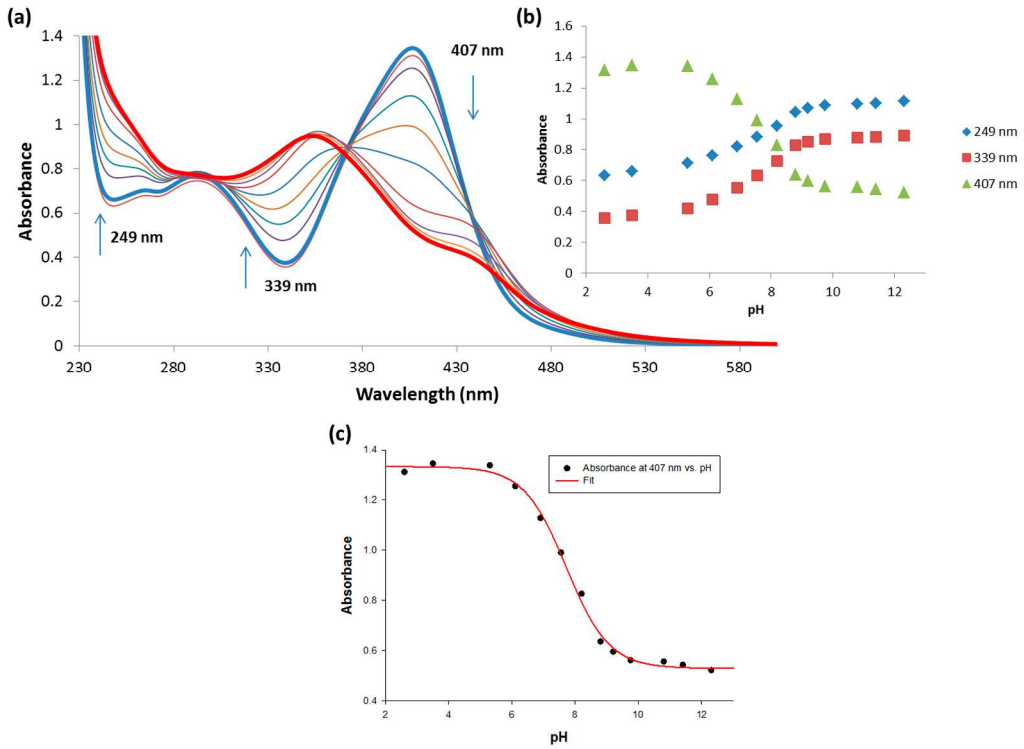

Figure S42: (a) Absorption spectra taken over the course of a pH-spectrophotometric titration of **8** (6×10^{-5} M) in an acetonitrile/water mixture (9/1 v/v; 0.1 M in $TBAPF_6$). (b) Comparison plots of absorbance at 249 nm (♦), 339 nm (■) and 407 nm (▲) vs. pH.(c) Four parameter sigmoid curve fit with the point of inflexion corresponding to the pK_a value.

Computational pK_a values were obtained using density functional theory (DFT) at the M06-2X/6-311+G(3df,2p) level, in conjunction with the SMD continuum solvation model. Two water molecules were included in the model in order to take into account explicit interactions (see Figure S43).

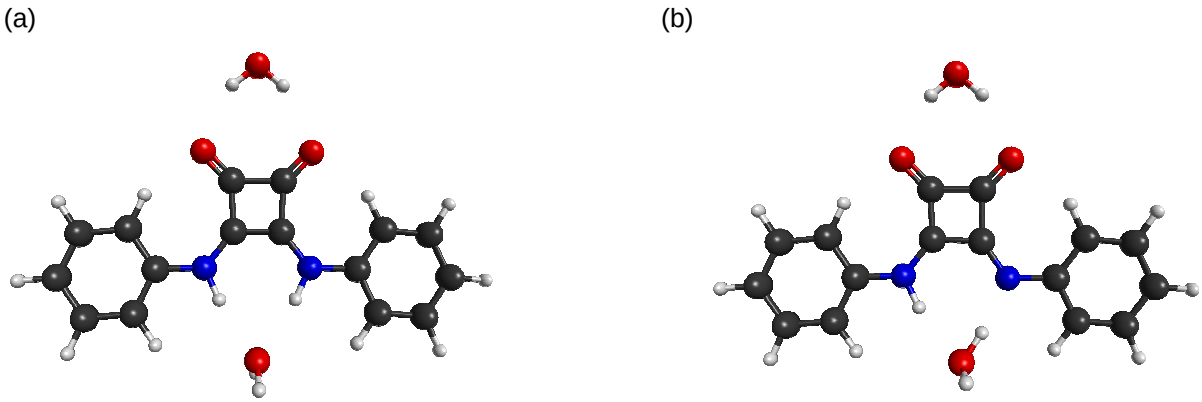

Figure S43: Model system (for **1**, as an example) used in the DFT calculations, (a) neutral **1**•$2H_2O$ and (b) deprotonated **1**•$2H_2O$

S7. Anion transport studies

S7.1. General protocol

This procedure describes a typical membrane transport tests. Internal and external solutions can vary and are detailed in the caption of the figures. Chloride concentrations during transport experiments were determined using an *Accumet* chloride-selective electrode. The electrode was calibrated against sodium chloride solutions of known concentrations prior to each experiment. POPC (1-palmitoyl-2-oleoyl-*sn*-glycero-3-phosphocholine) was supplied by *Genzyme* and was stored at –20°C as a solution in chloroform (1 g POPC in 35 mL chloroform). Cholesterol was supplied by *Sigma-Aldrich*. Octaethylene glycol monododecyl ether was used as detergent and was supplied by *TCI*.

A lipid film of POPC or 7:3 POPC:cholesterol was formed from a chloroform solution under reduced pressure and dried under vacuum for at least 4 hours. The lipid film was rehydrated by vortexing with a metal chloride (MCl) salt solution. The lipid suspension was then subjected to nine freeze-thaw cycles, where the suspension was alternatingly allowed to freeze in a liquid nitrogen bath, followed by thawing in a water bath. The lipid suspension was allowed to age for 30 min at room temperature and was subsequently extruded 25 times through a 200 nm polycarbonate membrane (*Nucleopore*^{TM}) using a LiposoFast-Basic extruder set (*Avestin, Inc*). The resulting unilamellar vesicles were dialyzed (*Spectra/Por® 2* Membrane MWCO 12-14 kD) against the external medium to remove unencapsulated MCl salts. Internal and external solutions vary from experiment to experiment, but in general an ionic strength of 500 mM was used.

S7.2. Chloride/nitrate transport at pH 7.2 and pH 4.0

Unilamellar POPC vesicles containing NaCl, prepared as described in Section S7.1., were suspended in the external medium consisting of $NaNO_3$ solution buffered to pH 7.2 or pH 4.0. The lipid concentration per sample was 1 mM. A DMSO solution of the carrier molecule was added to start the experiment and the chloride efflux was monitored using a chloride sensitive electrode. At 5 min, the vesicles were lysed with 50 μL of octaethylene glycol monododecyl ether (0.232 mM in 7:1 water:DMSO v/v) and a total chloride reading was taken at 7 min. The initial value was set at 0% chloride efflux and the final chloride reading (at 7 minutes) was set as 100% chloride efflux. All other data points were calibrated to these points.

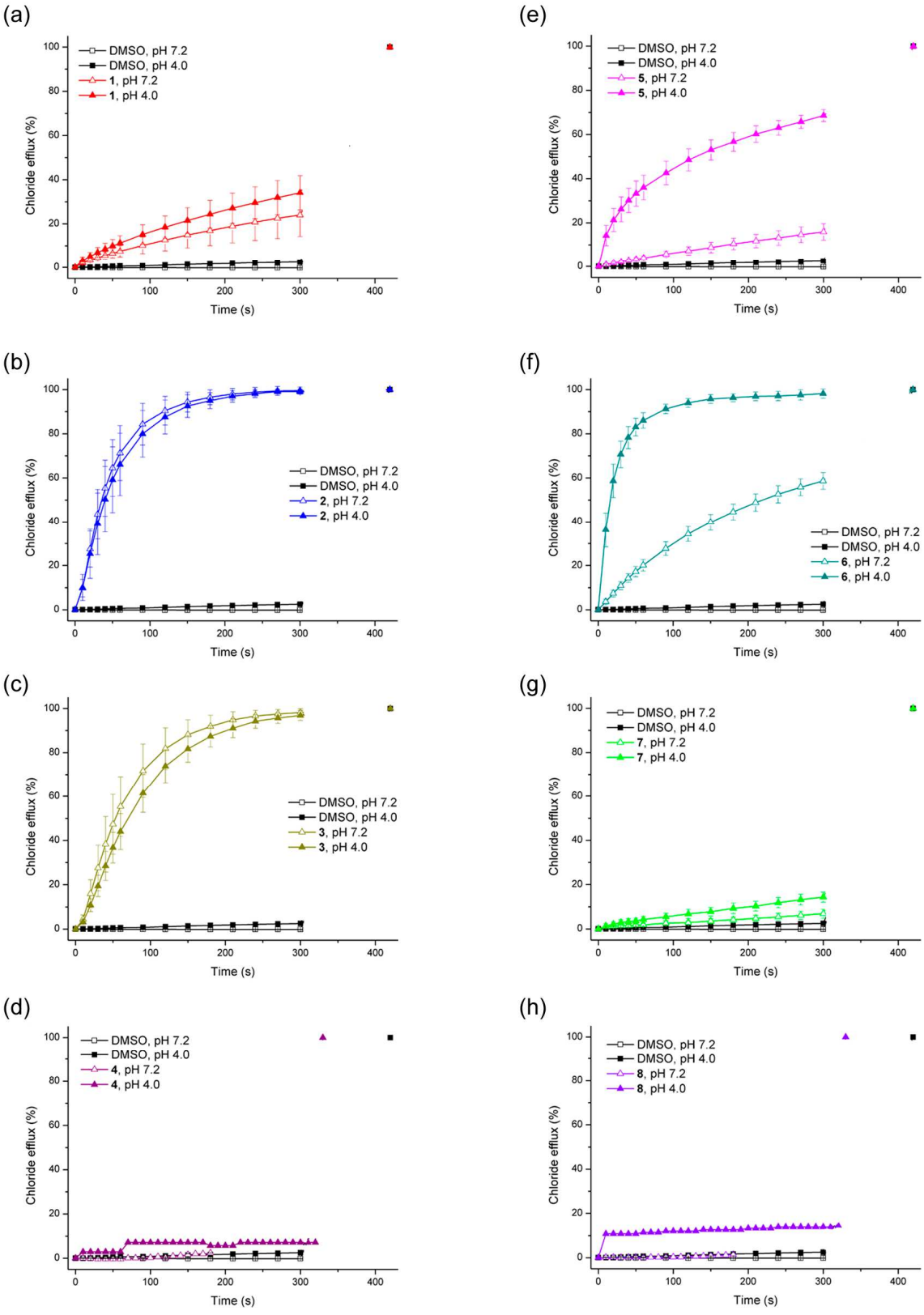

Figure S44: Chloride efflux from POPC vesicles at pH 7.2 (empty symbols) and pH 4.0 (filled symbols). POPC vesicles were loaded with a 489 mM NaCl solution buffered to pH 7.2 with 5 mM phosphate salts or to pH 4.0 with 5 mM citrate salts, and were suspended in a 489 mM $NaNO_3$ solution buffered to pH 7.2 with 5 mM phosphate salts or to pH 4.0 with 5 mM citrate salts. At the end of the experiment (300 s), detergent was added to lyse the vesicles and calibrate the ISE to 100% chloride efflux. Each point represents the average of a minimum of 6 independent trials. DMSO was used as a control. (a) **1**; (b) **2**; (c) **3**; (d) **4**; (e) **5**; (f) **6**; (g) **7**; (h) **8**.

S7.3. Hill plots

During Hill plots the chloride/nitrate transport assays are performed as described above for various concentrations of carrier. The chloride efflux (%) 270 s after the addition of carrier is plotted as a function of the carrier concentration. Data points can then be fitted to the Hill equation using *Origin 8.1*:

$$y = V_{\max}\frac{x^n}{k + x^n} = 100\%\frac{x^n}{EC_{50} + x^n}$$

where y is the chloride efflux at 270 s (%) and x is the carrier concentration (mol% carrier to lipid). V_{max}, k and n are the parameters to be fitted. V_{max} is the maximum efflux possible (often fixed to 100%, as this is physically the maximum chloride efflux possible), n is the Hill coefficient and k is the carrier concentration needed to reach $V_{max}/2$ (when V_{max} is fixed to 100%, k equals EC_{50}). From the Hill plot it is therefore possible to directly obtain $EC_{50,270s}$ values, defined as the carrier concentration (mol% carrier to lipid) needed to obtain 50% chloride efflux after 270 s. The Hill plots of compounds **1**-**3** at pH 7.2 have been previously published,[1] while compounds **4**, **7** and **8** were not active enough to allow Hill plots.

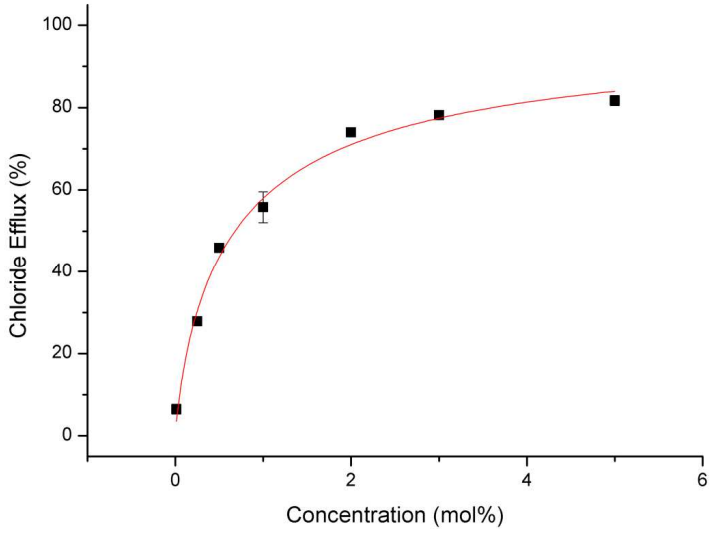

Model	Hill		
Equation	y=Vmax*x^n/(k^n+x^n)		
Reduced Chi-Sqr	7.86265		
Adj. R-Square	0.99007		
		Value	Standard Erro
Chloride Efflux	Vmax	100	0
	k	0.67804	0.04769
	n	0.82906	0.0572

Figure S45: Hill plot for chloride release mediated by receptor **6** from unilamellar POPC vesicles loaded with 489 mM NaCl buffered to pH 7.2 with 5 mM sodium phosphate salts. The vesicles were dispersed in 489 mM $NaNO_3$ buffered to pH 7.2 with 5 mM sodium phosphate salts. Chloride efflux was measured at 270 s. Each points represent the average of a minimum of three repeats and eror bars represent standard deviations. Concentrations used: 0.0125 mol%, 0.25 mol%, 0.5 mol%, 1 mol%, 2 mol%, 3 mol%, 5 mol% with respect to lipid.

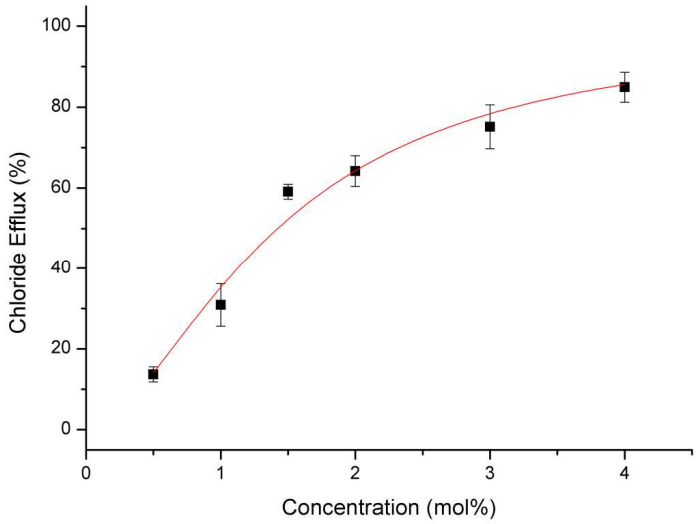

Model	Hill		
Equation	y=Vmax*x^n/(k^n+x^n)		
Reduced Chi-Sqr	19.19282		
Adj. R-Square	0.97401		
		Value	Standard Error
B	Vmax	100	0
	k	1.42311	0.07779
	n	1.72518	0.18128

Figure S46: Hill plot for chloride release mediated by receptor **1** from unilamellar POPC vesicles loaded with 489 mM NaCl buffered to pH 4.0 with 5 mM citrate salts. The vesicles were dispersed in 489 mM $NaNO_3$ buffered to pH 4.0 with 5 mM citrate salts. Chloride efflux was measured at 270 s. Each points represent the average of a minimum of three repeats and eror bars represent standard deviations. Concentrations used: 0.5 mol%, 1 mol%, 1.5 mol%, 2 mol%, 3 mol%, 4 mol% with respect to lipid.

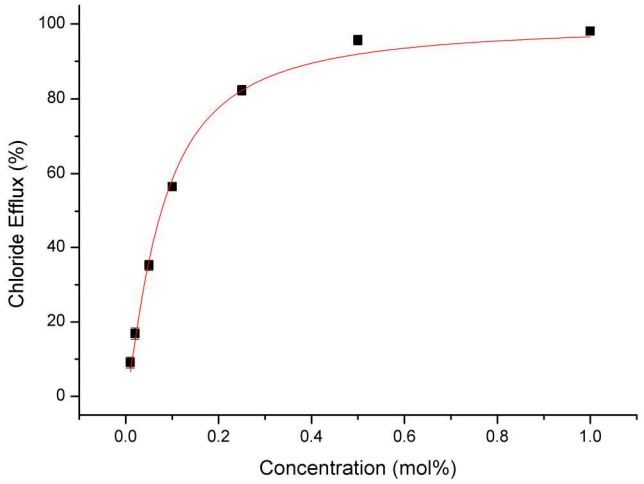

Model	Hill		
Equation	y=Vmax*x^n/(k^n+x^n)		
Reduced Chi-Sqr	6.37111		
Adj. R-Square	0.99534		
		Value	Standard Error
B	Vmax	100	0
	k	0.07683	0.00373
	n	1.29875	0.07442

Figure S47: Hill plot for chloride release mediated by receptor **2** from unilamellar POPC vesicles loaded with 489 mM NaCl buffered to pH 4.0 with 5 mM citrate salts. The vesicles were dispersed in 489 mM $NaNO_3$ buffered to pH 4.0 with 5 mM citrate salts. Chloride efflux was measured at 270 s. Each points represent the average of a minimum of three repeats and eror bars represent standard deviations. Concentrations used: 0.01 mol%, 0.02 mol%, 0.05 mol%, 0.1 mol%, 0.25 mol%, 0.5 mol%, 1 mol% with respect to lipid.

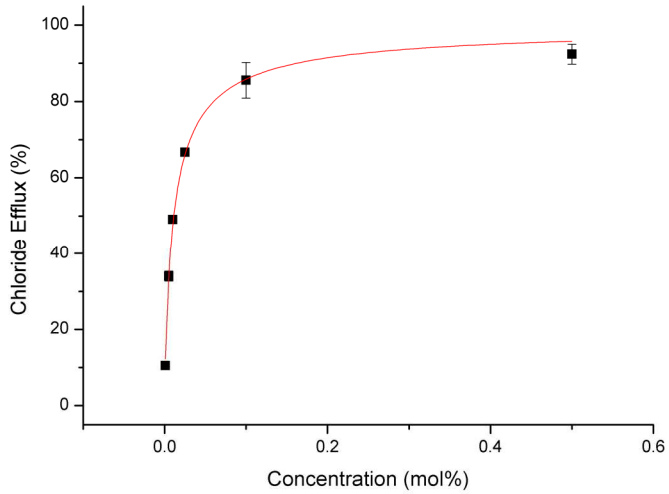

Model	Hill		
Equation	y=Vmax*x^n/(k^n+x^n)		
Reduced Chi-Sqr	4.09839		
Adj. R-Square	0.99583		
		Value	Standard Erro
B	Vmax	100	0
	k	0.01106	6.25375E-4
	n	0.81894	0.0424

Figure S48: Hill plot for chloride release mediated by receptor **3** from unilamellar POPC vesicles loaded with 489 mM NaCl buffered to pH 4.0 with 5 mM citrate salts. The vesicles were dispersed in 489 mM $NaNO_3$ buffered to pH 4.0 with 5 mM citrate salts. Chloride efflux was measured at 270 s. Each points represent the average of a minimum of three repeats and eror bars represent standard deviations. Concentrations used: 0.001 mol%, 0.005 mol%, 0.01 mol%, 0.025 mol%, 0.1 mol%, 0. 5 mol% with respect to lipid.

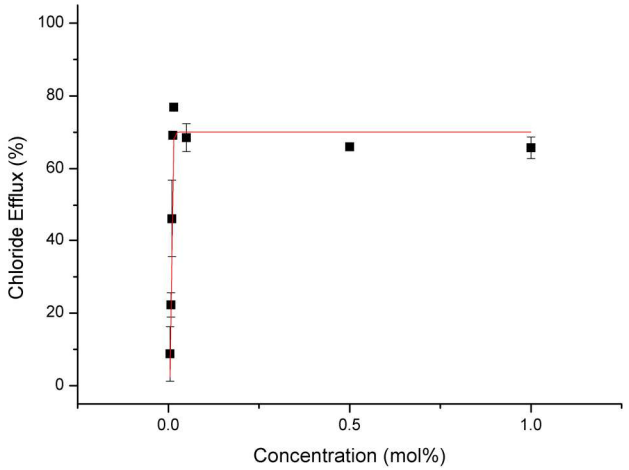

Model	Hill		
Equation	y=Vmax*x^n/(k^n+x^n)		
Reduced Chi-Sqr	41.05947		
Adj. R-Square	0.93397		
		Value	Standard Error
Chloride efflux at 270 s	Vmax	70.0651	3.3571
	k	0.00853	4.57085E-4
	n	6.26087	1.80548

Figure S49: Hill plot for chloride release mediated by receptor **5** from unilamellar POPC vesicles loaded with 489 mM NaCl buffered to pH 4.0 with 5 mM citrate salts. The vesicles were dispersed in 489 mM $NaNO_3$ buffered to pH 4.0 with 5 mM citrate salts. Chloride efflux was measured at 270 s. Each points represent the average of a minimum of three repeats and eror bars represent standard deviations. Concentrations used: 0.005 mol% (large error), 0.0075 mol% (large error), 0.01 mol% (large error), 0.0125 mol%, 0.015 mol%, 0.05 mol%, 0.5 mol%, 1 mol% with respect to lipid. Large errors at low concentration are due to high *n*-value and this prevented the accurate determination of the EC_{50}. However, all concentration above 0.0125 mol% carrier-to-lipid gave chloride effluxes above 50% with low errors and thus the EC_{50} value can be estimated around 0.0125 mol%

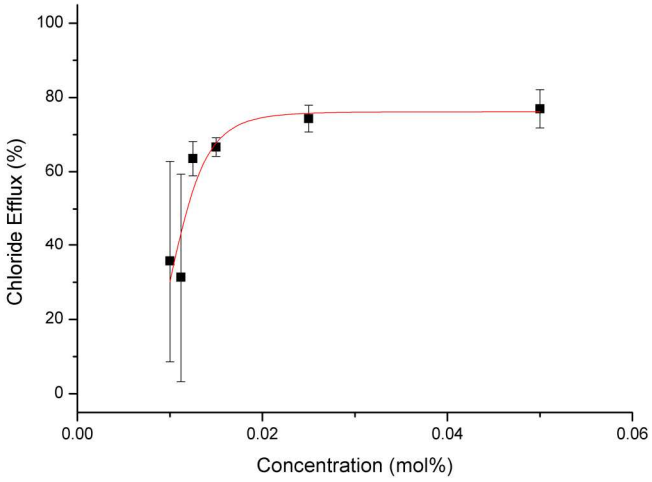

Model	Hill		
Equation	y=Vmax*x^n/(k^n+x^n)		
Reduced Chi-Sqr	83.98293		
Adj. R-Square	0.7837		
		Value	Standard Error
Chloride efflux at 270 s	Vmax	76.16022	6.59965
	k	0.01071	6.35779E-4
	n	6.18347	2.98695

Figure S50: Hill plot for chloride release mediated by receptor **6** from unilamellar POPC vesicles loaded with 489 mM NaCl buffered to pH 4.0 with 5 mM citrate salts. The vesicles were dispersed in 489 mM $NaNO_3$ buffered to pH 4.0 with 5 mM citrate salts. Chloride efflux was measured at 270 s. Each points represent the average of a minimum of three repeats and eror bars represent standard deviations. Concentrations used: 0.01 mol% (large error), 0.0112 mol% (large error), 0.0125 mol%, 0.015 mol%, 0.025 mol%, 0.05 mol% with respect to lipid. Large errors at low concentration are due to high *n*-value and this prevented the accurate determination of the EC_{50}. However, all concentration above 0.0125 mol% carrier-to-lipid gave chloride effluxes above 50% with low errors and thus the EC_{50} value can be estimated around 0.0125 mol%

S7.4. Cholesterol tests

For the cholesterol tests, the chloride/nitrate transport experiments (see Section S7.2) were repeated with vesicles consisting of 3:7 cholesterol:POPC. Cholesterol is believed to increase the viscosity of the membrane, hence slowing down diffusion in the lipid bilayer. This effect should be more pronounced in the case of a mobile carrier mechanism, while no effect is expected for an ion channel. Figure S51 and Figure S52 indicate that there is indeed a significant reduction in the transport ability of **1**-**8**, especially at pH 4.0. This suggests that the both squaramides and thiosquaramides operate via a mobile carrier mechanism at both low and high pH conditions. The results for oxosquaramides **1**-**3** at pH 7.2 have been previously published.[1] Cholesterol tests were not performed for compounds **4** and **8** due to their very low transport activity.

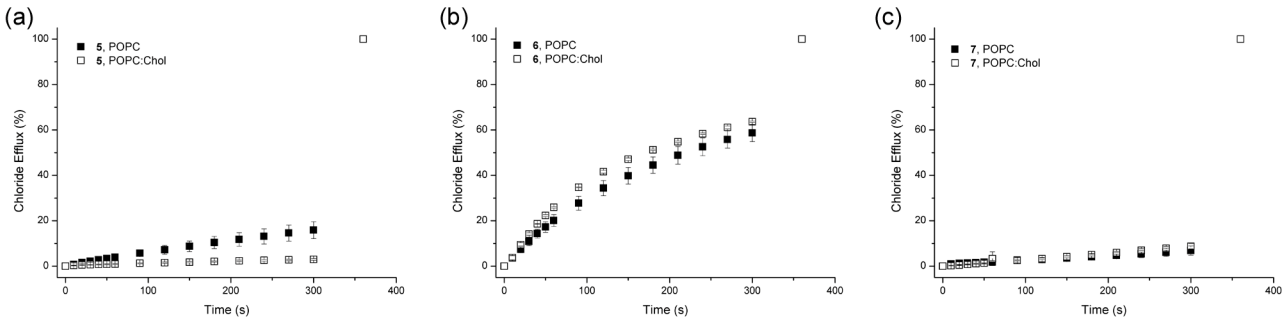

Figure S51: Chloride efflux promoted by compounds **5-7** from unilamellar POPC vesicles (filled symbols) or unilamellar 7:3 POPC:cholesterol vesicles (empty symbols) loaded with 489 mM NaCl buffered to pH 7.2 with 5 mM sodium phosphate salts. The vesicles were dispersed in 489 mM $NaNO_3$ buffered to pH 7.2 with 5 mM sodium phosphate salts. At the end of the experiment, detergent was added to lyse the vesicles and calibrate the ISE to 100% chloride efflux. Each point represents the average of three trials. (a) 1 mol% of compound **5**. (c) 1 mol% of compound **6**. (c) 1 mol% of compound **7**.

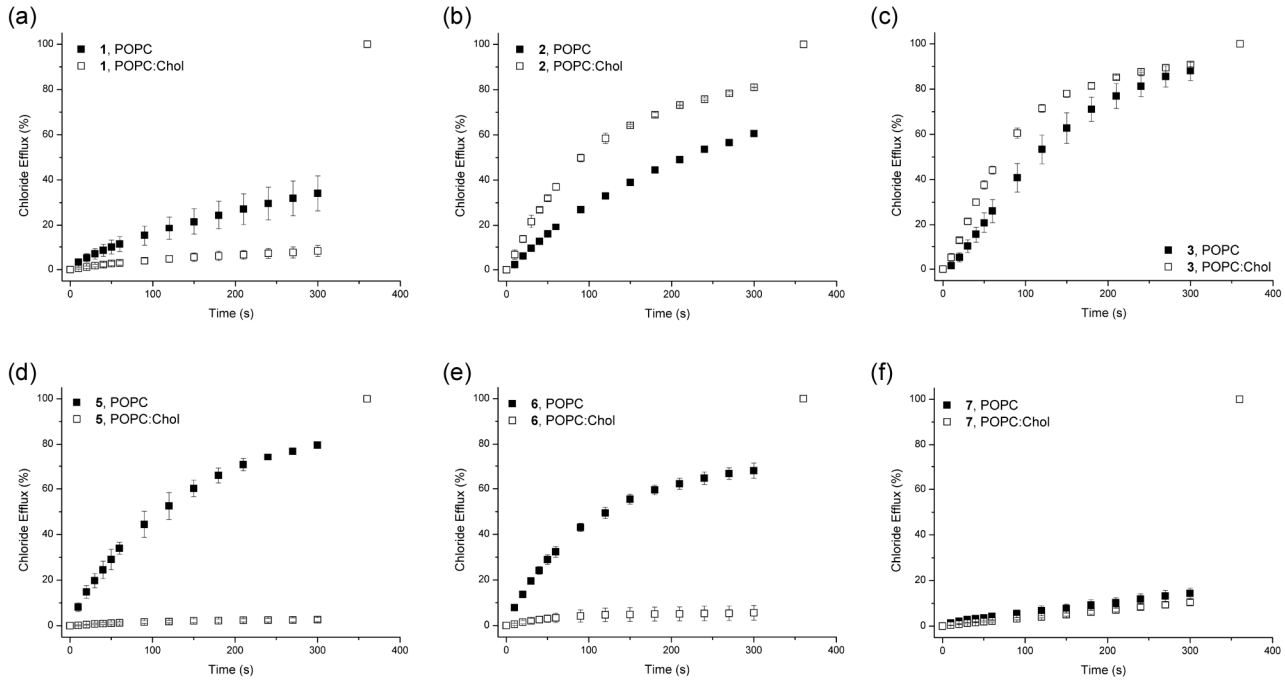

Figure S52: Chloride efflux promoted by compounds **1-8** from unilamellar POPC vesicles (filled symbols) or unilamellar 7:3 POPC:cholesterol vesicles (empty symbols) loaded with 489 mM NaCl buffered to pH 4.0 with 5 mM citrate salts. The vesicles were dispersed in 489 mM $NaNO_3$ buffered to pH 4.0 with 5 mM citrate salts. At the end of the experiment, detergent was added to lyse the vesicles and calibrate the ISE to 100% chloride efflux. Each point represents the average of three trials. (a) 1 mol% of compound **1**. (c) 0.1 mol% of compound **2**. (c) 0.1 mol% of compound **3;** (d) 0.015 mol% of compound **5**. (e) 0.015 mol% of compound **6**. (f) 1 mol% of compound **7**.

S7.5. Calcein leakage assays

A lipid film of POPC was formed from a chloroform solution under reduced pressure and dried under vacuum for at least 6 hours. The lipid film was rehydrated by vortexing with a NaCl solution (100 mM calcein, 489 mM NaCl, 5 mM phosphate buffer at pH 7.2 or 5 mM citrate buffer at pH 4.0). The lipid suspension was then subjected to nine freeze-thaw cycles and allowed to age for 30 min at room temperature before extruding 25 times through a 200 nm polycarbonate membrane. The unincorporated calcein was removed by size exclusion chromatography on a Sephadex G-50 column using a sodium sulfate or sodium nitrate solution as eluent (162 mM Na_2SO_4 or 489 mM $NaNO_3$, 5 mM phosphate buffer at pH 7.2 or 5 mM citrate buffer at pH 4.0).

The thus obtained unilamellar POPC were suspended in a Na_2SO_4 or $NaNO_3$ solution buffered to pH 7.2 with sodium phosphate salts or to pH 4.0 with citrate buffer. The lipid concentration per sample was 1 mM. The fluorescence emission of the encapsulated calcein at 520 nm after excitation at 490 nm was recorded using a *Varian Cary Eclipse Fluorescence Spectrophotometer*. At t = 10 s, a solution of the carrier molecule in DMSO (1 mol% w.r.t. lipid) was added to start ion transport. At the end of the experiment the vesicles were lysed with 30 µl of octaethylene glycol monododecyl ether (0.232 mM in 7:1 water:DMSO v/v). The fractional calcein release (FR) was calculated as follows (with I_t = fluorescence intensity at time t, I_0 = fluorescence intensity at time 0 and I_{max} = fluorescence intensity after addition of detergent):

$$FR = \frac{I_t - I_0}{I_{\max} - I_0}$$

The results depicted in Figure S53 and Figure S54 shown no sign of leakage of the calcein dye from the vesicles. This indicates that the vesicles are stable under the experimental conditions and that not the oxosquaramides nor the thiosquaramides induce vesicles leakage. This is additional evidence that compounds **1**-**8** do not cause the formation of large channels in the POPC membranes and most likely function as mobile carriers for chloride ions. Calcein leakage assays were not performed for compounds **4** and **8** due to their very low transport activity.

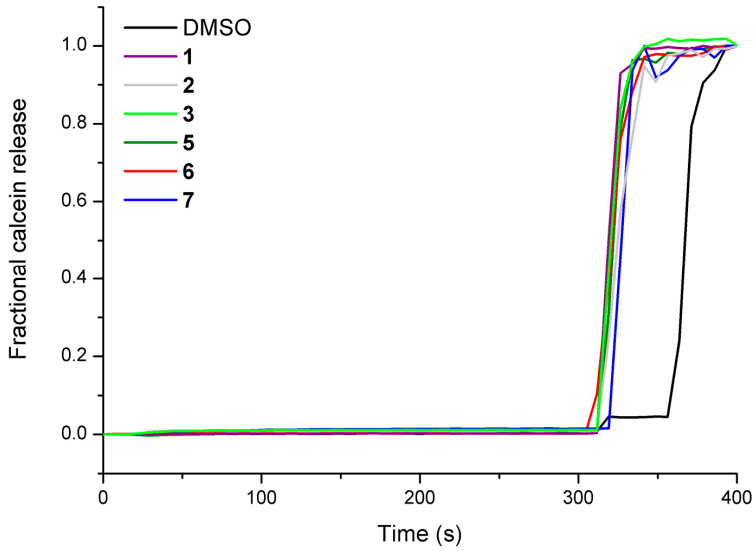

Figure S53: Calcein leakage by **1**-**8** (1 mol% carrier-to-lipid) from unilamellar POPC vesicles loaded with 100 mM calcein and 489 mM NaCl, buffered to pH 7.2 with 5 mM sodium phosphate salts. The vesicles were dispersed in 489 mM $NaNO_3$ buffered to pH 7.2 with 5 mM sodium phosphate salts. At t = 10 s, a DMSO solution of the transporter was added to start the experiment. At the end of the experiment, detergent was added to lyse the vesicles. The results are shown as the fraction of calcein leaked from the vesicles.

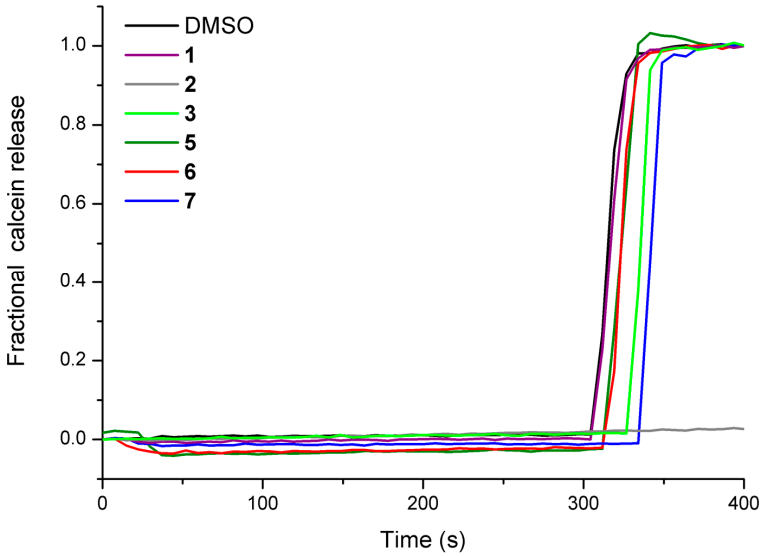

Figure S54: Calcein leakage by **1**-**8** (1 mol% carrier-to-lipid) from unilamellar POPC vesicles loaded with 100 mM calcein and 489 mM NaCl, buffered to pH 4.0 with 5 mM citrate salts. The vesicles were dispersed in 489 mM $NaNO_3$ buffered to pH 4.0 with 5 mM citrate salts. At t = 10 s, a DMSO solution of the transporter was added to start the experiment. At the end of the experiment, detergent was added to lyse the vesicles. The results are shown as the fraction of calcein leaked from the vesicles.

S7.6. Antiport tests

Unilamellar POPC vesicles containing 489 mM MCl (M = Na, Cs) solution buffered to pH 7.2 or pH 4.0 with 5 mM phosphate or citrate salts, prepared as described in Section S7.1., were suspended in the external medium consisting of a 162 mM Na_2SO_4 solution buffered to pH 7.2 or pH 4.0 with 5 mM phosphate or citrate salts. The lipid concentration per sample was 1 mM. A DMSO solution of the carrier molecule was added to start the experiment and chloride efflux was monitored using a chloride sensitive electrode. At 5 min, the vesicles were lysed with 50 μL of octaethylene glycol monododecyl ether (0.232 mM in 7:1 water:DMSO v/v) and a total chloride reading was taken at 7 min. The initial value was set at 0% chloride efflux and the final chloride reading was set as 100% chloride efflux. All other data points were calibrated to these points. For some experiments a pH gradient was applied. In these cases the vesicles were prepared containing a MCl solution buffered to pH 4.0 with citrate salts and they were dialysed with a $NaNO_3$ or Na_2SO_4 solution buffered to pH 4.0 with citrate salts. Immediately before the measurements, the vesicles were diluted with a $NaNO_3$ or Na_2SO_4 solution buffered to pH 7.2 with phosphate salts to create the gradient, followed by the addition of a DMSO solution of the transporter. The rest of the experiments was performed similar to the other ion-selective electrode tests. The antiport tests were not performed for compounds **4** and **8** due to their very low transport activity.

The following conclusions can be made based on the results shown in Figure S55:

- The small difference in chloride efflux from vesicles loaded with NaCl and vesicles loaded with CsCl indicates that the counterion does not play a significant role in the transport process. Metal-chloride symport by the (thio)squaramides is therefore unlikely.
- The large difference in activity seen when nitrate or sulfate is the external anion suggests that the anion in the external solution is important for the transport process. The most likely mechanism is therefore chloride/nitrate antiport.
- The absence of an increase in chloride transport mediated by the thiosquaramides when a pH gradient is applied, suggest that HCl symport does not occur. However, it must be noted that only a small amount of HCl needs to be transported to dissipate the pH gradient and this might not be picked up by the chloride-selective electrode.

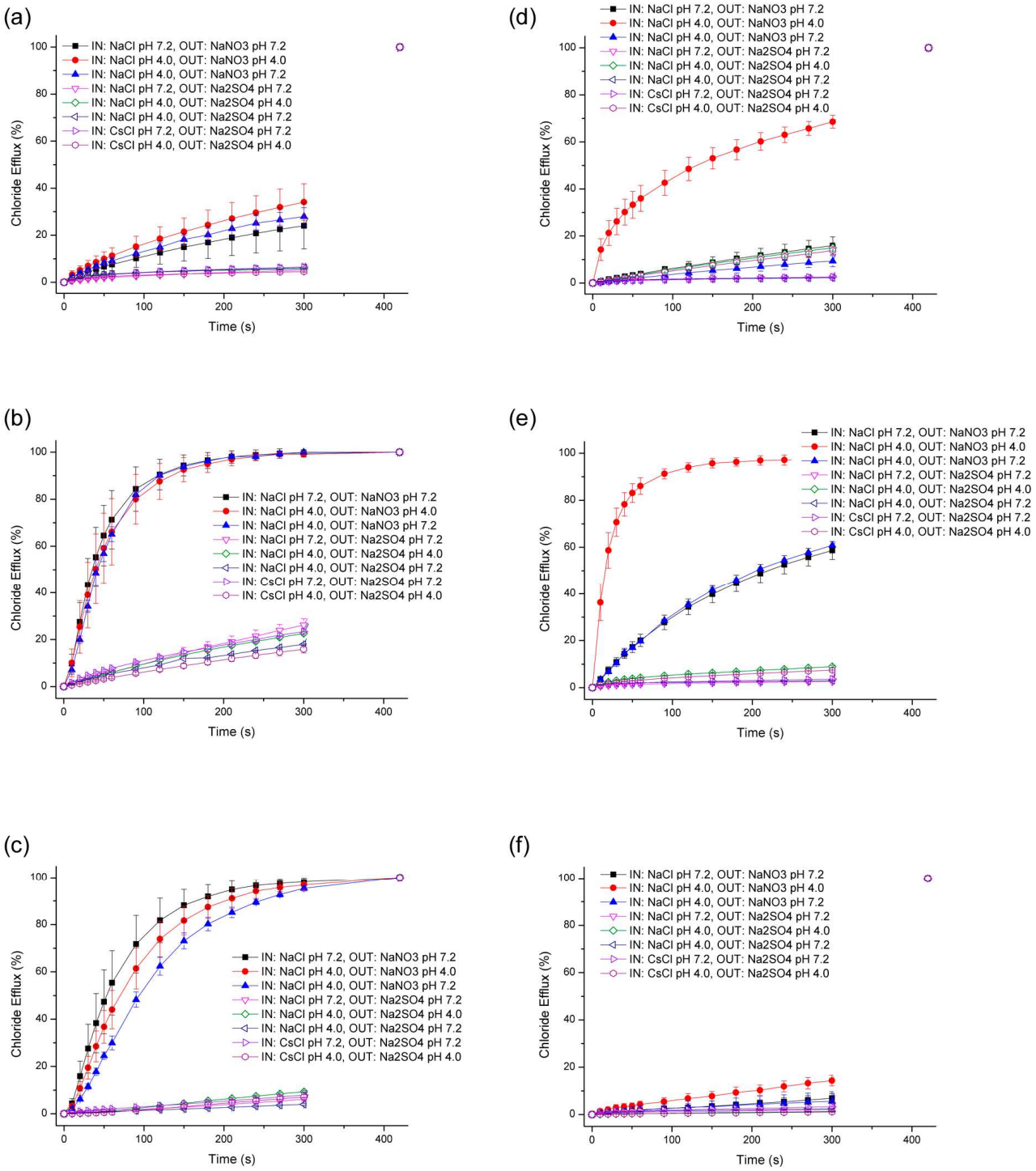

Figure S55: Chloride efflux from POPC vesicles at various conditions mediated by **1**-**8** (1 mol% with respect to lipid). POPC vesicles were loaded with a 489 mM MCl (M = Na, Cs) solution buffered to pH 7.2 with 5 mM phosphate salts or to pH 4.0 with 5 mM citrate salts (*IN*), and were suspended in a 489 mM $NaNO_3$ or 162 mM Na_2SO_4 solution buffered to pH 7.2 with 5 mM phosphate salts or to pH 4.0 with 5 mM citrate salts (*OUT*). At the end of the experiment (300 s), detergent was added to lyse the vesicles and calibrate the ISE to 100% chloride efflux. Conditions with NO_3^- as the external anion are shown in filled symbols, while conditions with SO_4^{2-} as the external anion are shown in empty symbols. Each point represents the average of a minimum of 3 independent trials. DMSO was used as a control. (a) **1**; (b) **2**; (c) **3**; (d) **5**; (e) **6**; (f) **7**.

S7.7. HPTS assays

The HPTS fluorescence in the conditions of the transport experiments was first calibrated against pH. For this, a lipid film of POPC was formed from a chloroform solution under reduced pressure and dried under vacuum for at least 6 hours. The lipid film was rehydrated by vortexing with a NaCl solution (1 mM HPTS (8-hydroxypyrene-1,3,6- trisulphonic acid), 489 mM NaCl, 5 mM citrate buffer at pH 6.0). The lipid suspension was then subjected to nine freeze-thaw cycles and allowed to age for 30 min at room temperature before extruding 25 times through a 200 nm polycarbonate membrane. The unincorporated HPTS was removed by size exclusion chromatography on a Sephadex G-25 column using a sodium sulfate or sodium nitrate solution as eluent (162 mM Na_2SO_4 or 489 mM $NaNO_3$, 5 mM citrate buffer at pH 6.0). The thus obtained unilamellar POPC liposomes were suspended in a Na_2SO_4 or $NaNO_3$ solution buffered to pH 6.0 with citrate buffer. The lipid concentration per sample was 1 mM. The vesicles were then lysed with octaethylene glycol monododecyl ether. Small aliquots of a concentrated NaOH solution were added to increase the pH (total range pH 6 – pH 8). At each addition, the pH of the solution was measured using a pH electrode and at the same time the HPTS fluorescence was monitored by excitation at both 403 nm and 460 nm and recording the emission at 510 nm using a *Varian Cary Eclipse Fluorescence Spectrophotometer*. A calibration curve could then be obtained by fitting a plot of the pH (y) against the ratio of HPTS emission after excitation at 460 nm and 403 nm (I_{460}/I_{403}, x) to the following equation (See Figure S56): $y = a + b \cdot ln(x+c)$.

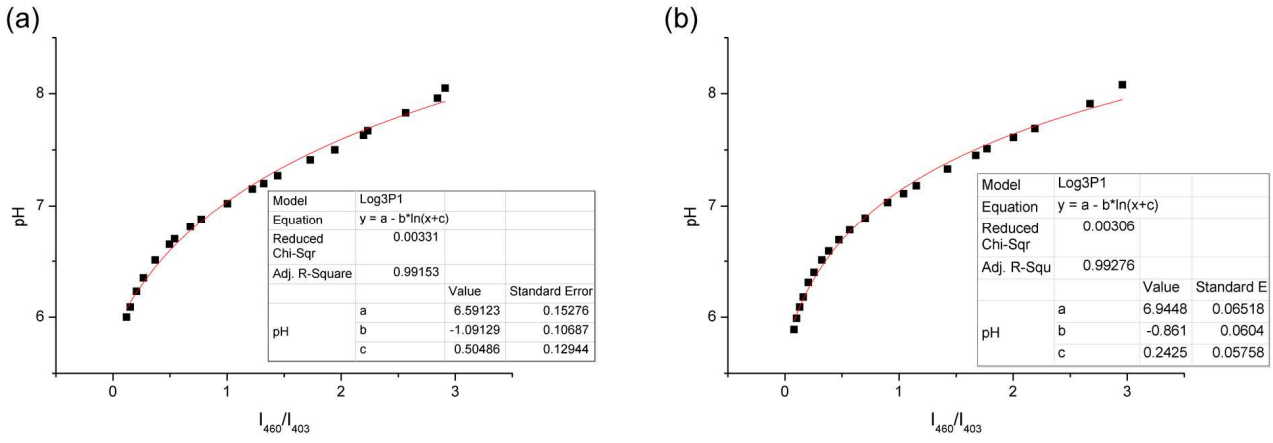

Figure S56: Calibration curve for pH (y) from the ratio of HPTS emission after excitation at 460 nm and 403 nm (I_{460}/I_{403}, x). (a) in the presence of $NaNO_3$; (b) in presence of $NaSO_4$.

For the actual HCl symport assays, a lipid film of POPC was formed from a chloroform solution under reduced pressure and dried under vacuum for at least 6 hours. The lipid film was rehydrated by vortexing with a NaCl solution (1 mM HPTS (8-hydroxypyrene-1,3,6-trisulphonic acid), 489 mM NaCl, 5 mM phosphate buffer at pH 7.2 or 5 mM citrate buffer at pH 6.0). The lipid suspension was then subjected to nine freeze-thaw cycles and allowed to age for 30 min at room temperature before extruding 25 times through a 200 nm polycarbonate membrane. The unincorporated HPTS was removed by size exclusion chromatography on a Sephadex G-25 column using a sodium sulfate or sodium nitrate solution as eluent (162 mM Na_2SO_4 or 489 mM $NaNO_3$, 5 mM phosphate buffer at pH 7.2 or 5 mM citrate buffer at pH 6.0). The thus obtained unilamellar POPC were suspended in a Na_2SO_4 or $NaNO_3$ solution buffered to pH 7.2 with sodium phosphate salts or to pH 6.0 with citrate buffer. The lipid concentration per sample was 1 mM. A DMSO solution of the carrier molecule was added to start the experiment (when a pH gradient was applied a small amount of the appropriate acid or base was added to the external solution just before the start of the experiment in order to achieve a pH gradient of one pH unit). The fluorescence of intravesicular HPTS was monitored by excitation at both 403 nm and 460 nm and recording the emission at 510 nm using a *Varian Cary Eclipse Fluorescence Spectrophotometer*. At the end of the experiment, the vesicles were lysed with 30 μL of octaethylene glycol monododecyl ether (0.232 mM in 7:1 water:DMSO v/v). The HPTS tests were not performed for compounds **4** and **8** due to their very low transport activity. The internal pH was obtained by fitting the data to the equation obtained after calibrating the HPTS fluorescence to pH:

$$pH = 6.59 + 1.09 \cdot \ln\left(\frac{I_{460}}{I_{403}} + 0.50\right) \quad \textit{for external nitrate}$$

$$pH = 6.94 + 0.86 \cdot \ln\left(\frac{I_{460}}{I_{403}} + 0.24\right) \quad \textit{for external sulfate}$$

When nitrate is the external anion (Figure S57-S59), the results reveal that in the absence of a pH gradient the intravesicular pH does not change upon the addition of (thio)squaramide based transporters (Figure S57-S58). However, when a pH gradient is applied across the phospholipid bilayer, a fast dissipation of the gradient is observed upon the addition of both oxosquaramides and thiosquaramides **1**–**8**, suggesting that H^+/Cl^- symport (or OH^-/Cl^- antiport) can occur under these conditions (Figure S59). However, when sulfate is the external anion, the results are slightly different (Figure S60-S62). In this case only a small increase in

internal pH was observed when both the intravesicular and extravesicular solution were buffered to pH 7.2 (Figure S60), while a large increase in internal pH was seen when a pH gradient was applied (Figure S62). However, unlike the nitrate tests (Figure S58), a large increase in internal pH was also observed when both intra- and extravesicular solution were buffered to pH 6.0 (Figure S61), hinting that H^+/Cl^- symport (or OH^-/Cl^- antiport) can occur without a pH gradient providing that sulfate is the external anion.

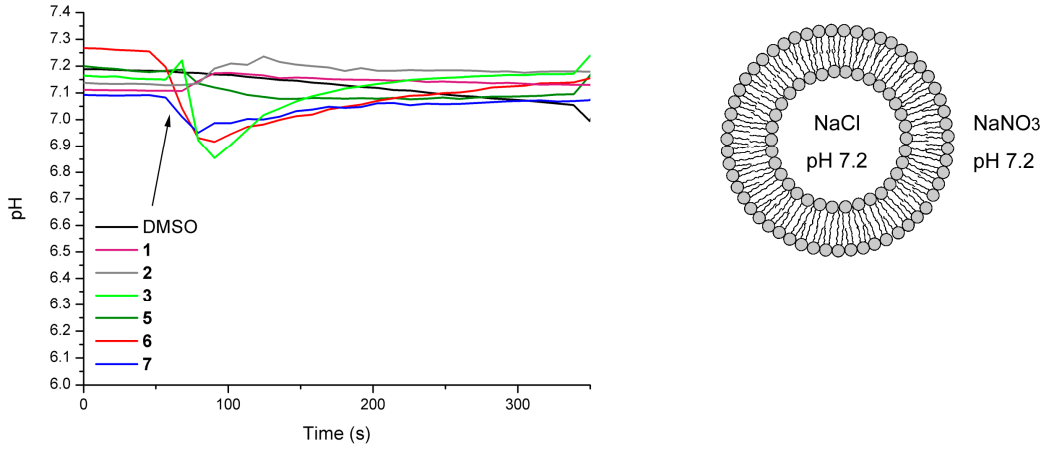

Figure S57: Investigation of HCl transport facilitated by **1**–**8** using the fluorescent dye HPTS to estimate the intravesicular pH. POPC vesicles were loaded with 489 mM NaCl, 1 mM HPTS, buffered to pH 7.2 with phosphate buffer and suspended in a solution of 489 mM $NaNO_3$ buffered to pH 7.2 with phosphate buffer. At time t = 50 s a DMSO solution of the transporter was added (1 mol% with respect to lipid) and at time t = 350 s detergent was added. Each line represents the average of 3 independent trials and DMSO was used as a control.

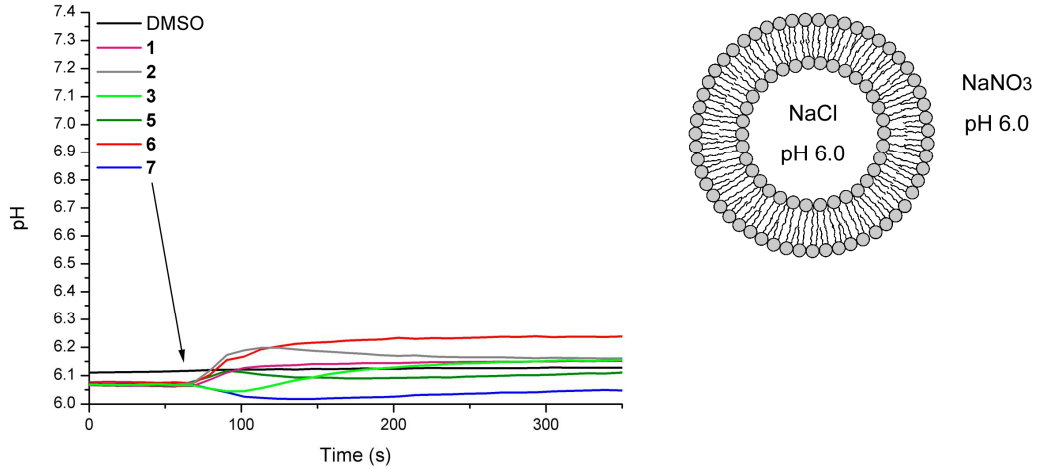

Figure S58: Investigation of HCl transport facilitated by **1**–**8** using the fluorescent dye HPTS to estimate the intravesicular pH. POPC vesicles were loaded with 489 mM NaCl, 1 mM HPTS, buffered to pH 6.0 with phosphate buffer and suspended in a solution of 489 mM $NaNO_3$ buffered to pH 7.2 with phosphate buffer. At time t = 50 s a DMSO solution of the transporter was added (1 mol% with respect to lipid) and at time t = 350 s detergent was added. Each line represents the average of 3 independent trials and DMSO was used as a control.

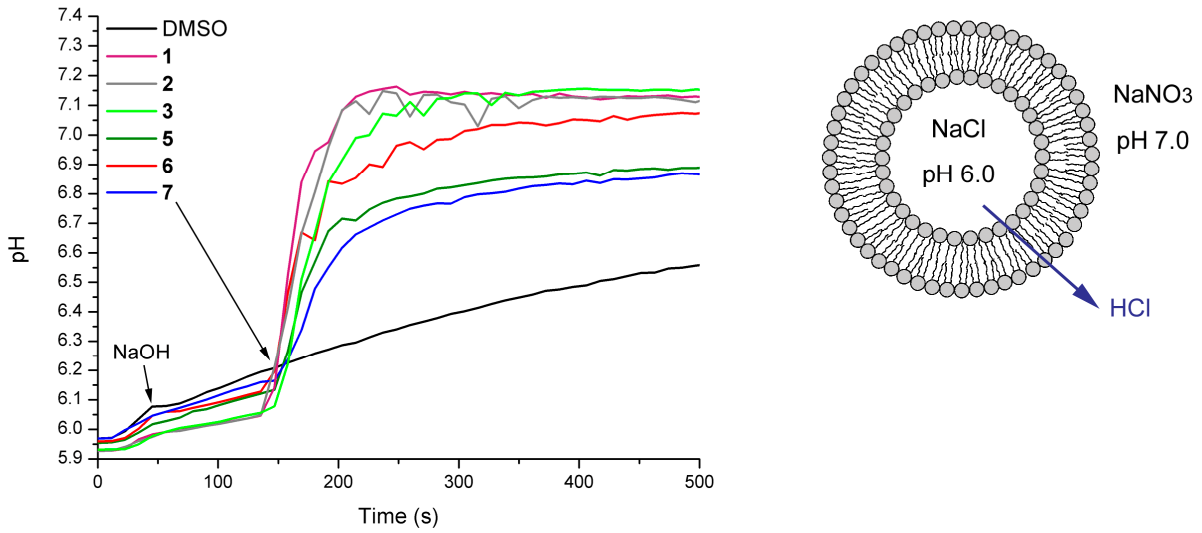

Figure S59: Investigation of HCl transport facilitated by **1**–**8** using the fluorescent dye HPTS to estimate the intravesicular pH. POPC vesicles were loaded with 489 mM NaCl, 1 mM HPTS, buffered to pH 6.0 with citrate buffer, and suspended in a solution of 489 mM $NaNO_3$ buffered to pH 6.0 with citrate buffer. At time t = 50 s a NaOH solution was added to achieve an external pH of 7.0. At time t = 150 s a DMSO solution of the transporter was added (1 mol% with respect to lipid) and at time t = 500 s detergent was added. Each line represents the average of 3 independent trials and DMSO was used as a control.

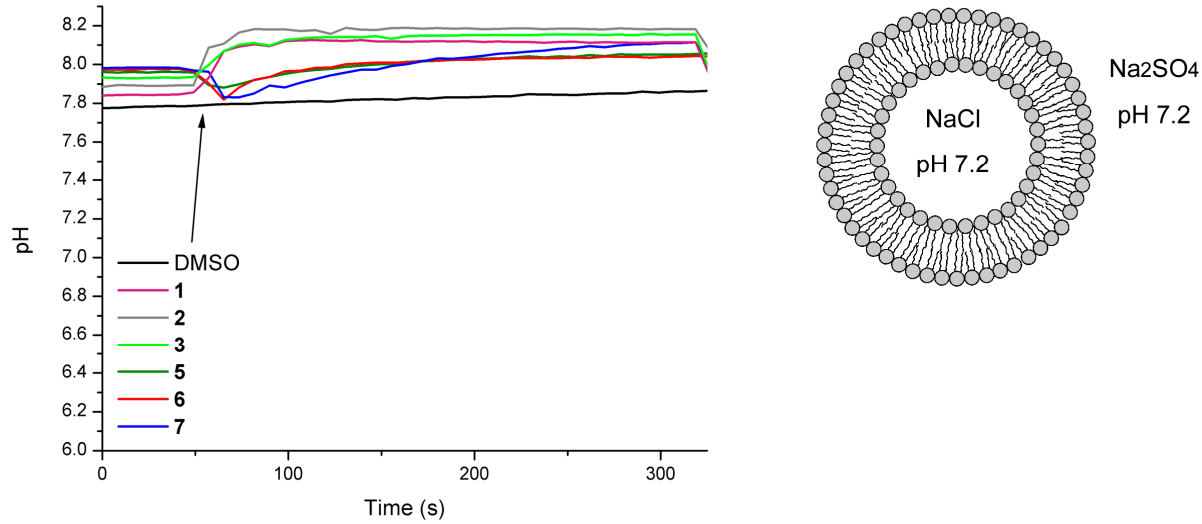

Figure S60: Investigation of HCl transport facilitated by **1**–**8** using the fluorescent dye HPTS to estimate the intravesicular pH. POPC vesicles were loaded with 489 mM NaCl, 1 mM HPTS, buffered to pH 7.2 with phosphate buffer and suspended in a solution of 162 mM Na_2SO_4 buffered to pH 7.2 with phosphate buffer. At time t = 50 s a DMSO solution of the transporter was added (1 mol% with respect to lipid) and at time t = 350 s detergent was added. Each line represents the average of 3 independent trials and DMSO was used as a control.

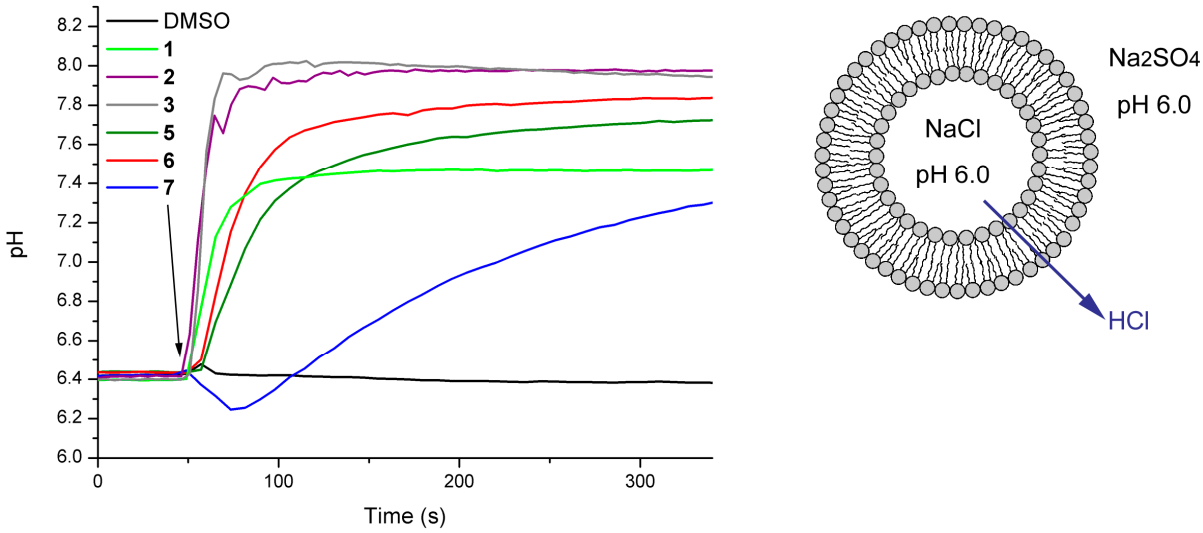

Figure S61: Investigation of HCl transport facilitated by **1**–**8** using the fluorescent dye HPTS to estimate the intravesicular pH. POPC vesicles were loaded with 489 mM NaCl, 1 mM HPTS, buffered to pH 6.0 with phosphate buffer and suspended in a solution of 162 mM Na_2SO_4 buffered to pH 7.2 with phosphate buffer. At time t = 50 s a DMSO solution of the transporter was added (1 mol% with respect to lipid) and at time t = 350 s detergent was added. Each line represents the average of 3 independent trials and DMSO was used as a control.

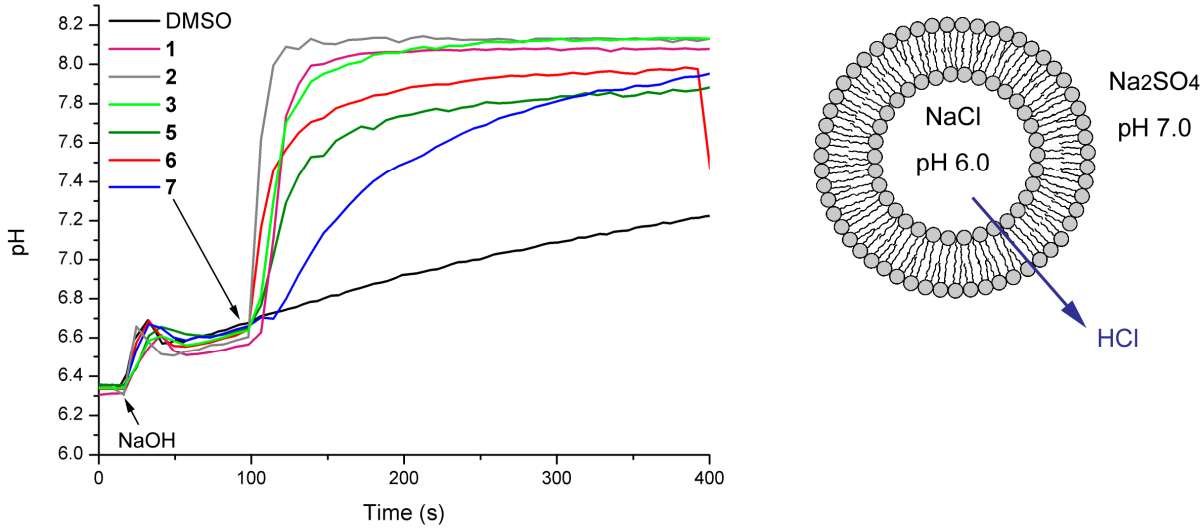

Figure S62: Investigation of HCl transport facilitated by **1**–**8** using the fluorescent dye HPTS to estimate the intravesicular pH. POPC vesicles were loaded with 489 mM NaCl, 1 mM HPTS, buffered to pH 6.0 with citrate buffer, and suspended in a solution of 162 mM Na_2SO_4 buffered to pH 6.0 with citrate buffer. At time t = 20 s a NaOH solution was added to achieve an external pH of 7.0. At time t = 100 s a DMSO solution of the transporter was added (1 mol% with respect to lipid) and at time t = 400 s detergent was added. Each line represents the average of 3 independent trials and DMSO was used as a control.

In order to see if any other acids can be transported across POPC bilayers, the HPTS tests were repeated with the internal and external solutions exchanged or with the pH gradient in opposite directions. The results shown in Figures S63-S66 indicated that HCl and HNO_3 can be transported by **1-8**, but HSO_4^- (or H_2SO_4) cannot be transported by these compounds.

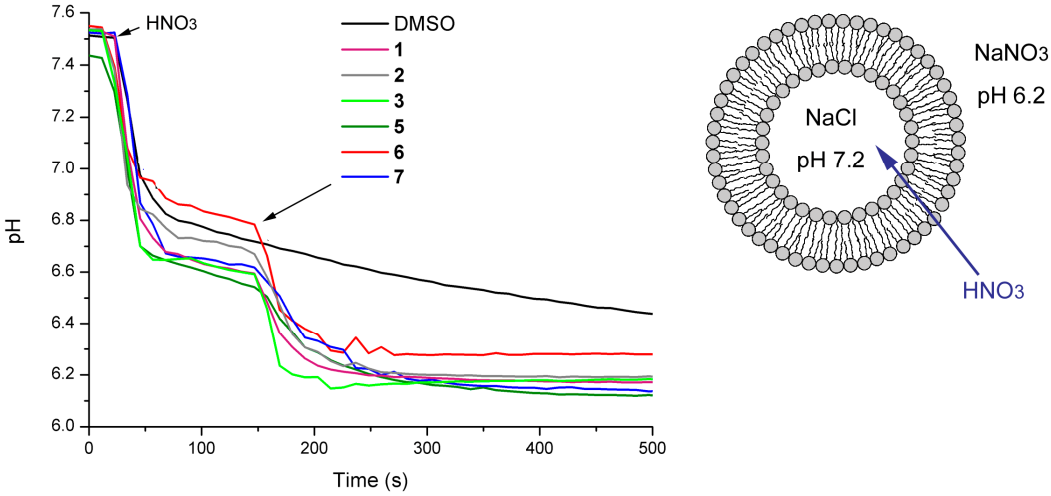

Figure S63: Investigation of HNO_3 transport facilitated by **1**–**8** using the fluorescent dye HPTS to estimate the intravesicular pH. POPC vesicles were loaded with 489 mM NaCl, 1 mM HPTS, buffered to pH 7.2 with phosphate buffer, and suspended in a solution of 489 mM $NaNO_3$ buffered to pH 7.2 with phosphate buffer. At time t = 10 s a HNO_3 solution was added to achieve an external pH of 6.2. At time t = 150 s a DMSO solution of the transporter was added (1 mol% with respect to lipid) and at time t = 450 s detergent was added. Each line represents the average of 3 independent trials and DMSO was used as a control.

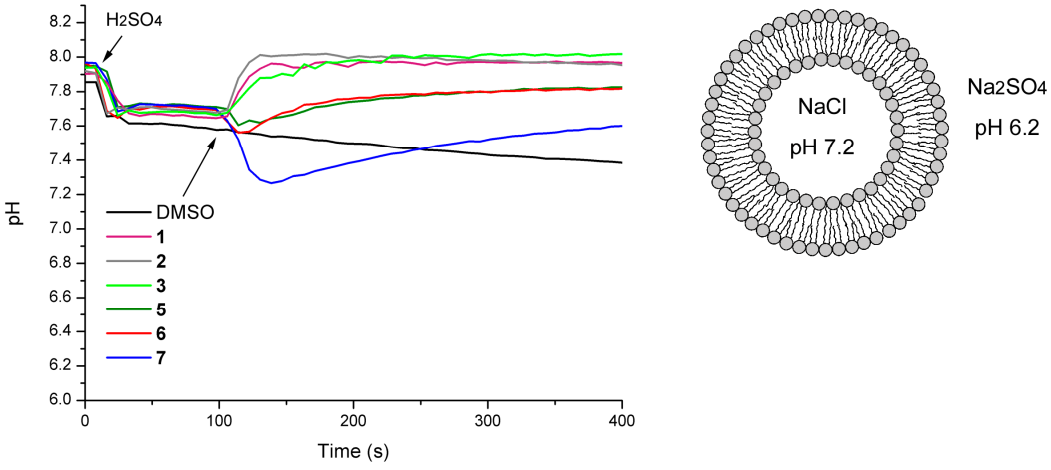

Figure S64: Investigation of HSO_4^- transport facilitated by **1**–**8** using the fluorescent dye HPTS to estimate the intravesicular pH. POPC vesicles were loaded with 489 mM NaCl, 1 mM HPTS, buffered to pH 7.2 with phosphate buffer, and suspended in a solution of 162 mM Na_2SO_4 buffered to pH 7.2 with phosphate buffer. At time t = 10 s a H_2SO_4 solution was added to achieve an external pH of 6.2. At time t = 100 s a DMSO solution of the transporter was added (1 mol% with respect to lipid) and at time t = 400 s detergent was added. Each line represents the average of 3 independent trials and DMSO was used as a control.

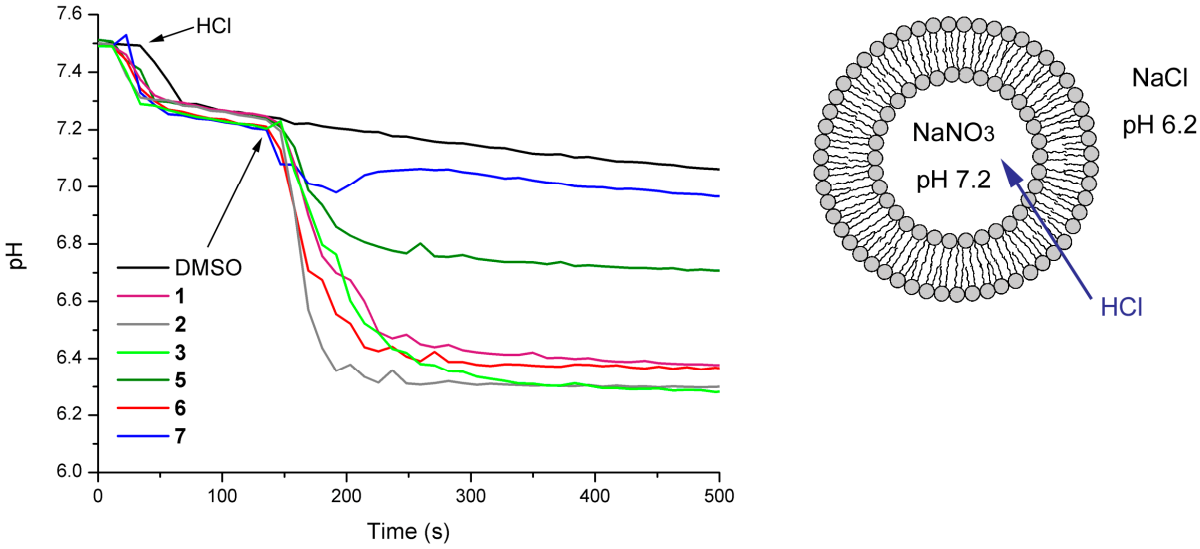

Figure S65: Investigation of HCl transport facilitated by **1**–**8** using the fluorescent dye HPTS to estimate the intravesicular pH. POPC vesicles were loaded with 489 mM $NaNO_3$, 1 mM HPTS, buffered to pH 7.2 with phosphate buffer, and suspended in a solution of 489 mM NaCl buffered to pH 7.2 with phosphate buffer. At time t = 10 s a HCl solution was added to achieve an external pH of 6.2. At time t = 150 s a DMSO solution of the transporter was added (1 mol% with respect to lipid) and at time t = 450 s detergent was added. Each line represents the average of 3 independent trials and DMSO was used as a control.

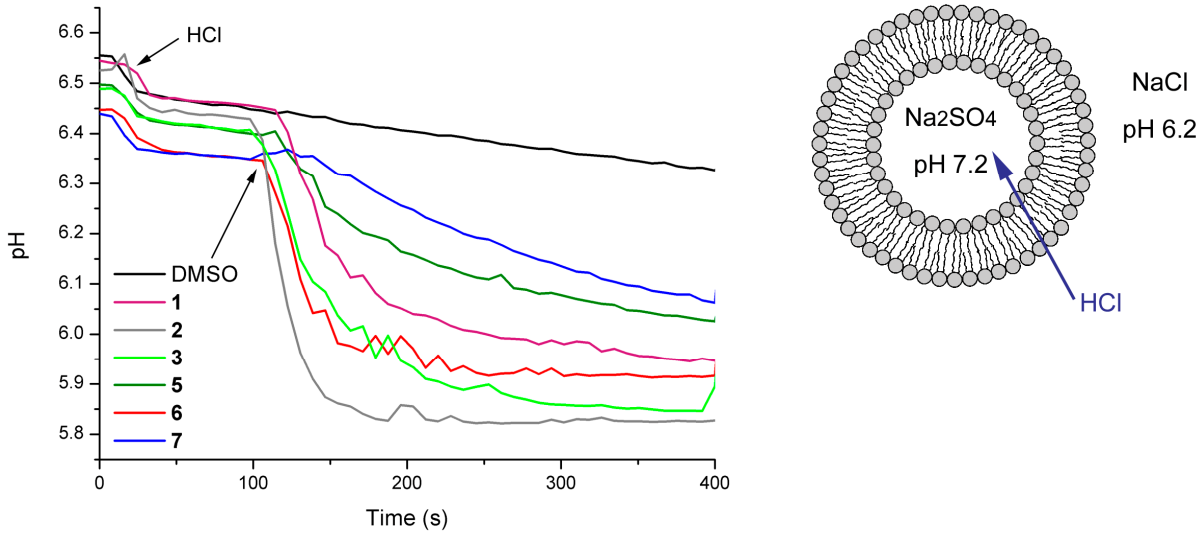

Figure S66: Investigation of HCl transport facilitated by **1**–**8** using the fluorescent dye HPTS to estimate the intravesicular pH. POPC vesicles were loaded with 162 mM Na_2SO_4, 1 mM HPTS, buffered to pH 7.2 with phosphate buffer, and suspended in a solution of 489 mM NaCl buffered to pH 7.2 with phosphate buffer. At time t = 10 s a HCl solution was added to achieve an external pH of 6.2. At time t = 100 s a DMSO solution of the transporter was added (1 mol% with respect to lipid) and at time t = 400 s detergent was added. Each line represents the average of 3 independent trials and DMSO was used as a control.

There is a spectral overlap between the absorbance region of the thiosquaramides and HPTS (400-500 nm), which might cause interference. To test whether interference was an issue, aqueous HPTS solutions were prepared (1 mM HPTS, 489 mM NaCl, buffered with 5 mM phosphate salts to pH 7.2 or with 5 mM citrate salts to pH 6.0) and diluted with a NaCl solution (489 mM NaCl, buffered with 5 mM phosphate salts to pH 7.2 or with 5 mM citrate salts to pH 6.0) so that the fluorescence intensity of HPTS was similar to those obtained during the transport experiments and the emission spectra after excitation at 403 nm and 460 nm were then collected. A small amount of transporter was subsequently added (aliquots of 6 µL of a 5 mM DMSO solution were added to a 3 mL cuvette, to mimic the conditions of the transport experiments) and the emission spectra were collected. The results shown in Figures S67-S72 reveal that there is some interference in the HPTS fluorescence due to the thiosquaramides, resulting in a reduction in fluorescence intensity. However, when the ratios of the HPTS fluorescence intensity at 510 nm after excitation at 403 nm and 460 nm are calculated, as well as the pH values based on these ratios, it is clear that the interference from the thiosquaramides does not affect the ratio of the fluorescence intensity at 510 nm. This implies that the results shown in Figures S57-S66 are due to real changes in intravesicular pH and not due to interference.

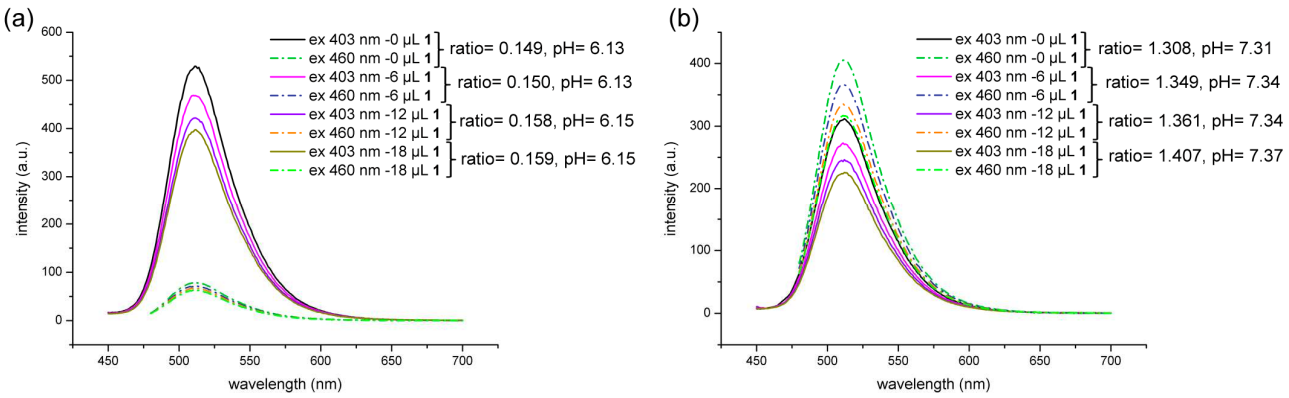

Figure S67: Investigation of possible interference in HPTS fluorescence by compound **1**. Some interference is present, but this does not affect the pH determination. (a) HPTS solution at pH 6.0 using 5 mM citrate buffer; (b) HPTS solution at pH 7.2 using 5 mM phosphate buffer.

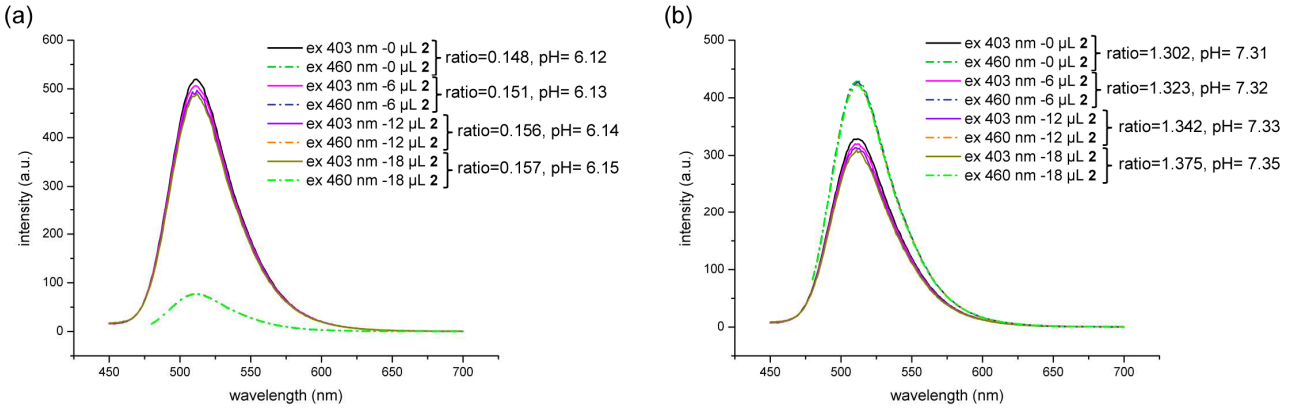

Figure S68: Investigation of possible interference in HPTS fluorescence by compound **2**. Very little interference is present. (a) HPTS solution at pH 6.0 using 5 mM citrate buffer; (b) HPTS solution at pH 7.2 using 5 mM phosphate buffer.

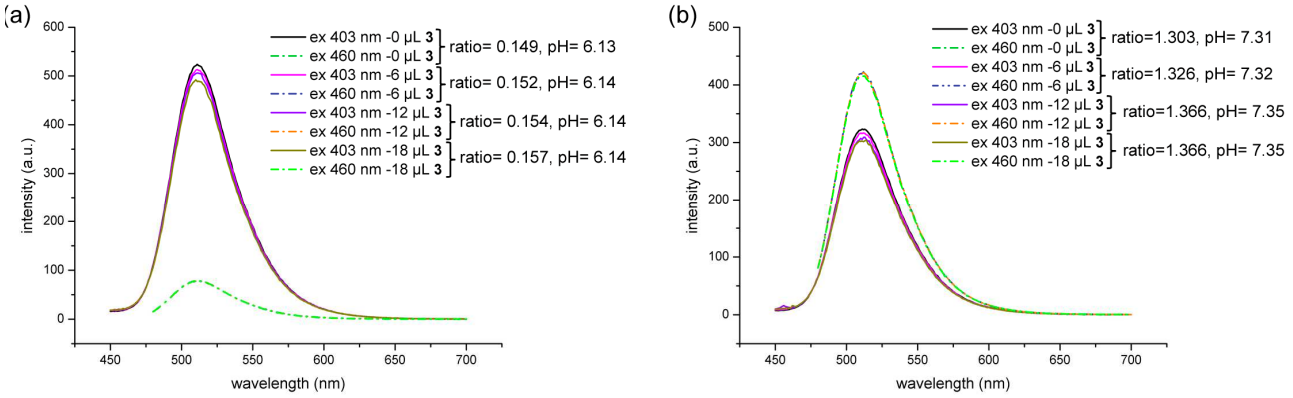

Figure S69: Investigation of possible interference in HPTS fluorescence by compound **3**. Very little interference is present. (a) HPTS solution at pH 6.0 using 5 mM citrate buffer; (b) HPTS solution at pH 7.2 using 5 mM phosphate buffer.

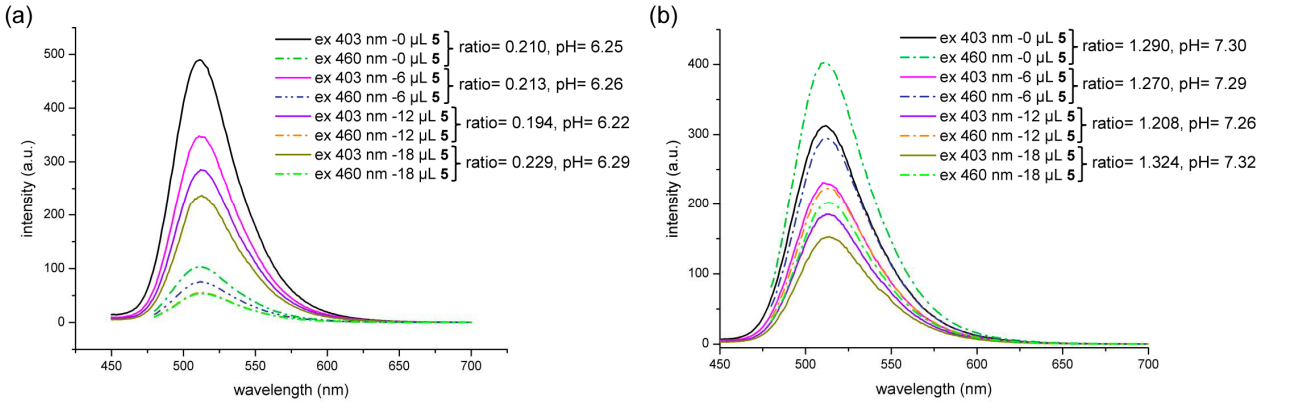

Figure S70: Investigation of possible interference in HPTS fluorescence by compound **5**. Some interference is present, but this does not affect the pH determination. (a) HPTS solution at pH 6.0 using 5 mM citrate buffer; (b) HPTS solution at pH 7.2 using 5 mM phosphate buffer.

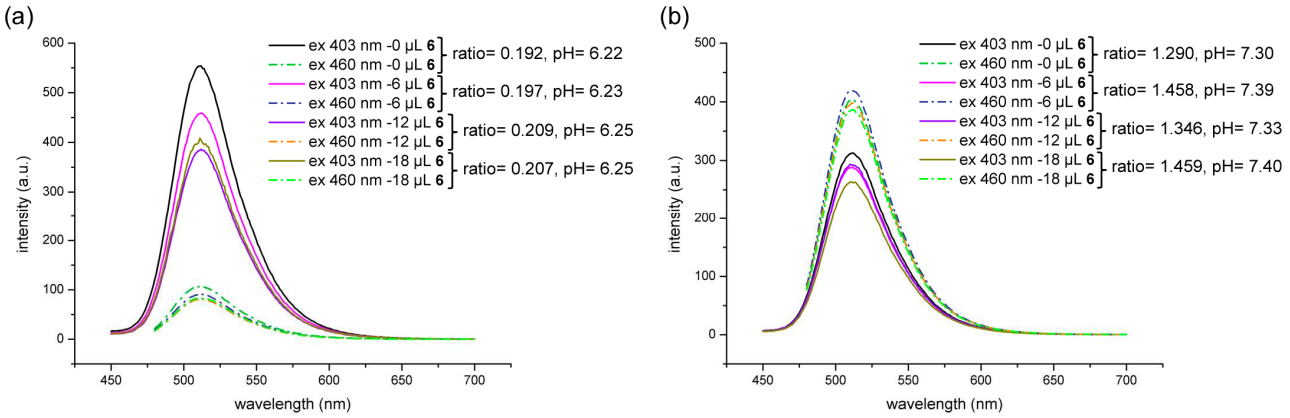

Figure S71: Investigation of possible interference in HPTS fluorescence by compound **6**. Some interference is present, but this does not affect the pH determination. (a) HPTS solution at pH 6.0 using 5 mM citrate buffer; (b) HPTS solution at pH 7.2 using 5 mM phosphate buffer.

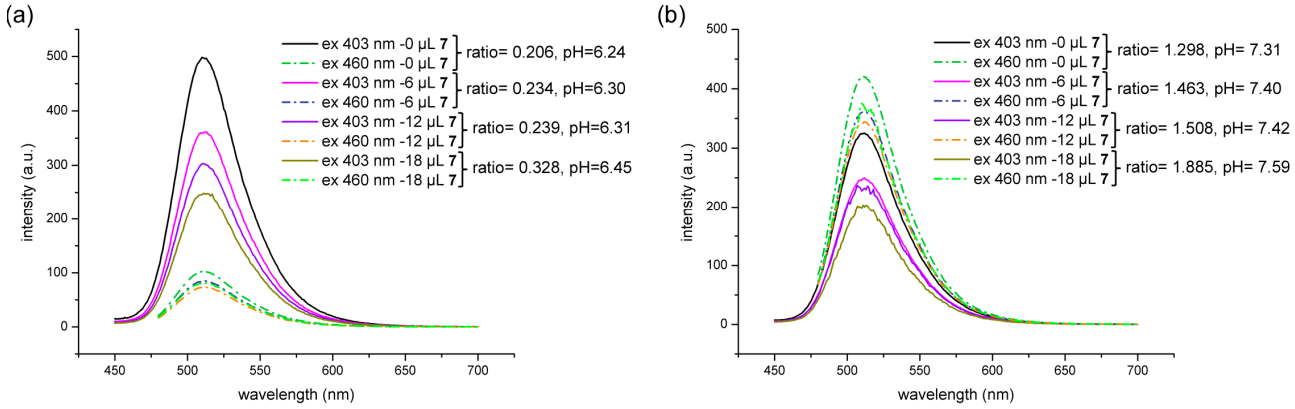

Figure S72: Investigation of possible interference in HPTS fluorescence by compound **7**. Some interference is present, but this does not affect the pH determination. (a) HPTS solution at pH 6.0 using 5 mM citrate buffer; (b) HPTS solution at pH 7.2 using 5 mM phosphate buffer.

S7.8. Apparent pK_a determination

Unilamellar POPC vesicles containing NaCl, prepared as described in Section S7.1., were suspended in the external medium consisting of $NaNO_3$ solution buffered to various pH. For the preparation of the buffer of both the internal and external solutions, an online application was used (http://www.biomol.net/en/tools/buffercalculator.htm), whereby the concentration of buffer was set to 5 mM and the ionic strength to 500 mM (the following buffers were used:

pH 4.0 – pH 6.0 = citrate, pH 7.2 = phosphate, pH 8.0 – pH 9.0 = Tris, pH 10.0 = ethanolamine, pH 11.0 = methylamine, pH 11.5 – pH 12.5 = phosphate). The lipid concentration per sample was 1 mM. A DMSO solution of the carrier molecule was added (to achieve 1 mol% carrier-to-lipid concentration) to start the experiment and the chloride efflux was monitored using a chloride sensitive electrode. At 5 min, the vesicles were lysed with 50 μL of octaethylene glycol monododecyl ether (0.232 mM in 7:1 water:DMSO v/v) and a total chloride reading was taken at 7 min. The initial value was set at 0% chloride efflux and the final chloride reading (at 7 minutes) was set as 100% chloride efflux. All other data points were calibrated to these points.

In order to calculate apparent pK_a values from this data, plots were made of the transport activity versus pH and subsequently fitted to the following equation (where *y* is a measure of transport activity, *x* is the pH, *MIN* is the minimum transport activity and *MAX* is the maximum transport activity):

$$y = MAX + \frac{(MIN - MAX)}{(1+10^{pKa-x})}$$

In theory there are various measures of transport activity that can be use, *e.g.* percentage of chloride efflux at a given time or initial rate of chloride efflux (k_{ini}). However, when using the single-point data of percentage of chloride efflux at a given time, artificially high pK_a values can be obtained for highly active chloride transporters (see Figures S73-S77). This is because the maximum efflux that can be achieved is 100%. A highly active transporter can achieve this 100% chloride efflux in 60 s, 90s, 300 s, etc. This means that when you plot the chloride efflux at 300 s versus pH for a highly active transporter, a platform at 100% chloride efflux is maintained for a wider range of pH than when a plot was made of the chloride efflux at 60 s versus pH. This is because in the first case 100% chloride efflux could be achieved in 60 s or in 300 s and no distinction is made between these values while they correspond to an actual difference in transport activity. In order to avoid this error, it is better to use the initial rate of chloride efflux (k_{ini}) as a measure of transport activity. The k_{ini} values were obtained by fitting the chloride efflux versus time plots with the following asymptotic function using Origin 8.1: $y = a - b \cdot c^x$, where *y* is the chloride efflux (%) and *x* is time (s). The initial rate of chloride release (k_{ini}) is then given by $k_{ini} = -b \cdot ln(c)$ and is obtained in % s^{-1}. In order to give more comparable values between the different compounds with different activities, the k_{ini} values were normalised to the highest k_{ini} value (at pH = 4.0).

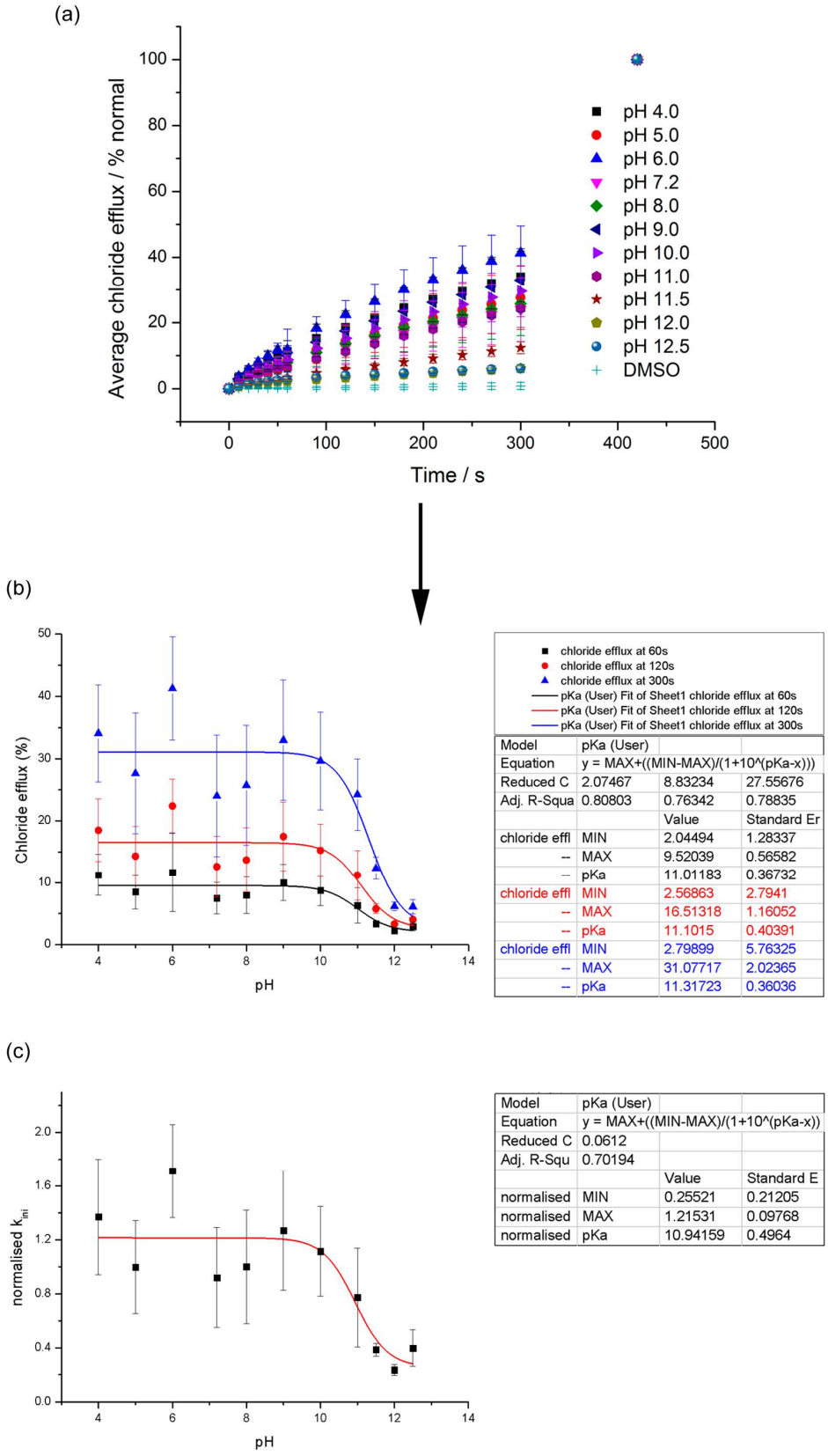

Model	pKa (User)		
Equation	y = MAX+((MIN-MAX)/(1+10^(pKa-x)))		
Reduced C	2.07467	8.83234	27.55676
Adj. R-Squa	0.80803	0.76342	0.78835
		Value	Standard Er
chloride effl	MIN	2.04494	1.28337
--	MAX	9.52039	0.56582
--	pKa	11.01183	0.36732
chloride effl	MIN	2.56863	2.7941
--	MAX	16.51318	1.16052
--	pKa	11.1015	0.40391
chloride effl	MIN	2.79899	5.76325
--	MAX	31.07717	2.02365
--	pKa	11.31723	0.36036

Model	pKa (User)		
Equation	y = MAX+((MIN-MAX)/(1+10^(pKa-x))		
Reduced C	0.0612		
Adj. R-Squ	0.70194		
		Value	Standard E
normalised	MIN	0.25521	0.21205
normalised	MAX	1.21531	0.09768
normalised	pKa	10.94159	0.4964

Figure S73: Apparent pK_a determination of receptor **1**. (a) Chloride efflux mediated by 1 mol% **1** from unilamellar POPC vesicles loaded with 489 mM NaCl buffered to various pH. The vesicles were dispersed in 489 mM $NaNO_3$ buffered to the same pH as the internal solution. Each points represent the average of a minimum of three repeats and error bars represent standard deviations. (b) pK_a determination based on the percentage of chloride efflux at 60 s, 120 s and 300 s. (c) pK_a determination based on normalised k_{ini} values.

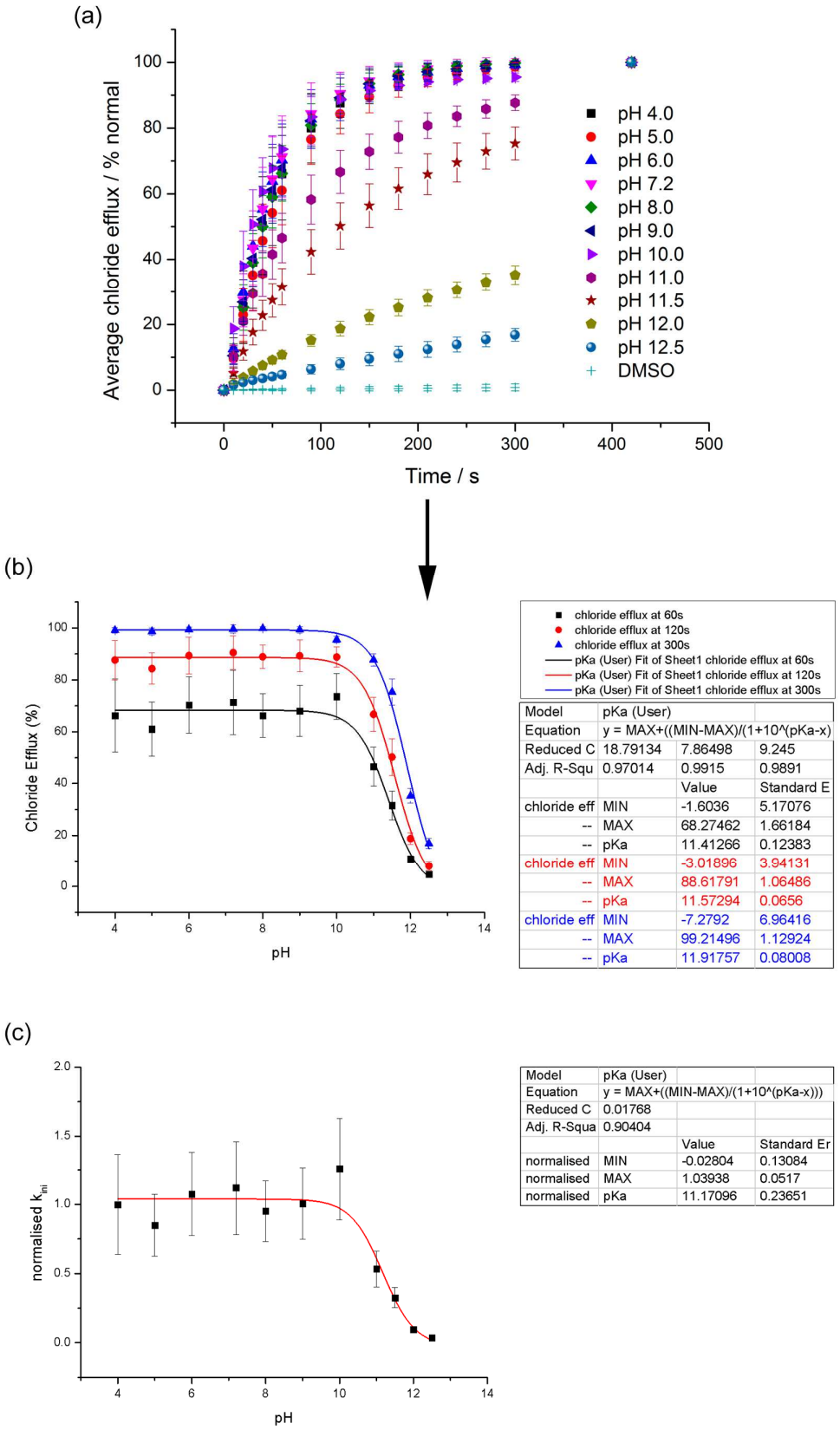

Model	pKa (User)		
Equation	y = MAX+((MIN-MAX)/(1+10^(pKa-x)		
Reduced C	18.79134	7.86498	9.245
Adj. R-Squ	0.97014	0.9915	0.9891
		Value	Standard E
chloride eff	MIN	-1.6036	5.17076
--	MAX	68.27462	1.66184
--	pKa	11.41266	0.12383
chloride eff	MIN	-3.01896	3.94131
--	MAX	88.61791	1.06486
--	pKa	11.57294	0.0656
chloride eff	MIN	-7.2792	6.96416
--	MAX	99.21496	1.12924
--	pKa	11.91757	0.08008

Model	pKa (User)		
Equation	y = MAX+((MIN-MAX)/(1+10^(pKa-x)))		
Reduced C	0.01768		
Adj. R-Squa	0.90404		
		Value	Standard Er
normalised	MIN	-0.02804	0.13084
normalised	MAX	1.03938	0.0517
normalised	pKa	11.17096	0.23651

Figure S74: Apparent pK_a determination of receptor **2**. (a) Chloride efflux mediated by 1 mol% **2** from unilamellar POPC vesicles loaded with 489 mM NaCl buffered to various pH. The vesicles were dispersed in 489 mM $NaNO_3$ buffered to the same pH as the internal solution. Each points represent the average of a minimum of three repeats and error bars represent standard deviations. (b) pK_a determination based on the percentage of chloride efflux at 60 s, 120 s and 300 s. (c) pK_a determination based on normalised k_{ini} values.

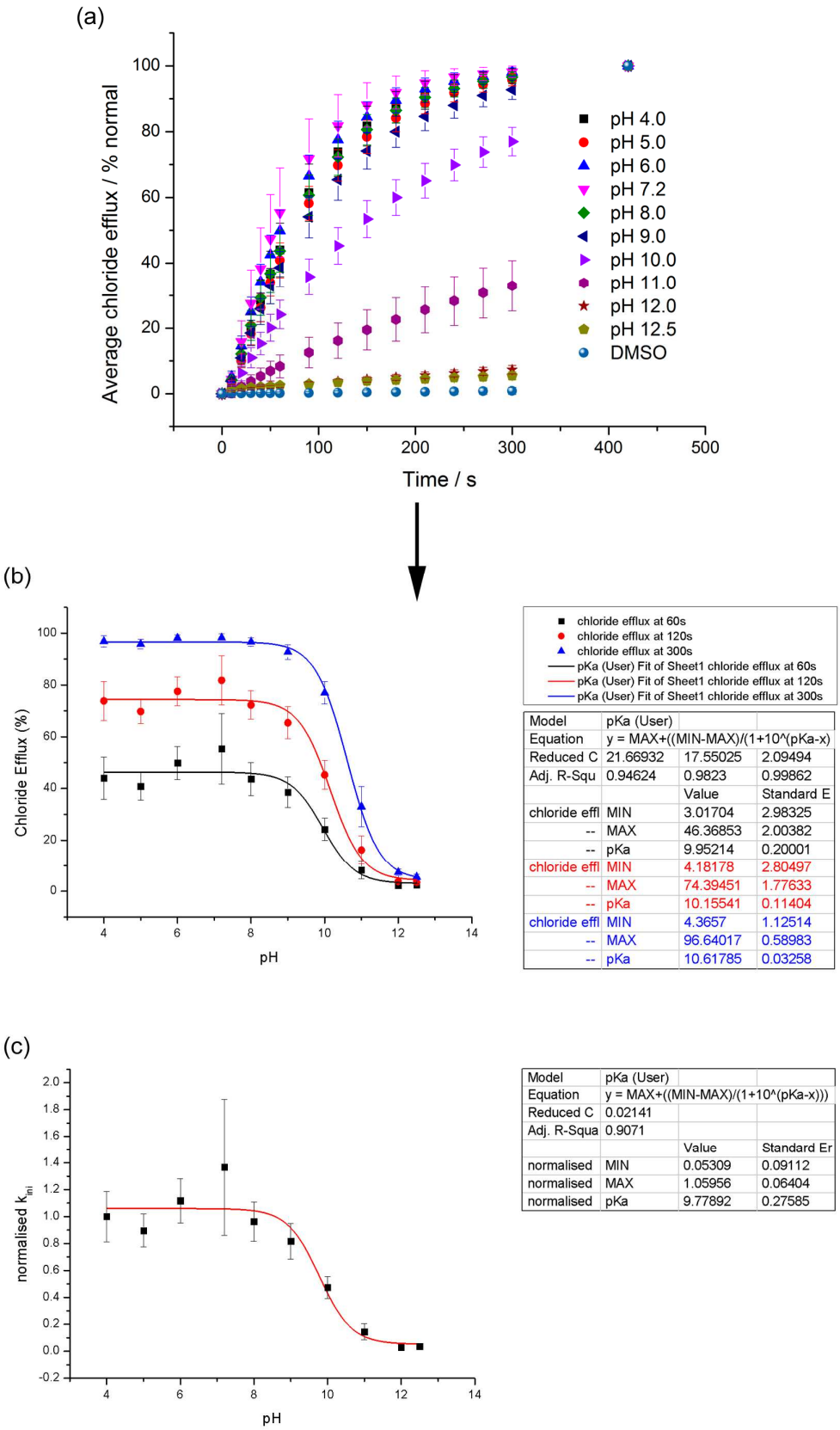

Model	pKa (User)		
Equation	y = MAX+((MIN-MAX)/(1+10^(pKa-x)		
Reduced C	21.66932	17.55025	2.09494
Adj. R-Squ	0.94624	0.9823	0.99862
		Value	Standard E
chloride effl	MIN	3.01704	2.98325
--	MAX	46.36853	2.00382
--	pKa	9.95214	0.20001
chloride effl	MIN	4.18178	2.80497
--	MAX	74.39451	1.77633
--	pKa	10.15541	0.11404
chloride effl	MIN	4.3657	1.12514
--	MAX	96.64017	0.58983
--	pKa	10.61785	0.03258

Model	pKa (User)		
Equation	y = MAX+((MIN-MAX)/(1+10^(pKa-x)))		
Reduced C	0.02141		
Adj. R-Squa	0.9071		
		Value	Standard Er
normalised	MIN	0.05309	0.09112
normalised	MAX	1.05956	0.06404
normalised	pKa	9.77892	0.27585

Figure S75: Apparent pK_a determination of receptor **3**. (a) Chloride efflux mediated by 1 mol% **3** from unilamellar POPC vesicles loaded with 489 mM NaCl buffered to various pH. The vesicles were dispersed in 489 mM $NaNO_3$ buffered to the same pH as the internal solution. Each points represent the average of a minimum of three repeats and error bars represent standard deviations. (b) pK_a determination based on the percentage of chloride efflux at 60 s, 120 s and 300 s. (c) pK_a determination based on normalised k_{ini} values.

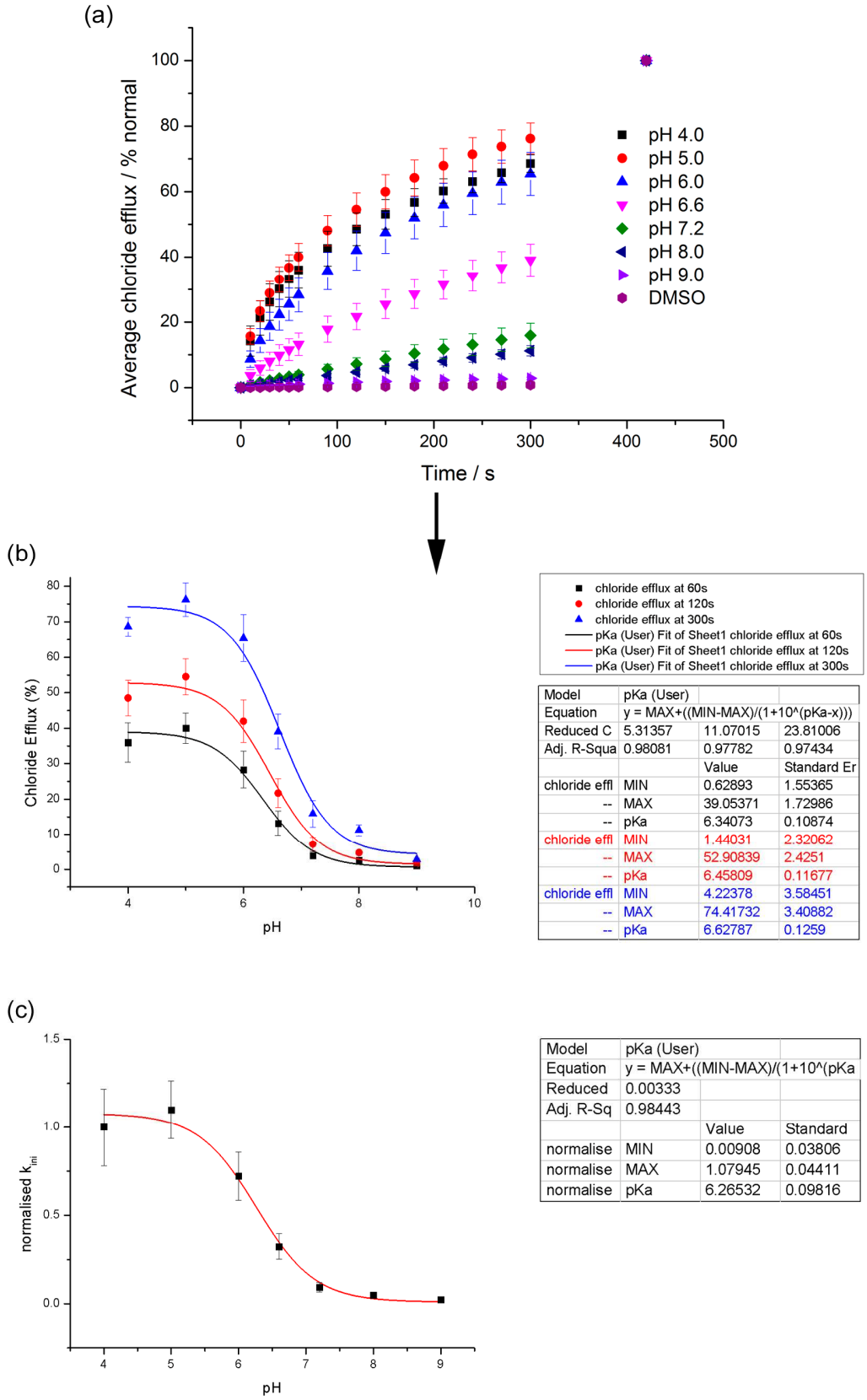

Model	pKa (User)		
Equation	y = MAX+((MIN-MAX)/(1+10^(pKa-x)))		
Reduced C	5.31357	11.07015	23.81006
Adj. R-Squa	0.98081	0.97782	0.97434
		Value	Standard Er
chloride effl	MIN	0.62893	1.55365
--	MAX	39.05371	1.72986
--	pKa	6.34073	0.10874
chloride effl	MIN	1.44031	2.32062
--	MAX	52.90839	2.4251
--	pKa	6.45809	0.11677
chloride effl	MIN	4.22378	3.58451
--	MAX	74.41732	3.40882
--	pKa	6.62787	0.1259

Model	pKa (User)		
Equation	y = MAX+((MIN-MAX)/(1+10^(pKa		
Reduced	0.00333		
Adj. R-Sq	0.98443		
		Value	Standard
normalise	MIN	0.00908	0.03806
normalise	MAX	1.07945	0.04411
normalise	pKa	6.26532	0.09816

Figure S76: Apparent pK_a determination of receptor **5**. (a) Chloride efflux mediated by 1 mol% **5** from unilamellar POPC vesicles loaded with 489 mM NaCl buffered to various pH. The vesicles were dispersed in 489 mM $NaNO_3$ buffered to the same pH as the internal solution. Each points represent the average of a minimum of three repeats and error bars represent standard deviations. (b) pK_a determination based on the percentage of chloride efflux at 60 s, 120 s and 300 s. (c) pK_a determination based on normalised k_{ini} values.

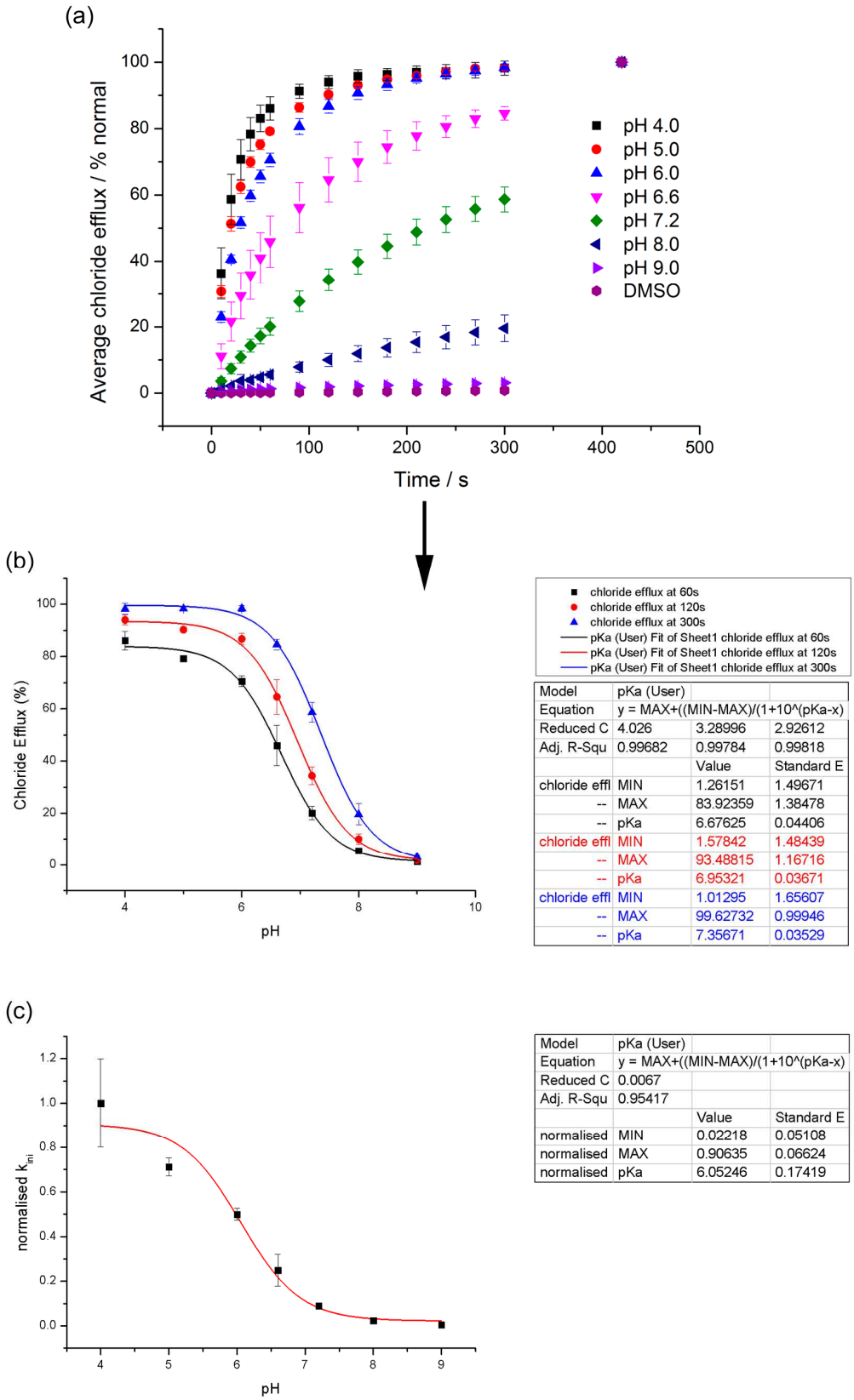

Model	pKa (User)		
Equation	y = MAX+((MIN-MAX)/(1+10^(pKa-x)		
Reduced C	4.026	3.28996	2.92612
Adj. R-Squ	0.99682	0.99784	0.99818
		Value	Standard E
chloride effl	MIN	1.26151	1.49671
--	MAX	83.92359	1.38478
--	pKa	6.67625	0.04406
chloride effl	MIN	1.57842	1.48439
--	MAX	93.48815	1.16716
--	pKa	6.95321	0.03671
chloride effl	MIN	1.01295	1.65607
--	MAX	99.62732	0.99946
--	pKa	7.35671	0.03529

Model	pKa (User)		
Equation	y = MAX+((MIN-MAX)/(1+10^(pKa-x)		
Reduced C	0.0067		
Adj. R-Squ	0.95417		
		Value	Standard E
normalised	MIN	0.02218	0.05108
normalised	MAX	0.90635	0.06624
normalised	pKa	6.05246	0.17419

Figure S77: Apparent pK_a determination of receptor **6**. (a) Chloride efflux mediated by 1 mol% **6** from unilamellar POPC vesicles loaded with 489 mM NaCl buffered to various pH. The vesicles were dispersed in 489 mM $NaNO_3$ buffered to the same pH as the internal solution. Each points represent the average of a minimum of three repeats and error bars represent standard deviations. (b) pK_a determination based on the percentage of chloride efflux at 60 s, 120 s and 300 s. (c) pK_a determination based on normalised k_{ini} values.

S8. Thiosquaramide stability

Some of the thiosquaramides (especially **6** and **7**) were found to be unstable in DMSO. It was found that the UV/Vis absorbance spectra of **6** changes over time due to degradation of the thiosquaramide (Figure S78). On the other hand, this behaviour was not seen in acetonitrile solutions of the thiosquaramides, indicating that the thiosquaramides are more stable in this solvent (see Figure S79). In acetonitrile degradation only became important after more than 24 hours (see Figure S80). Unfortunately, not all of the compounds were soluble in acetonitrile and therefore DMSO was still used as the solvent of choice for the anion binding and anion transport studies. To overcome the issue of instability, all of the experiments were performed on freshly made DMSO solutions that were used immediately. The ^{1}H NMR spectra obtained during the anion binding studies, indicated that the thiosquaramides remained stable over the course of the experiment. To check if the instability had an effect on the anion transport studies, some of the anion transport experiments were repeated with acetonitrile solutions of the thiosquaramides (this was only possible for **6** and 7, because the other compounds were not soluble in acetonitrile). It was found that using acetonitrile stock solutions gave identical results as using fresh DMSO stock solution (see Figures S81-S82), indicating that the instability of the thiosquaramides had no effect on the results of the anion transport studies. However, when old DMSO stock solutions were used (7 days old) a significant change in anion transport ability was seen, suggesting that the thiosquaramides had degraded. All of the transport experiments described above and in the manuscript were performed with freshly made DMSO solutions and should therefore be valid.

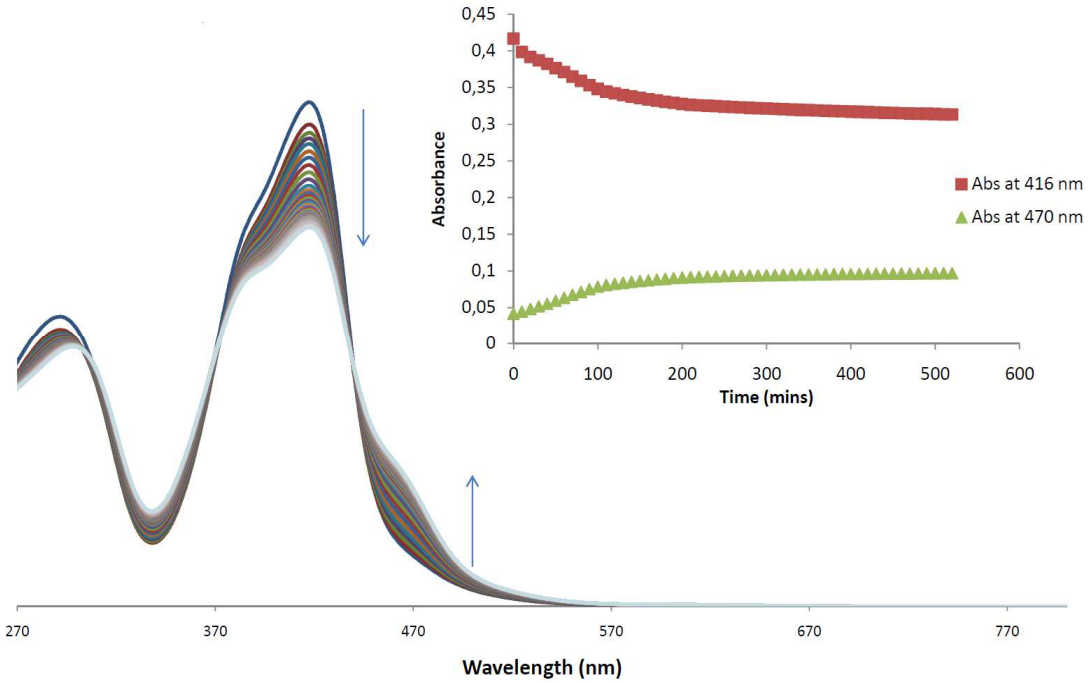

Figure S78: Changes in absorbance of a DMSO solution of compound **6** over time.

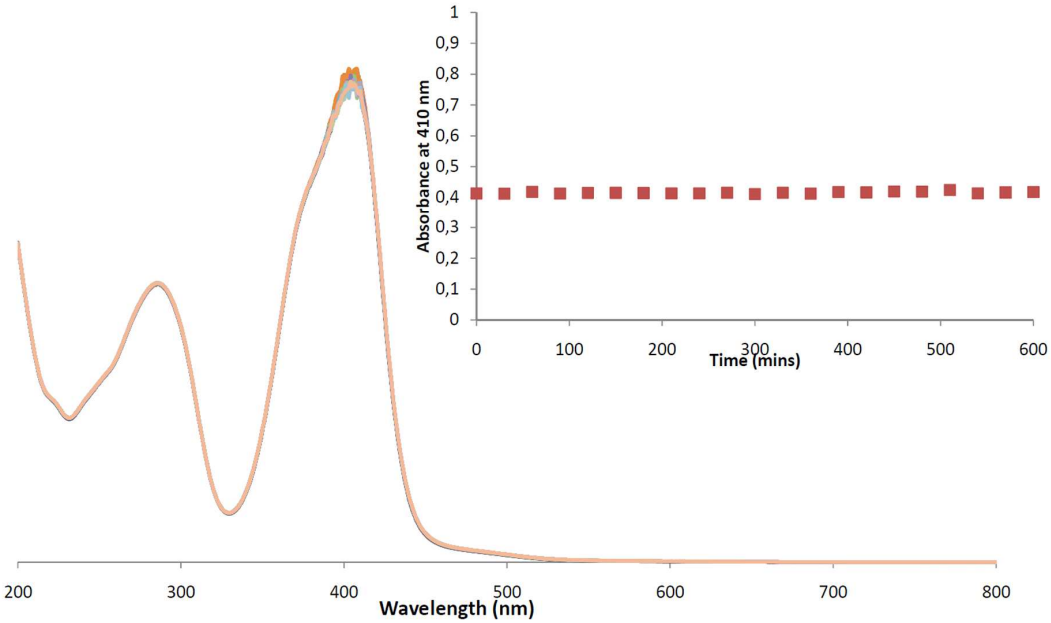

Figure S79: Changes in absorbance of a MeCN solution of compound **6** over time.

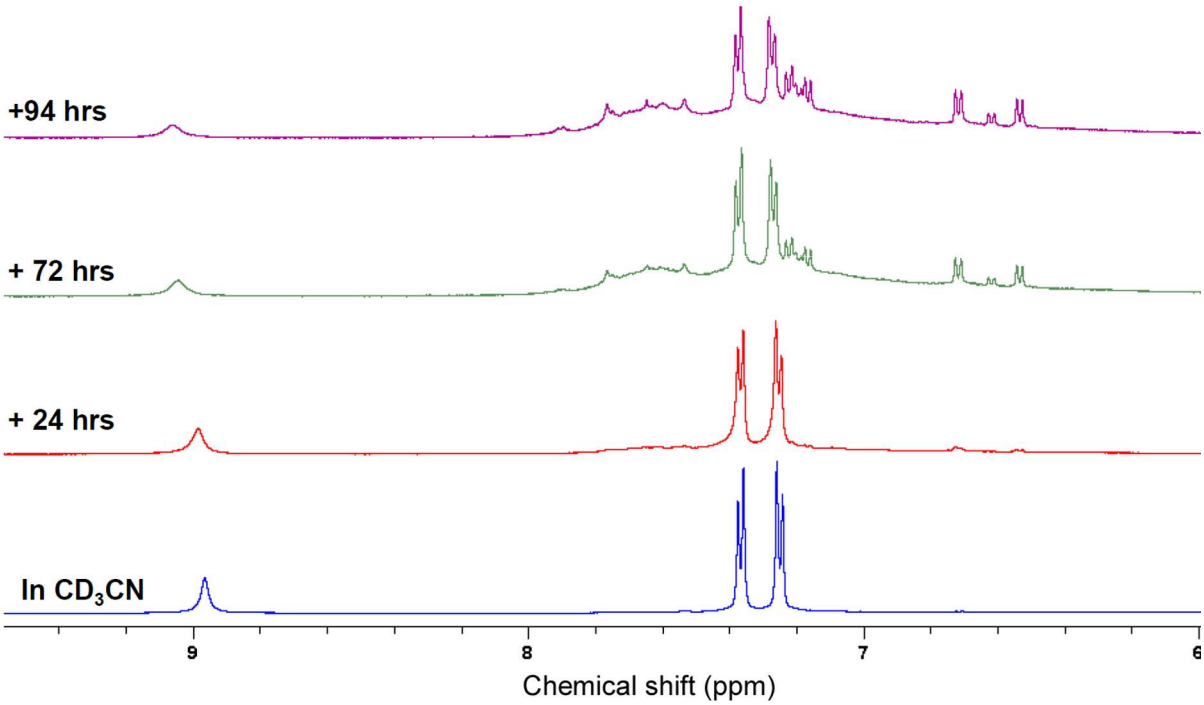

Figure S80: Changes in ^{1}H NMR spectra of a MeCN solution of compound **6** over time.

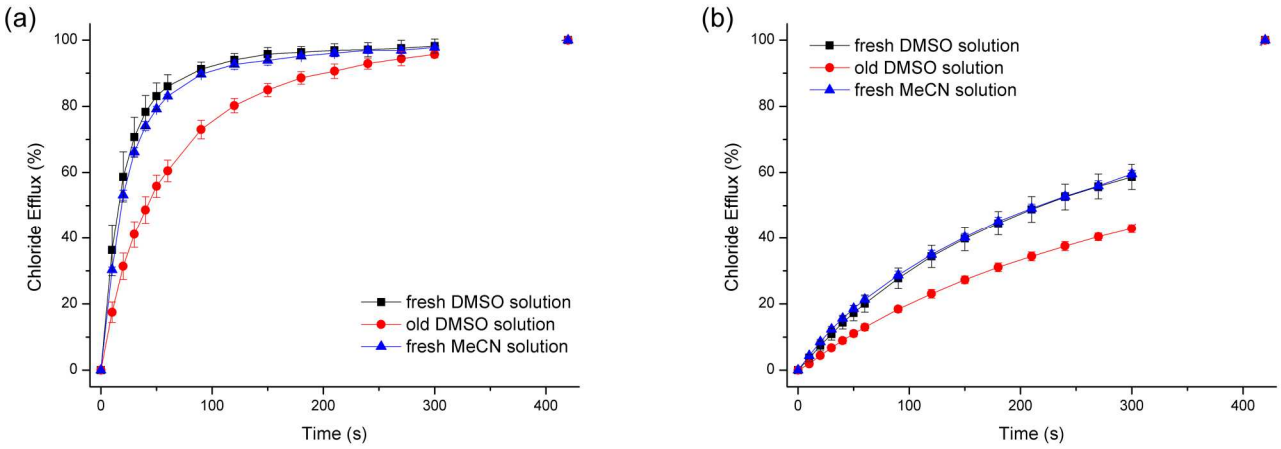

Figure S81: Chloride efflux from POPC vesicles at pH 4.0 (a) and pH 7.2 (b) mediated by compound **6** (1 mol% with respect to lipid). POPC vesicles were loaded with a 489 mM NaCl solution buffered to pH 7.2 with 5 mM phosphate salts or to pH 4.0 with 5 mM citrate salts, and were suspended in a 489 mM $NaNO_3$ solution buffered to pH 7.2 with 5 mM phosphate salts or to pH 4.0 with 5 mM citrate salts. The experiment was started by the addition of a DMSO or MeCN solution of compound **6** (10 µL of a 5 mM stock solution). At the end of the experiment (300 s), detergent was added to lyse the vesicles and calibrate the ISE to 100% chloride efflux. Each point represents the average of a minimum of 3 independent trials.

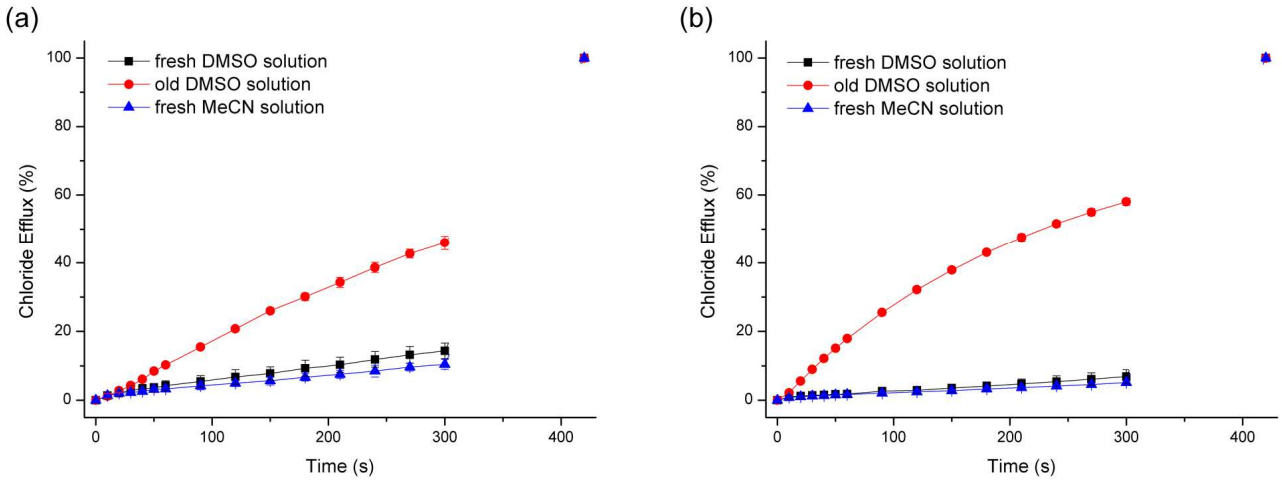

Figure S82: Chloride efflux from POPC vesicles at pH 4.0 (a) and pH 7.2 (b) mediated by compound **7** (1 mol% with respect to lipid). POPC vesicles were loaded with a 489 mM NaCl solution buffered to pH 7.2 with 5 mM phosphate salts or to pH 4.0 with 5 mM citrate salts, and were suspended in a 489 mM $NaNO_3$ solution buffered to pH 7.2 with 5 mM phosphate salts or to pH 4.0 with 5 mM citrate salts. The experiment was started by the addition of a DMSO or MeCN solution of compound **7** (10 µL of a 5 mM stock solution). At the end of the experiment (300 s), detergent was added to lyse the vesicles and calibrate the ISE to 100% chloride efflux. Each point represents the average of a minimum of 3 independent trials.

S9. References

(1) Busschaert, N.; Kirby, I. L.; Young, S.; Coles, S. J.; Horton, P. N.; Light, M. E.; Gale, P. A. *Angew. Chem. Int. Ed.***2012**, *51*, 4426-4430.

(2) Bergman, J.; Pettersson, B.; Hasimbegovic, V.; Svensson, P. H. *J. Org. Chem.***2011**, *76*, 1546-1553.

(3) Rostami, A.; Colin, A.; Li, X. Y.; Chudzinski, M. G.; Lough, A. J.; Taylor, M. S. *J. Org. Chem.* **2010**, *75*, 3983-3992.

(4) R Ian Storer, C Aciro and L H Jones, *Chem. Soc. Rev.*, 2011, **40**, 2330-2346.

(5) M. C. Rotger, M. N. Pina, A. Frontera, G. Martorell, P. Ballester, P. M. Deya and A. Costa, J. Org. Chem., 2004, 69, 2302–2308.

(6) S. Tomas, R. Prohens, M. Vega, M. C. Rotger, P. M. Deya, P. Ballester and A. Costa, J. Org. Chem., 1996, 61, 9394

(7) D. Quinonero, A. Frontera, P. Ballester and P. M. Deya, Tetrahedron Lett., 2000, 41, 2001–2005